2011

Modulation and Multiple Access Techniques for Ultra-Wideband Communication Systems

Song Cui
Cleveland State University

MODULATION AND MULTIPLE ACCESS TECHNIQUES FOR ULTRA-WIDEBAND COMMUNICATION SYSTEMS

SONG CUI

Bachelor of Engineering in Mechanical Engineering

Guangxi University

June, 1997

Master of Engineering in Electrical Engineering

Guangxi University

July, 2004

submitted in partial fulfillment of the requirements for the degree

DOCTOR OF ENGINEERING

at the

CLEVELAND STATE UNIVERSITY

November 2011

This dissertation has been approved for the

Department of **ELECTRICAL AND COMPUTER ENGINEERING**

and the College of Graduate Studies by

_____

Dissertation Committee Chairperson, Dr. Fuqin Xiong

_____

Department/Date

_____

Dr. Ching L Chang

_____

Department/Date

_____

Dr. Pong Chu

_____

Department/Date

_____

Dr. Murad Hizlan

_____

Department/Date

_____

Dr. Chansu Yu

_____

Department/Date

_____

Dr. Wenbing Zhao

_____

Department/Date

ACKNOWLEDGMENTS

I am very grateful to my advisor, Dr. Fuqin Xiong, for his consistent guidance, encouragement, and support during the whole period of my study. I would like to thank Dr. Ching L Chang, Dr. Pong Chu, Dr. Murad Hizlan, Dr. Chansu Yu, and Dr. Wenbing Zhao, who are on my dissertation committee, for reviewing this dissertation as well as for their suggestions to my research.

I am also grateful to my friends in our department, especially Rick Rarick, Stanley Siwale, Mehmet Ergezer, Sheng Zhao, Qing Zheng, Gang Tian, Honglei Zhang, Tianning Shen, Dawei Du, Yuanchao Lu, Yidong Qian, Hua Chai, Zhuolei Wang.

I also will express my gratitude to my friend Dr. Jiangli Zhu, who is with Cadence company as a hardware engineer in present and a previous doctoral student from Case Western Reserve University. During my research period, Dr. Zhu provided very supportive help to search documents for me. I also obtain great help from the engineer of Viasat company Dr. Fan Mo and Mr. Mike Dollard who gave me very helpful suggestions in simulation experiment.

Finally, I will express my deepest gratitude to my wife Zongling Han. Without her love, patience, encouragement, and sacrifice, I would not have accomplished this dissertation.

MODULATION AND MULTIPLE ACCESS TECHNIQUES FOR ULTRA-WIDEBAND COMMUNICATION SYSTEMS

SONG CUI

ABSTRACT

Two new energy detection (ED) Ultra-Wideband (UWB) systems are proposed in this dissertation. The first one is an ED UWB system based on pulse width modulation (PWM). The bit error rate (BER) performance of this ED PWM system is slightly worse than ED pulse position modulation (PPM) system in additive white Gaussian noise (AWGN) channels. However, the BER performance of this ED PWM system surpasses that of a PPM system in multipath channels since a PWM system does not suffer cross-modulation interference (CMI) as a PPM system. In the presence of synchronization errors, the BER performance of a PWM system also surpasses that of a PPM system. The second proposed ED UWB system is based on using two pulses, which are the different-order derivatives of the Gaussian pulse, to transmitted bit 0 or 1. These pulses are appropriately chosen to separate their spectra in frequency domain. The receiver is composed of two energy detection branches and each branch has a filter which captures the signal energy of either bit 0 or 1. The outputs of two branches are subtracted from each other to generate the decision statistic and the value of this statistic is compared to a threshold to determine the transmitted bits. This system is named as Gaussian FSK (GFSK) system in this dissertation

and it exhibits the same BER performance as a PPM system in AWGN channels. In multipath channels, a GFSK system surpasses a PPM system because it does not suffer CMI. And the BER performance of a GFSK system is better than a PPM system in the presence of synchronization errors. When a GFSK system is compared to a PWM system, it will always achieve approximately 2 dB improvement in AWGN channels, multipath channels, and in the presence synchronization errors. However, a PWM system uses lower-order derivatives of the Gaussian pulse to transmit signal, and this leads to a simple pulse generator. In this dissertation, an optimal threshold is applied to improve PPM system performance. The research results show that the application of an optimal threshold can effectively mitigate the effect of CMI and synchronization errors and achieve performance improvement. Finally, the multiple access schemes are discussed and time hopping is chosen as the multiple access scheme for PWM and GFSK systems.

TABLE OF CONTENTS

LIST OF TABLES

LIST OF FIGURES

ACRONYMS

AWGN additive white Gaussian noise

BER bit error rate

CMI cross-modulation interference

CDMA code division multiple access

DF differential detection

DS-CDMA direct sequence CDMA

ED energy detection

EDGE enhanced data rates for GSM evolution

FCC federal communication commission

FDMA frequency division multiple access

FH-CDMA frequency hopping CDMA

GFSK Gaussian FSK

GPRS general packet radio service

HSPA High speed packet access

IFI inter-frame interference

IR impulse radio

MAI multiple access interference

OOK on-off keying

PAM pulse amplitude modulation

PPM pulse position modulation

PWM Pulse width modulation

QAM quadrature amplitude modulation

SNR signal-to-noise ratio

SRD step recovery diode

TDMA time division multiple access

TH time hoping

TR transmitted reference

UWB Ultra-Wideband

CHAPTER I

INTRODUCTION

1.1 Definition of Ultra-Wideband Signals

Ultra-Wideband (UWB) impulse radio (IR) systems convey information by transmitting sub-nano second short pulses. These extremely short pulses produce ultra-wide bandwidth, and thus these systems are called ultra-wideband systems. According to the regulation of the federal communication commission (FCC), a signal is defined as an UWB signal if the absolute bandwidth of a signal $B \geq 500MHz$ or the fractional bandwidth $B_f \geq 0.2$. The definition of B_f is [1]

$$B_f = \frac{f_H - f_L}{(f_H + f_L)/2} \tag{1.1}$$

where f_H and f_L are the highest and lowest cut-off frequencies of the signal bandwidth, and $(f_H + f_L)/2$ is equal to the center frequency. The bandwidth has different definition, such as null-to-null bandwidth, -3 dB bandwidth, -10 dB bandwidth, and son on. In UWB systems, -10 dB bandwidth is used.

1.2 History of UWB Technology

UWB technology becomes a popular research topic in recent ten years, but the earliest prototype of UWB technology can be traced back to 1901 when Guglielmo Marconi transmitted Morse code using spark gap radio transmitters [1]. However, this impulse radio technology did not attract too much attention at that time and the potential ability to provide an ultra-wide bandwidth of this technology has been buried for many years since then. Approximately in the 1950s, impulse radio was applied in military to develop radars. From the 1960s to the 1990s, UWB technology was developed for military and defence applications, such as secure communications, under the strict management. With the increasing demand of high-data-rate service, more and more organizations and institutes appealed the governments to release the regulation to allow the development of UWB technology for commercial applications. In 2002, the FCC of USA issued its rule for UWB commercial applications, and this initiate the new times of UWB technology [1]. After that, Japan, South Korea and Europe also published their regulations on September 2005, July 2006, and February 2007, respectively [2]. Now, more and more academic institutes and companies join the research alliance to develop UWB technology and these research activities generate a large number of valuable papers published on different journals and international conferences. Furthermore, the industry takes part in not only the theoretical research but also the hardware implementation which will provide pioneer experiment platforms for UWB hardware-based research. These leading companies include Intel, Time Domain, Mitsubishi, Bosch, XtremeSpectrum, Motorola and so on. IEEE has published its standard of UWB applications such as IEEE 802.15.3 and IEEE 802.15.4a.

1.3 Advantages and Applications of UWB Technology

When compared to narrow band systems, UWB systems have many advantages: large channel capacity, ability to work under low signal-to-noise ratio, immunity to intercept and detection, resistance to jamming, high performance in multipath channels, super penetrating property, and simple transceiver structure [1]. These advantages make UWB technology a candidate for many applications. For example, UWB technology can be applied to covert communication, such as secure communications, and covert wireless sensor network. Also UWB technology is suitable to short-range, low-power wireless application [3,4], high-data-rate wireless personal area network, wireless Ethernet interface link, intelligent wireless area network and outdoor peer-to-peer network [5]. The special penetrating ability of UWB signals is exploited to develop ground-penetrating radar, through-wall imaging, medical imaging, surveillance, and monitoring systems [1]. UWB technology is applied to localization system such as personnel identification, inventory tracking, asset management, tagging and identification [1].

1.4 Challenges of UWB Technology

Although UWB technology has many advantages and potential applications, there are still many technology problems need to be resolved before UWB products really enter the market.

Channel estimation: In UWB multipath channels, the number of the multipath components of a signal is pretty large. The estimator needs to obtain a large number of the amplitude and phase response informations of these multipath components and this leads to the great complexity of channel estimation [4].

Synchronization: The signals of UWB systems are transmitted at extremely short duration on the order of sub-nano second. Thus UWB receivers must work under a stringent synchronization requirement, and a tiny timing mis-alignment will result in a great degradation of the system performance [4].

Multiple-Access Interference: In multi-user or multiple access systems, different users transmit signals into the channels simultaneously. An user's receiver receives not only the useful signals but also multiple access interference (MAI) from neighbour users [1]. MAI degrades the system performance greatly if it is not affectively avoided. The appropriate multiple access schemes need to be developed to prevent the collision of signals from different users. If MAI can not be avoid, methods should be developed to mitigate the effect of MAI.

Modulation and Receiver: UWB systems transmit short pulse to convey information, so the modulation can be achieved by changing the amplitude, position and width of the pulses. The modulation methods of UWB systems are very limited and not so abundant as continuous waveform systems. The receiver can use coherent or non-coherent methods to demodulate the received signals and all these methods all have their advantages and disadvantages.

In this dissertation, we focus on developing modulation and receiver methods, so we will introduce the existing methods in the following.

1.5 Modulation Methods

The popular modulation methods used in UWB systems are pulse position modulation (PPM) and pulse amplitude modulation (PAM). Pulse width modulation (PWM) has been proved a suitable modulation method for UWB recently [6].

1.5.1 PPM

Fig. 1 is the modulation diagram of PPM. PPM carries out modulation by shift pulse position. When the transmitted bit is 0, pulse does not shift. When bit is 1, pulse shift a specific amount δ, where δ is called modulation index.

1.5.2 OOK

Fig. 2 is the modulation diagram of on-off keying (OOK). When the transmitted bit is 1, a pulse is transmitted. When the bit is 0, no pulse is transmitted.

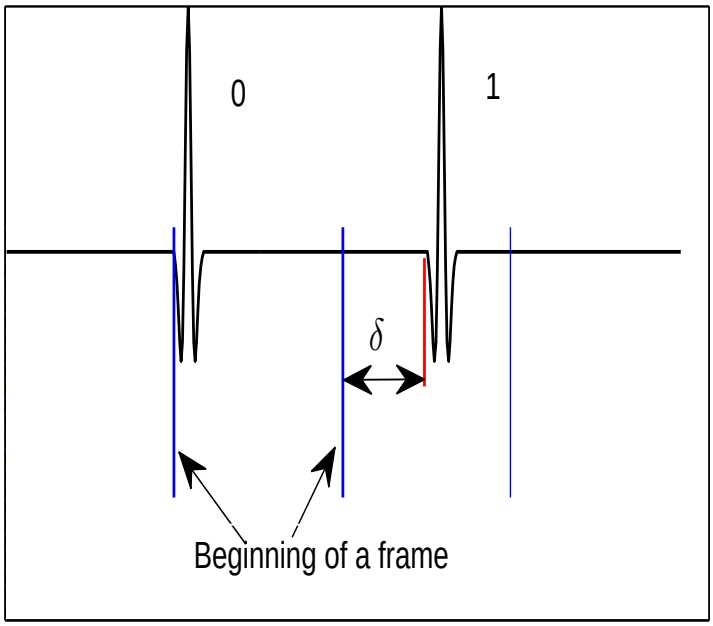

Figure 1: PPM Modulation

1.5.3 PAM

Fig. 3 is the diagram of PAM. When the transmitted bit is 1, a positive pulse is transmitted. When the bit is 0, a negative pulse is transmitted.

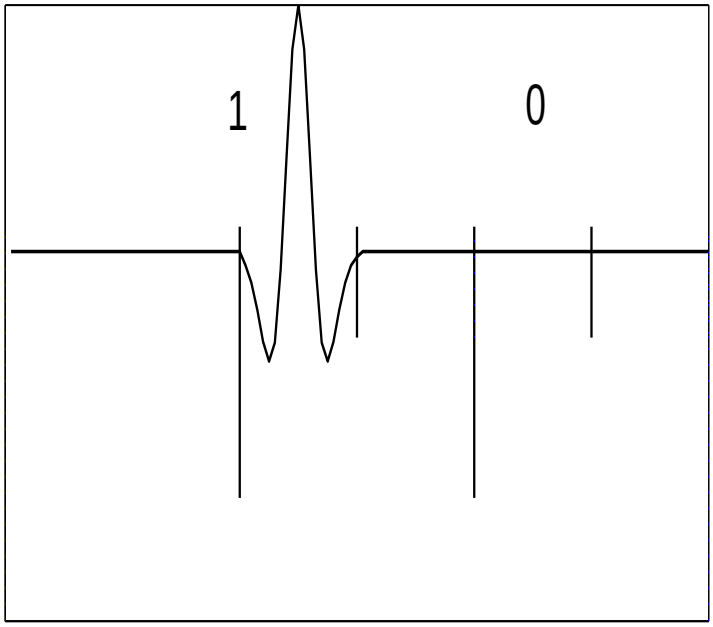

Figure 2: OOK Modulation

1.5.4 PWM

Fig. 4 is the diagram of PWM. When the transmitted bit is 1, a wide pulse is transmitted. When the bit is 0, a narrow pulse is transmitted.

1.6 Receiver Methods

The receiver methods of UWB systems are separated into two categories: coherent and non-coherent methods. The coherent receiver method includes rake receiver, and the non-coherent methods include energy detection, transmitted- reference and differential detection. These methods will be introduced in the following.

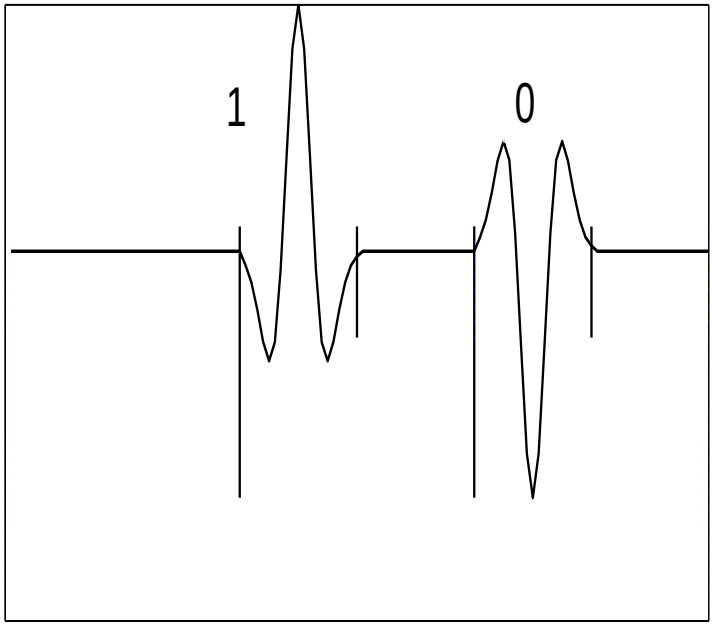

Figure 3: PAM Modulation

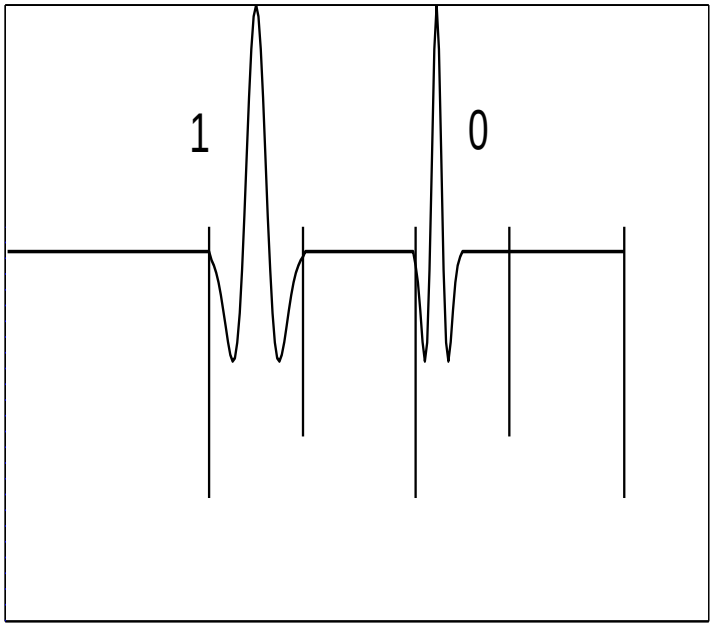

Figure 4: PWM Modulation

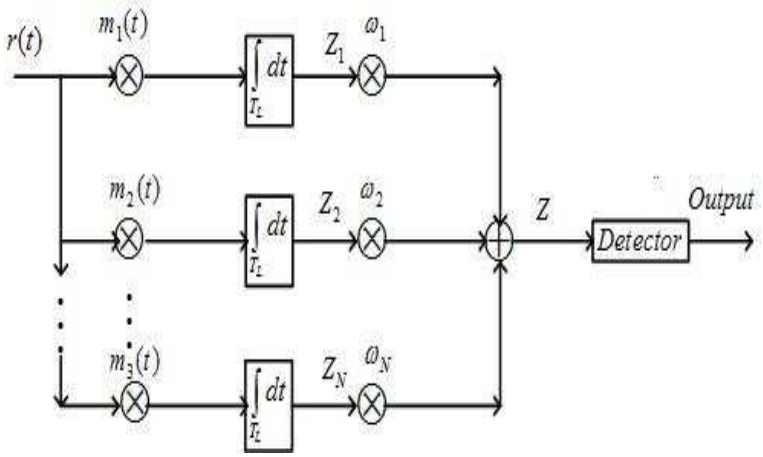

Figure 5: The structure of a rake receiver (from [7])

1.6.1 Rake Receiver

Fig. 5 is the structure of the rake receiver [7], where $r(t)$ denotes the received signal. The term $m_j(t) = m(t - \tau_j)$ denotes correlator template, where τ_j is the time delay of the jth multipath component relative to the first component. The integration time is T_L which is equal to one pulse duration and Z_j is the output of the jth correlator. These correlator outputs are multiplied by weighting factors ω_i and then are summed together to generate Z. Finally, Z is sent to detector to obtain the output data bit. Each branch of the rake receiver includes a correlator and these correlators need the information of channel impulse response.

1.6.2 Energy Detection

Fig. 6 is the structure of energy detection (ED) receiver [8], where $s(t)$ denotes the signal arriving at the receiver, $n(t)$ is additive white Gaussian noise (AWGN) and $r(t) = s(t) + n(t)$ denotes the composition of signal and noise. The filter is designed to capture as much signal energy as possible and suppress out-of-band noise simultaneously. ED has been applied to OOK and PPM systems.

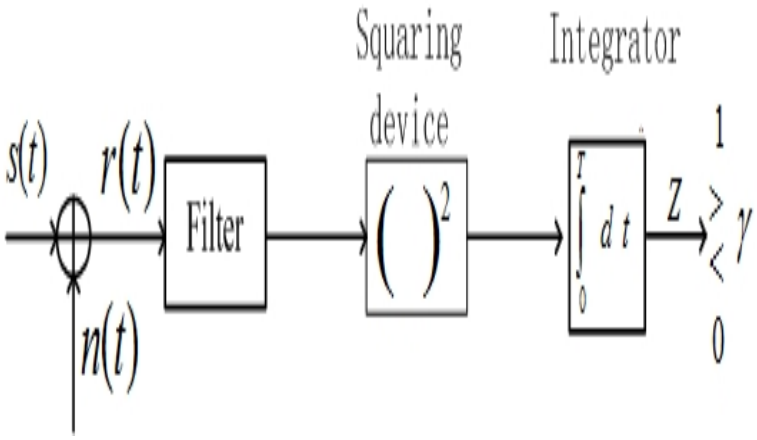

Figure 6: The structure of energy detection receiver(from [8])

1.6.3 Transmitted Reference

Fig. 7 is the frame structures of a transmitted reference system. In every frame period T_f, two pulses are transmitted with a interval D. The first pulse is the reference pulse and it is known by the receiver. The second pulse is the data pulse and its polarity is positive and negative for data bits 1 and 0, respectively. At the receiver, the reference pulse and the data pulse are aligned and correlated to finish demodulation. Because the reference and the data pulses experience the same channel, so the data pulse is demodulated with the knowledge of correct channel impulse response. The equation of the transmitted signal is [9]

$$s(t) = \sum_j \sqrt{E_p} p(t - jT_f) + L_j \sqrt{E_p} p(t - jT_f - D) \tag{1.2}$$

where E_p denotes signal energy, $p(t)$ denotes the transmitted waveform, T_f denotes frame period and D denotes the delay between the reference and data pulses and $L_j \in \{-1, 1\}$ is used to change the pole of the pulses. Transmitted reference system is also a popular method in UWB systems, and its application can be found in many papers [10–19].

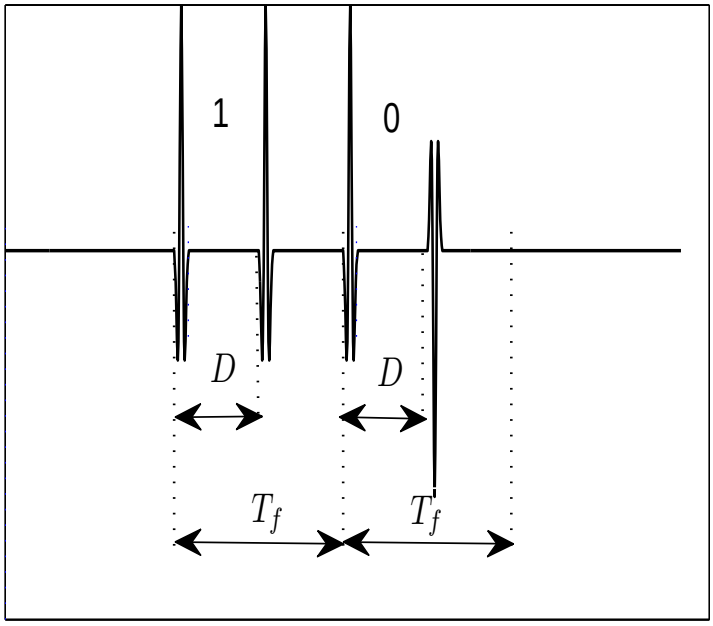

Figure 7: Frame structures of a transmitted reference system(from [9])

1.6.4 Differential Detection

The transmitters of differential detection (DF) differentially encode the data bits and use these encoded bits to modulate the pulses as follows [9, 20, 21]:

$$s(t) = \sum_j L_j \sqrt{E_p} p(t - jT_f) \tag{1.3}$$

where E_p denotes the signal energy, T_f is frame period and $L_j \in \{-1, 1\}$ is the encoded data.

At the receiver, the received signal is passed through a bandpass filter, delayed a symbol period and then correlated with itself.

1.6.5 Comparisons of Different Receivers

In UWB systems, the data are carried by sub-nanosecond pulses and each of these short pulses will generate a large number of multipath components with fine

time resolution in multipath channels. These multipath components can be resolved and combined in a rake receiver with multiple fingers [22]. However, the raker receiver needs a large number of fingers to capture enough signal energy to demodulate the received signals, so this leads to a very complex receiver and great computational burden of channel estimation [9, 22]. In a rake receiver, each finger includes a correlator and these correlators need extremely accurate synchronization to align the received signals with the template signals to perform correlation. The acceptable synchronization error is much smaller than one pulse duration, and a small synchronization error can severely degrade the system performance [9].

Non-coherent technologies have been developed to avoid the challenges in rake receivers. Non-coherent methods include transmitted reference (TR), DF and ED. A TR system transmits an un-modulated reference pulse prior to each data pulse and this reference pulse is used to demodulate data pulse at the receiver. The reference and data pulses pass through the same channel, so the same channel impulse response acts on these two pulses and the data pulses will be demodulated with the perfect channel knowledge [10]. The drawback of a TR system is that it results in a signal-to-noise ratio (SNR) loss of 6 dB compared to perfect matched filter: noise corrupted reference pulses can induce 3 dB loss and two pulses in one bit can bring another 3 dB loss [17]. A DF system delays the first one of two consecutive pulses and uses the first one as the template pulse to demodulate the second one. A DF system does not need channel estimation, so the complexity of receiver can be reduced. However, the delay between two pulses requires to be aligned accurately, and this is not easy to achieve. The performance of DF only arrives to that of single-finger rake receiver at low SNR and even at high SNR it just slightly surpasses the single-finger rake receiver. And a DF system is also very sensitive to inter-symbol and narrowband interference [20].

ED has been a conventional receiver scheme in the communication field for

many years. In recent year, ED is applied to UWB systems for OOK [8, 23–25] and PPM systems [8, 24, 194]. Although ED is a sub-optimal technology, it has many advantages. Its receiver structure is very simple and channel estimation is not required. Also ED does not need as accurate synchronization as a rake receiver because ED does not use correlators. Now, ED is attracting more and more researchers in the field of UWB.

1.7 Dissertation Motivation

As aforementioned, ED UWB systems show many advantages and are more and more popular, so we focus our research in the field of ED UWB systems. ED UWB technology has been applied to PPM and OOK systems. In OOK systems, the transmitter does not transmit a pulse when the data bit is 0, so it has difficult to achieve synchronization, especially when a zeros stream is transmitted [1]. And PPM systems suffer from cross-modulation interference and the system performance is severely degraded in the presence of cross-modulation interference. Also, synchronization errors can lead to performance degradation if symbol timing is not accurate. These drawbacks in the existing methods motivate us to develop new ED UWB systems to circumvent the challenges in UWB systems. Although popular modulation methods in UWB are PPM and PAM, PWM has been proved to be a suitable scheme for UWB systems [6]. The receiver structure in [6] is a rake receiver, so we develop the ED receiver for PWM in this dissertation. Also other ED UWB systems based on new modulation methods will be developed. We also will find some solutions to resolve the issues in the existing methods.

1.8 Dissertation Contributions

The contribution of this dissertation is composed of several aspects. Firstly, a new ED UWB systems based on PWM is proposed. The performance of this ED PWM system is analyzed and compared with an ED PPM system in AWGN and multipath channels, and in the presence of synchronization errors. The research results show that this ED PWM system exhibits better BER performance than an ED PPM system in multipath channels and when synchronization errors occur. Secondly, another new ED UWB system based on different-order derivatives of the Gaussian pulse is proposed. This system is called an ED GFSK UWB system in this dissertation. Also The performances of this ED GFSK UWB system is compared to an ED PPM system in AWGN channels, multipath channels, and in the presence of synchronization errors. The research results show that this GFSK system achieves better BER performance than a PPM system in multipath channels and in the presence of synchronization errors. Thirdly, we compare the performance of our new two systems PWM and GFSK. The research results show that GFSK has better performance but PWM need simpler pulse generators. Fourthly, we analyze these two new systems under the constraint of FCC emission mask and find suitable approach and parameters to match the requirement of the FCC mask. Fifthly, an optimal threshold is applied to PPM systems to mitigate the effect of cross-modulation interference and synchronization errors, the research results show that the system BER performance is improved after an optimal threshold is applied. Finally, we analyze and compare miscellaneous multiple access schemes and find the appropriate multiple access scheme for our two new systems.

1.9 Dissertation Outline

The structure of this dissertation is as follows. In Chapter 1, the introduction of UWB systems is given: the definition, history, advantages, applications, challenges and existing technologies are described. In Chapter 2, a new ED PWM UWB system is proposed, and the BER performance of this system is compared to that of a PPM system in AWGN and multipath channels. Also the BER performances are compared in the presence of synchronization errors. In Chapter 3, a new ED UWB system called GFSK which is based on using different-order derivatives of the Gaussian pulse is proposed. And the BER performance of this system is compared to that of a PPM system in AWGN and multipath channels. The BER performances are compared when the synchronization errors occur. In Chapter 4, the performance of PWM and GFSK systems are compared. In Chapter 5, an optimal threshold is applied to PPM systems to improve performance. In Chapter 6, PWM and GFSK systems are analyzed under the constraint of the FCC emission mask. In Chapter 7, the multiple access schemes are discussed. In Chapter 8, the conclusion of this dissertation is stated and the future work is presented.

CHAPTER II

AN ENERGY DETECTION UWB SYSTEM BASED ON PULSE WIDTH MODULATION

A new energy detection UWB system based on pulse width modulation is proposed in this chapter. And the bit error rate (BER) performance of this system is analyzed in AWGN channels, multipath channels, and in the presence of synchronization errors. Although BER performance of this new system is slightly worse than PPM in additive white Gaussian noise channels, it exhibits better BER performance than PPM in multipath channels. And this system is more robust to synchronization errors than a PPM system. When synchronization errors occur, the BER performance of this system surpasses that of PPM.

The structure of this chaper is as follows: Section 2.1 introduces the system models, Section 2.2 analyzes the BER performance of systems in AWGN channels, Section 2.3 analyzes the BER performance of systems in multipath channels, Section 2.4 analyzes the BER performance of systems in the presence of synchronization

errors. Section 2.6 summarizes this chapter.

2.1 System Models

2.1.1 System Model of PWM

In a PWM system, the modulation is achieved by transmitting the pulses with different width to denote bit 0 or 1. The model of the transmitter in [6] is used here, and the transmitted signal of the mth user is

$$s_{PWM}^{(m)} = \sum_{j} \sqrt{E_p} p_{b_{\lfloor j/N_s \rfloor}^{(m)}} (t - j\,T_f - c_j^{(m)}\,T_c) \tag{2.1}$$

where $p_{b_{\lfloor j/N_s \rfloor}^{(m)}}(t)$ means the jth transmitted pulse of the mth user. The value of $b_{\lfloor j/N_s \rfloor}^{(m)}$ is $\{0,1\}$, and it denotes transmitted bit is 0 or 1. The index $\lfloor j/N_s \rfloor$, the integer part of j/N_s, represents the index of the data bit modulating the waveform in the jth frame. Usually a bit is repeated N_s times and transmitted over N_s frame to improve performance, so the waveform having same $\lfloor j/N_s \rfloor$ value will be modulated by the same bit. When bit 0 or 1 is transmitted, the transmitted pulse waveform is $p_0(t)$ or $p_1(t)$, respectively, where $p_0(t)$ and $p_1(t)$ are amplitude-normalized pulse waveforms with different widths. The symbol period to transmit a bit is $T_s = N_s T_f$, where T_f is the frame period. To realize multi-user communications, a frame is separated into several chip intervals and the period of a chip interval is T_c. The user chooses the chip interval by time hoping (TH) code $c_j^{(m)}$, which is generated from specific pseudo-random code, and the value of $c_j^{(m)}$ can be any numbers in the set of $0 \le c_j^{(m)} \le N_h - 1$, where N_h denotes the number of chip intervals in a frame. The energy of pulses is changed by E_p, and the energies of pulses to transmit bit 0 and 1 are different because $p_0(t)$ and $p_1(t)$ have different widths.

Without loss of generality, we only research single-user communication in this

dissertation, and a bit is transmitted only once. So equation (2.1) is simplified to

$$s_{PWM}(t) = \sum_j \sqrt{E_p} p_{b_j}(t - jT_f) \tag{2.2}$$

where T_f denotes the frame period, and $p_{b_j}(t)$ denotes the pulse waveform for jth transmitted data bit b_j. The data bit has binary value of either 0 or 1. When bit 0 or 1 are transmitted, the transmitted pulse waveform is $p_0(t)$ or $p_1(t)$, respectively, where $p_0(t)$ and $p_1(t)$ are amplitude-normalized pulse waveforms with different widths. The signal energy is adjusted by E_p, and the energy of $p_0(t)$ and $p_1(t)$ are different. Therefore, we define the energies of pulses for bits 0 and 1, E_0 and E_1, by $E_i = E_p \int_{-T_{p_i}/2}^{T_{p_i}/2} [p_i(t)]^2 dt, (i = 0, 1)$, where T_{p_i} is the pulse width. The ratio E_0/E_1 depends on which pulse waveforms are chosen [6]. In this dissertation, we will use the second-order derivative of the Gaussian pulse [7]

$$p(t) = (1 - 4\pi t^2/\alpha_i^2) \exp(-2\pi t^2/\alpha_i^2) \tag{2.3}$$

where α_i is the shape factor. The pulse width T_{p_i} is set to $2.4\alpha_i$, and the detailed method to chose the pulse width for a specific α_i value can be found in [7]. Fig. 8 shows the waveform of the 2nd-order derivative of the Gaussian pulse with $\alpha_i = 0.5 \times 10^{-9}$ and normalized energy. After the second-order derivative of the Gaussian pulse is chosen, the modulation is achieved by using different α_i values for bits 0 and 1. Increasing α_i will increase T_{p_i} and thus decrease the bandwidth. We set $\alpha_1 = 2\alpha_0$ to achieve modulation, where α_1 and α_0 are the shape factors for $p_1(t)$ and $p_0(t)$, respectively. So we have $T_{p_1} = 2T_{p_0}$, where T_{p_1} and T_{p_0} denote the width of $p_1(t)$ and $p_0(t)$, respectively. Based on these assignments, the relationship between E_0 and E_1 is

$$E_0 = 0.5E_1 \tag{2.4}$$

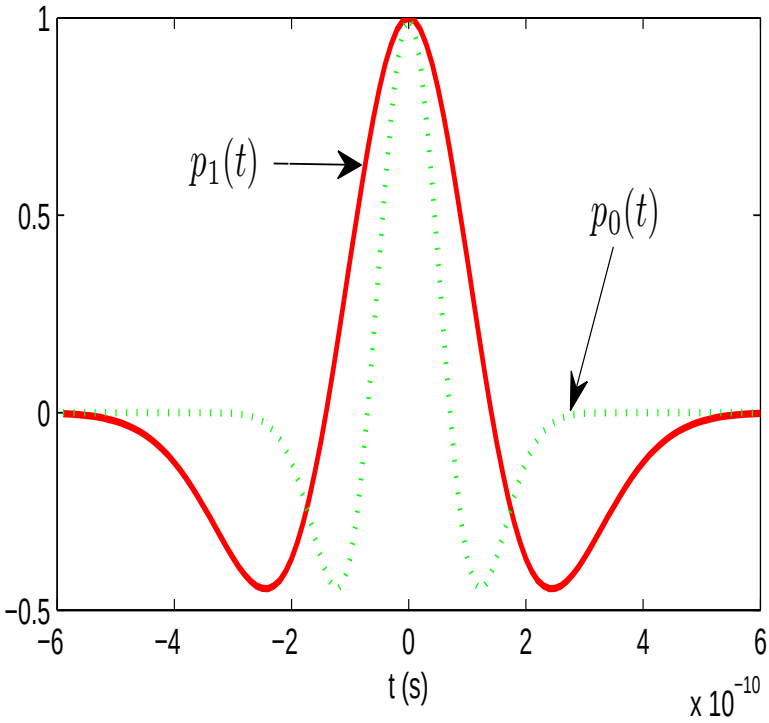

Figure 8: The waveform of the 2nd-order derivative of the Gaussian pulse with different shaping factors: $\alpha_1 = 2\alpha_0$

The proof is given as follows:

$$E_0 = E_p \int_{-1.2\alpha_0}^{1.2\alpha_0} [p_0(t)]^2 dt = E_p \int_{-1.2\alpha_0}^{1.2\alpha_0} \left(1 - 4\pi t^2/\alpha_0^2\right)^2 e^{-4\pi t^2/\alpha_0^2} dt \tag{2.5}$$

$$E_1 = E_p \int_{-1.2\alpha_1}^{1.2\alpha_1} [p_1(t)]^2 dt = E_p \int_{-1.2\alpha_1}^{1.2\alpha_1} \left(1 - 4\pi t^2/\alpha_1^2\right)^2 e^{-4\pi t^2/\alpha_1^2} dt \tag{2.6}$$

Let $\tau = t/2$, we have $dt = 2d\tau$ and $t = 2\tau$. When $t = -1.2\alpha_1$, $\tau = (-1.2\alpha_1)/2 = -1.2\alpha_0$. Similarly, when $t = 1.2\alpha_1$, $\tau = 1.2\alpha_0$. Substituting these values into equation (2.6), E_1 becomes

$$\begin{aligned} E_1 &= E_p \int_{-1.2\alpha_0}^{1.2\alpha_0} \left(1 - \tfrac{4\pi(2\tau)^2}{(2\alpha_0)^2}\right)^2 e^{-\frac{4\pi(2\tau)^2}{(2\alpha_0)^2}} 2d\tau \\ &= 2E_p \int_{-1.2\alpha_0}^{1.2\alpha_0} \left(1 - \tfrac{4\pi\tau^2}{\alpha_0{}^2}\right)^2 e^{-\frac{4\pi\tau^2}{\alpha_0{}^2}} d\tau = 2E_0 \end{aligned} \tag{2.7}$$

The design idea of the receiver originates from the spectral characteristics of the Gaussian pulse. The Fourier transform X_f and center frequency f_c of the kth-order

derivative of the Gaussian pulse are [7]

$$X_f \propto f^k \exp(-\pi f^2 \alpha_i^2/2) \tag{2.8}$$

$$f_c = \sqrt{k}/(\alpha_i \sqrt{\pi}) \tag{2.9}$$

where f is the frequency. Using equation (2.8), the spectra of $p_0(t)$ and $p_1(t)$ are

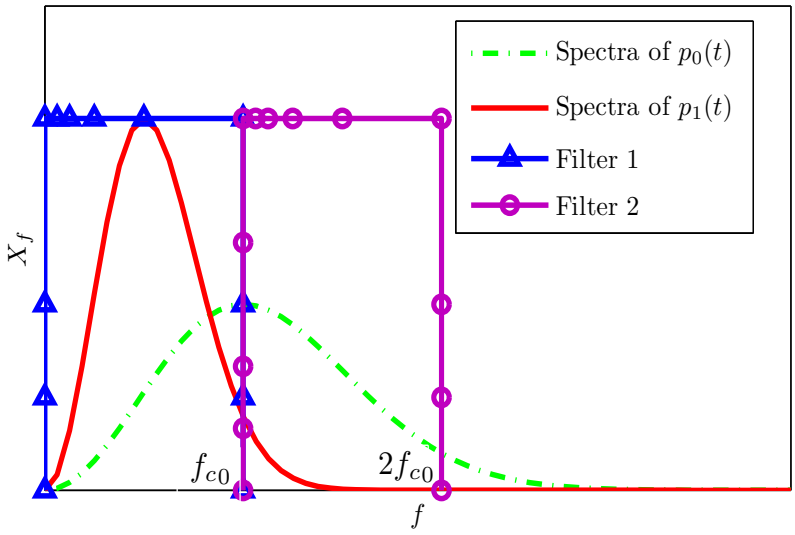

Figure 9: Spectral curves

plotted in Fig. 9. The bandwidth of $p_0(t)$ is almost twice that of $p_1(t)$. The center frequency of $p_0(t)$ is f_{c0}. Two ideal filters, Filter 1 and 2, are also shown in Fig. 9. The passband of Filter 1 is $[0, f_{c0}]$ and that of Filter 2 is $[f_{c0}, 2f_{c0}]$. When $p_0(t)$ is transmitted, both Filter 1 and 2 pass about half of its energy. If we subtract the energies of filtered signals, the resultant energy is approximately 0. When $p_1(t)$ is transmitted, Filter 1 passes almost all of the energy of $p_1(t)$ but Filter 2 rejects the energy of $p_1(t)$. Therefore, if we subtract the energies of filtered signals, the resultant energy is approximately E_1. We can decide the transmitted bit is 0 or 1 by measuring the energy difference of the filtered signals. This leads us to design the receiver as in Fig. 10. To make sure that our design idea of the receiver is based on strict theoretical

support rather than direct observable results, we use MAPLE to perform numerical calculation as follows:

The energy distributions of $p_0(t)$ and $p_1(t)$ in the passbands of Filter 1 and 2 are derived as follows:

$$E_{01} = \int_0^{\sqrt{2}/(\alpha_0\sqrt{\pi})} [X_f]^2 df = \int_0^{\sqrt{2}/(\alpha_0\sqrt{\pi})} \left(f^2 e^{-\pi f^2 \alpha_0^2/2}\right)^2 df \tag{2.10}$$

$$E_{02} = \int_{\sqrt{2}/(\alpha_0\sqrt{\pi})}^{2\sqrt{2}/(\alpha_0\sqrt{\pi})} [X_f]^2 df = \int_{\sqrt{2}/(\alpha_0\sqrt{\pi})}^{2\sqrt{2}/(\alpha_0\sqrt{\pi})} \left(f^2 e^{-\pi f^2 \alpha_0^2/2}\right)^2 df \tag{2.11}$$

$$E_{11} = \int_0^{\sqrt{2}/(\alpha_0\sqrt{2})} [X_f]^2 df = \int_0^{\sqrt{2}/(\alpha_0\sqrt{\pi})} \left(f^2 e^{-\pi f^2 \alpha_1^2/2}\right)^2 df \tag{2.12}$$

$$E_{12} = \int_{\sqrt{2}/(\alpha_0\sqrt{\pi})}^{2\sqrt{2}/(\alpha_0\sqrt{\pi})} [X_f]^2 df = \int_{\sqrt{2}/(\alpha_0\sqrt{\pi})}^{2\sqrt{2}/(\alpha_0\sqrt{\pi})} \left(f^2 e^{-\pi f^2 \alpha_1^2/2}\right)^2 df \tag{2.13}$$

where E_{01}, $E_{0,2}$, E_{11} and E_{12} denote the signal energy distributing in the passbands of the filters. The first subscript denotes the transmitted bit is 0 or 1 and the second subscript means Filter 1 or 2. After substitute the values of α_0 and $\alpha_1 = 2\alpha_0$ into these four equations and use MAPLE to obtain

$$E_{01} - E_{02} \approx 0.451E_0 - 0.543E_0 = -0.09E_0 = -0.06E_b \approx 0 \tag{2.14}$$

$$E_{01} + E_{02} \approx 0.451E_0 + 0.543E_0 = 0.994E_0 \approx E_0 \tag{2.15}$$

where E_b denotes the average bit energy. Because E_1=$2E_0$ and $E_b = 0.5(E_1 + E_0)$, it is straightforward to obtain $E_0 = 2/3E_b$ and $E_1 = 4/3E_b$. UWB signals are transmitted in a very low power, so $0.06E_b$ is very small. Also, when we evaluate the BER performance of a system in terms of E_b/N_0, this $0.06E_b/N_0$ is very small when compared to E_b/N_0. So it is reasonable to round off $0.06E_b/N_0$ to 0.

$$E_{11} - E_{12} \approx 0.993E_1 - 0.0068E_1 = 0.986E_1 \approx E_1 \tag{2.16}$$

$$E_{11} + E_{12} \approx 0.993E_1 + 0.0068E_1 = 0.9998E_1 \approx E_1 \tag{2.17}$$

The results of equations (2.14), (2.15), (2.16) and (2.17) are verified by different α_0 and $\alpha_1 = 2\alpha_0$ values, and they all generate the same results. The results of equations (2.14) and (2.16) provide strong theory support for our design ideal. The

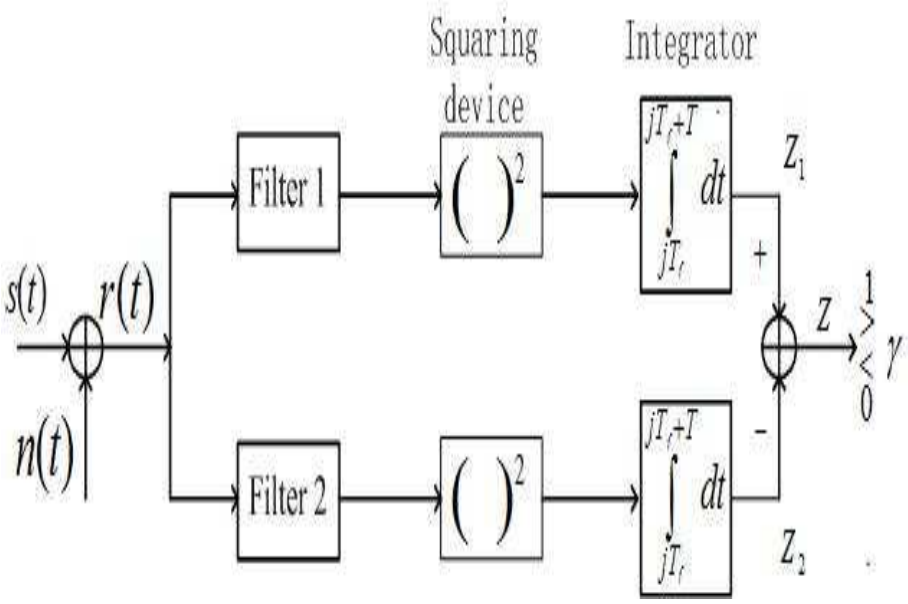

Figure 10: PWM Receiver

receiver is separated into two branches, and each branch is a conventional energy detection receiver. The only difference between the two branches is the passbands of the filters. The passbands of Filter 1 and 2 are like that in Fig. 9. The signal arriving at the receiver is denoted by $s(t)$, the AWGN is denoted by $n(t)$, and the sum of $s(t)$ and $n(t)$ is denoted by $r(t)$. The integration interval $T \leq T_f$. The decision statistic is given by $Z = Z_1 - Z_2$, where Z_1 and Z_2 are the outputs of branch 1 and 2, respectively. Finally, Z is compared with threshold γ to determine the transmitted bit. If $Z \geq \gamma$, the transmitted bit is 1, otherwise it is 0.

In this dissertation, the performance of this new system is compared with the existing systems, the models of those systems are simply stated as follows: the OOK system does not transmit a signal when data is 0. It has difficulty to achieve

synchronization, especially when a stream of zeros is transmitted [1], so it is not compared in this dissertation. We only compare PPM with our new system. In Section 2.1.2, the system model of PPM is depicted.

2.1.2 System Model of PPM

The transmitted signal of a PPM system is [3]

$$s(t)_{PPM} = \sum_{j} \sqrt{E_p} p(t - jT_f - \delta b_j) \tag{2.18}$$

where δ is called the modulation index, and the pulse shift amount is determined by δb_j. The frame period is denoted by T_f, $p(t)$ is the pulse waveform and E_p denotes signal energy. At the receiver, after the received signal pass through a square-law device and an integrator, the decision statistic Z is obtained as [27]

$$Z = Z_1 - Z_2 = \int_{jT_f}^{jT_f+T} r^2(t)dt - \int_{jT_f+\delta}^{jT_f+\delta+T} r^2(t)dt \tag{2.19}$$

where $T \leq \delta$ denotes the length of integration interval. The decision threshold of PPM is $\gamma = 0$. If $Z \geq \gamma = 0$, the transmitted bit is 0, otherwise it is 1.

2.2 BER Performance in AWGN Channels

2.2.1 PWM in AWGN channels

In Fig. 10, Z_1 and Z_2 are the outputs of conventional energy detectors, and they are defined as chi-square variables with approximately a degree of $2TW$ [28], where T is the integration time and W is the bandwidth of the filtered signal. A popular method for energy detection, called Gaussian approximation, has been developed to simplify the derivation of the BER formula. When $2TW$ is large enough, a chi-square variable can be approximated as a Gaussian variable. This method is commonly

used in energy detection communication systems [8, 27, 29, 30]. The mean value and variance of this approximated Gaussian variable are [31]

$$\mu = N_0TW + E \tag{2.20}$$

$$\sigma^2 = N_0^2TW + 2N_0E \tag{2.21}$$

where μ and σ^2 are the mean value and variance, respectively. The double-sided power spectral density of AWGN is $N_0/2$. The signal energy which passes through the filter is denoted by E. If the filter rejects all of the signal energy, then $E = 0$. In Fig. 10, when bit 1 is transmitted, the signal energy almost passes through Filter 1 entirely. The probability density function (pdf) of Z_1 and Z_2 can be expressed as $Z_1 \sim N(N_0TW+E_{11}, N_0^2TW+2N_0E_{11})$ and $Z_2 \sim N(N_0TW+E_{12}, N_0^2TW+2N_0E_{12})$. Since $Z = Z_1 - Z_2$, the pdf of Z is $Z \sim N(E_{11} - E_{12}, 2N_0^2TW + 2N_0(E_{11} + E_{12}))$. Using equations (2.16) and (2.17), the pdf of Z becomes

$$H_1 : Z \sim N(E_1, 2N_0^2TW + 2N_0E_1) \tag{2.22}$$

When bit 0 is transmitted, the signal energy almost distributes equally in the frequency ranges of Filter 1 and 2. The pdfs of Z_1 and Z_2 are $Z_1 \sim N(N_0TW + E_{01}, N_0^2TW + 2N_0E_{01})$ and $Z_2 \sim N(N_0TW + E_{02}, N_0^2TW + 2N_0E_{02})$. And then we have $Z \sim N(E_{01}-E_{02}, 2N_0^2TW+2N_0(E_{01}+E_{02}))$. Using equations (2.14) and (2.15), the pdf of Z is

$$H_0 : Z \sim N(0, 2N_0^2TW + 2N_0E_0) \tag{2.23}$$

Because E_0 and E_1 have different values, we will denote them using average bit energy E_b. Assume bits 0 and 1 are randomly transmitted at the same probability, we obtain $E_b = (1/2)(E_0 + E_1)$ [8, 24]. From equation (2.4), we have $E_0 = 0.5E_1$, so E_0 and E_1 can be expressed as

$$E_0 = \frac{2}{3}E_b \tag{2.24}$$

$$E_1 = \frac{4}{3}E_b \tag{2.25}$$

Substituting equations (2.25) and (2.24) into (2.22) and (2.23), respectively, we obtain

$$H_0 : Z \sim N(0, 2N_0^2TW + \frac{4}{3}N_0E_b) \tag{2.26}$$

$$H_1 : Z \sim N(\frac{4}{3}E_b, 2N_0^2TW + \frac{8}{3}N_0E_b) \tag{2.27}$$

We follow the method in [29] to derive BER using equation (2.27) and (2.26). Firstly, we calculate the BER when bits 0 and 1 are transmitted as follows:

$$P_0 = \int_{\gamma}^{\infty} f_0(x)dx = \int_{\gamma}^{\infty} \frac{1}{\sqrt{2\pi}\sigma_0} e^{-\frac{(x-\mu_0)^2}{2\sigma_0^2}} dx \tag{2.28}$$

$$P_1 = \int_{-\infty}^{\gamma} f_1(x)dx = \int_{-\infty}^{\gamma} \frac{1}{\sqrt{2\pi}\sigma_1} e^{-\frac{(x-\mu_1)^2}{2\sigma_1^2}} dx \tag{2.29}$$

where $f_0(x)$ and $f_1(x)$ denote the probability density functions, and γ denotes the decision threshold. From equation (2.27) and (2.26), it is straightforward to obtain $\mu_0 = 0$, $\sigma_0^2 = 2N_0^2TW + \frac{4}{3}N_0E_b)$, $\mu_1 = \frac{4}{3}E_b$, $\sigma_1^2 = 2N_0^2TW + \frac{8}{3}N_0E_b$. Substituting these parameter values into equations (2.28) and (2.29), and then expressing P_0 and P_1 in terms of the complementary error function $Q(\cdot)$, we obtain

$$P_0 = Q(\gamma/\sqrt{2N_0^2TW + \frac{4}{3}N_0E_b}) \tag{2.30}$$

$$P_1 = Q((\frac{4}{3}E_b - \gamma)/\sqrt{2N_0^2TW + \frac{8}{3}N_0E_b}) \tag{2.31}$$

The optimal threshold is obtained by setting $P_0 = P_1$ [8, 29]

$$\frac{\gamma}{\sqrt{2N_0^2TW + \frac{4}{3}N_0E_b}} = \frac{(\frac{4}{3}E_b - \gamma)}{\sqrt{2N_0^2TW + \frac{8}{3}N_0E_b}} \tag{2.32}$$

Solving equation (2.32), the optimal threshold is obtained as

$$\gamma = \frac{(\frac{4}{3}E_b)\sqrt{2N_0^2TW + \frac{4}{3}N_0E_b}}{\sqrt{2N_0^2TW + \frac{8}{3}N_0E_b} + \sqrt{2N_0^2TW + \frac{4}{3}N_0E_b}} \tag{2.33}$$

The total BER is $P_e = 0.5(P_0 + P_1)$. Since $P_0 = P_1$, it follows that $P_e = P_0$. Substituting equation (2.33) into (2.30), the total BER of PWM in AWGN channels is

$$P_e = Q\left(\frac{\frac{4}{3}\frac{E_b}{N_0}}{\sqrt{2TW + \frac{8}{3}\frac{E_b}{N_0}} + \sqrt{2TW + \frac{4}{3}\frac{E_b}{N_0}}}\right) \tag{2.34}$$

2.2.2 PPM in AWGN Channels

The BER equation of ED PPM has been derived in [8], and its expression is as followed:

$$P_e = Q\left(\frac{E_b/N_0}{\sqrt{2TW + 2E_b/N_0}}\right) \tag{2.35}$$

2.3 BER Performance in Multipath Channels

In this section, the BER performances of PPM and PWM in multipath channels are researched. The channel model of the IEEE 802.15.4a standard [32] is used in this paper. After the signal travels through a multipath channel, it is convolved with the channel impulse response. The received signal becomes

$$r(t) = s(t) \otimes h(t) + n(t) \tag{2.36}$$

where $h(t)$ denotes the channel impulse response and $n(t)$ is AWGN. The symbol $\otimes$ denotes the convolution operation. The IEEE 802.15.4a model is an extension of the Saleh-Valenzeula (S-V) model. The channel impulse response is

$$h(t) = \sum_{l=0}^{L}\sum_{k=0}^{K} \alpha_{k,l} \exp(j\phi_{k,l})\delta(t - T_l - \tau_{k,l}) \tag{2.37}$$

where $\delta(t)$ is Dirac delta function, and $\alpha_{k,l}$ is the tap weight of the kth component in the lth cluster. The delay of the lth cluster is denoted by T_l and $\tau_{k,l}$ is the delay of the kth multipath component (MPC) relative to T_l. The phase $\phi_{k,l}$ is uniformly distributed in the range $[0, 2\pi]$.

2.3.1 PPM in Multipath Channels

In PPM systems, the modulation index δ in equation (2.18) must be chosen appropriately. If it is designed to be less than the maximum channel spread D, the cross-modulation interference (CMI) will occur [27, 30, 33]. When CMI occurs, the system performance will be degraded greatly. Even increasing the transmitting power will not improve the performance because of the proportional increase of interference [33]. The effect of δ on BER performance of PPM has been analysed in [30]. But the BER equation in [30] is not expressed with respect to E_b/N_0. For convenience in the following analysis, the BER equation will be expressed in terms of E_b/N_0 here. Fig. 11 is frame structures of PPM in the presence of CMI. The relationship of δ with

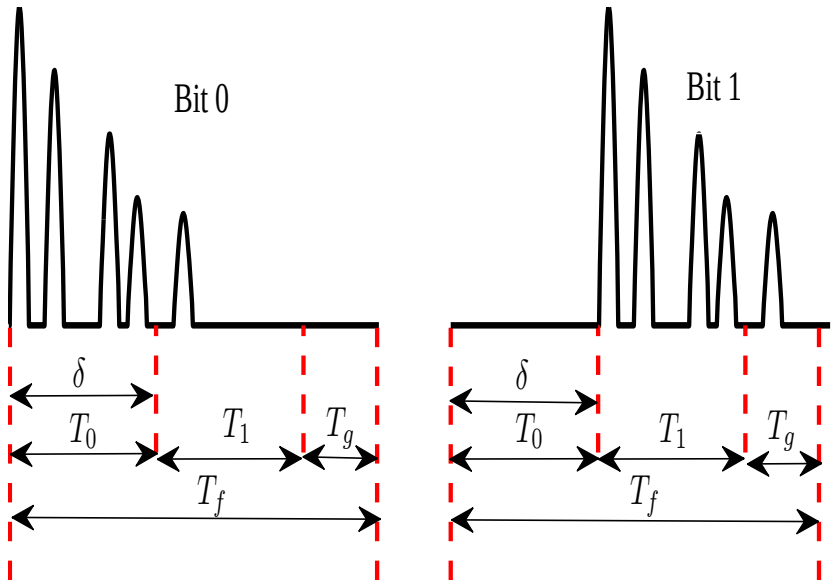

Figure 11: PPM frame structures in multipath channels

T_0 and T_1 is set to $\delta = T_0 = T_1$ as in [27], and T_0 and T_1 are the time intervals reserved for multipath components of bits 0 and 1, respectively. Synchronization is assumed to be perfect here. When δ is less than the maximum channel spread D, some multipath components of bit 0 fall into the interval T_1, and therefore CMI occurs. But the multipath components of bit 1 do not cause CMI. Some of them fall

into the guard interval T_g, which is designed to prevent inter-frame interference (IFI). The frame period is $T_f = T_0 + T_1 + T_g$. If T_g is chosen to be too large, it will waste transmission time. So we follow the method in [27] and set $T_f = \delta + D$. This will always achieve as high a data rate as possible without inducing IFI .

When bit 0 is transmitted, the pdfs of Z_1 and Z_2 are $Z_1 \sim N(N_0TW + \beta_a E_b, N_0^2TW + 2N_0\beta_a E_b)$, $Z_2 \sim N(N_0TW + \beta_b E_b, N_0^2TW + 2N_0\beta_b E_b)$. Since $Z = Z_1 - Z_2$, we have

$$H_{0:}\ \ Z \sim N((\beta_a - \beta_b)E_b, 2N_0^2TW + 2N_0(\beta_a + \beta_b)E_b) \tag{2.38}$$

where $\beta_a = E_{T_0}/E_b$ and $\beta_b = E_{T_1}/E_b$. The meanings of E_{T_0} and E_{T_1} are the captured signal energies in integration interval T_0 and T_1, respectively. The values of β_a and β_b are in the range $[0, 1]$. When bit 1 is transmitted, $E_{T_0} = 0$, the pdfs become $Z_1 \sim N(N_0TW, N_0^2TW)$ and $Z_2 \sim N(N_0TW + \beta_a E_b, N_0^2TW + 2N_0\beta_a E_b)$. The pdf of Z is

$$H_{1:}\ \ Z \sim N(-\beta_a E_b, 2N_0^2TW + 2N_0\beta_a E_b) \tag{2.39}$$

where the β_a in equation (2.39) has the same value as that in equation (2.38), but their meaning are different. In equation (2.39), $\beta_a = E_{T_1}/E_b$. Since the threshold is $\gamma = 0$, the BER formula of PPM is

$$P_e = 0.5\int_{-\infty}^{0} f_0(x)dx + 0.5\int_{0}^{\infty} f_1(x)dx \tag{2.40}$$

where $f_0(x)$ and $f_1(x)$ are the pdfs corresponding to equations (2.38) and (2.39). Therefore, the BER is

$$P_e = \frac{1}{2}Q\left(\frac{(\beta_a - \beta_b)(E_b/N_0)}{\sqrt{2TW + 2(\beta_a + \beta_b)(E_b/N_0)}}\right) + \frac{1}{2}Q\left(\frac{\beta_a(E_b/N_0)}{\sqrt{2TW + 2\beta_a(E_b/N_0)}}\right) \tag{2.41}$$

When there is no CMI, $\beta_a = 1$ and $\beta_b = 0$, equation (2.41) reduces to equation (2.35).

2.3.2 PWM in Multipath Channels

Fig. 12 is the frame structure of PWM in multipath channels. CMI does not occur as it does in PPM systems. In order to compare PWM to PPM under the same energy capture condition, the integration interval T_0 of PWM has the same length as the T_0 of PPM. Also synchronization is assumed to be perfect as in PPM. The guard interval is T_g, and the frame period is set to $T_f = T_0 + T_g = D$. This will achieve the maximum data rate and prevent IFI simultaneously. This frame structure is applied to both bits 0 and 1. We assume λ denotes the ratio of the captured signal energy to the total signal energy of each branch. When bit 0 is transmitted, the signal energy distributes equally to two branches, that is $E_{0,1} = E_{0,2} = E_b/3$. So the captured signal energy E_{T_0} in two branches are all $\lambda E_b/3$, and the resultant pdf of Z is

$$H_0 : Z \sim N(0, 2N_0^2TW + N_0\lambda\frac{4}{3}E_b) \tag{2.42}$$

When bit 1 is transmitted, the signal energy almost distributes to Branch 1 and the signal energy of Branch 2 is approximately 0. so we have $E_{1,1} = 4\lambda E_b/3$ and $E_{1,2} = 0$. The pdf of Z is

$$H_1 : Z \sim N(\lambda\frac{4}{3}E_b, 2N_0^2TW + N_0\lambda\frac{8}{3}E_b) \tag{2.43}$$

Using equations (2.28) and (2.29), and following the method in Section 2.2.1, we obtain the threshold γ and BER

$$\gamma = \frac{(\frac{4}{3}\lambda E_b)\sqrt{2N_0^2TW + \frac{4}{3}N_0\lambda E_b}}{\sqrt{2N_0^2TW + \frac{8}{3}N_0\lambda E_b} + \sqrt{2N_0^2TW + \frac{4}{3}N_0\lambda E_b}} \tag{2.44}$$

$$P_e = Q(\frac{\frac{4}{3}\lambda\frac{E_b}{N_0}}{\sqrt{2TW + \frac{8}{3}\lambda\frac{E_b}{N_0}} + \sqrt{2TW + \frac{4}{3}\lambda\frac{E_b}{N_0}}}) \tag{2.45}$$

The decision threshold γ is adaptive.

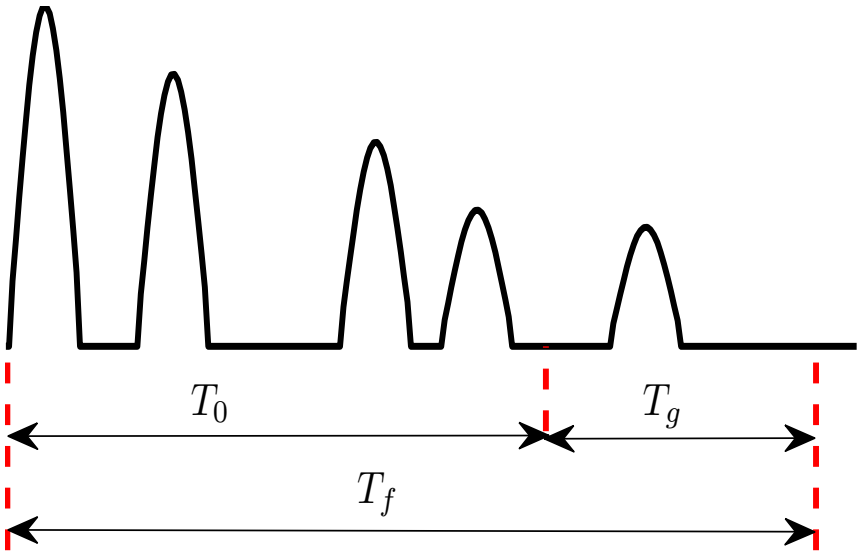

Figure 12: PWM frame structures in multipath channels

2.4 Performance Analysis in The Presence of Synchronization Errors

2.4.1 PPM Performance in The Presence of Synchronization Errors

Fig. 13 depicts PPM frame structures when synchronization errors ε occur. The modulation index is set to $\delta = D = T_0 = T_1$, so no CMI occurs. Assuming that coarse synchronization has been achieved, the BER performance of PPM and GFSK are compared in the range $\varepsilon \in [0, D/2]$. To prevent IFI, the frame length is set to $T_f = 2D + T_g$, where the guard interval T_g equals to $D/2$, the maximum synchronization error used in this paper. When bit 0 is transmitted, we have $Z_1 \sim N(N_0TW + \eta E_b, N_0^2TW + 2\eta E_b N_0)$ and $Z_2 \sim N(N_0TW, N_0^2TW)$. The pdf of Z is

$$H_0: \quad Z \sim N(\eta E_b, 2N_0^2TW + 2\eta E_b N_0) \tag{2.46}$$

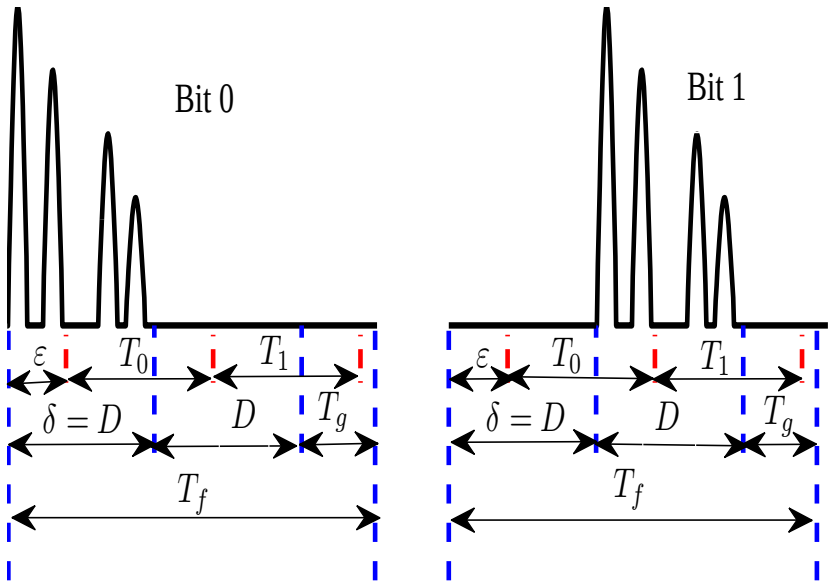

Figure 13: PPM frame structures in the presence of synchronization errors

where $\eta = E_{T_0}/E_b$, and $E_{T_1} = 0$. When bit 1 is transmitted, we have $Z_1 \sim N(N_0TW + (1-\eta)E_b, N_0^2TW + 2(1-\eta)E_bN_0)$ and $Z_2 \sim N(N_0TW + \eta E_b, N_0^2TW + 2\eta E_bN_0)$. And then we obtain

$$H_1: \quad Z \sim N((1-2\eta)E_b, 2N_0^2TW + 2E_bN_0) \tag{2.47}$$

where η in equation (2.47) has the same value as that in equation (2.46), but in equation (2.47), $\eta = E_{T_1}/E_b$, and $E_{T_0} = (1-\eta)E_b$. Using equation (2.40), the total BER is

$$P_e = \frac{1}{2}Q\left(\frac{\eta E_b/N_0}{\sqrt{2TW + 2\eta E_b/N_0}}\right) + \frac{1}{2}Q\left(\frac{(2\eta-1)E_b/N_0}{\sqrt{2TW + 2E_b/N_0}}\right) \tag{2.48}$$

2.4.2 PWM Performance in The Presence of Synchronization Errors

Fig. 14 depicts the PWM frame structure in the presence of synchronization errors. The integration interval $T_0 = D$ is the same as that of PPM. The frame length

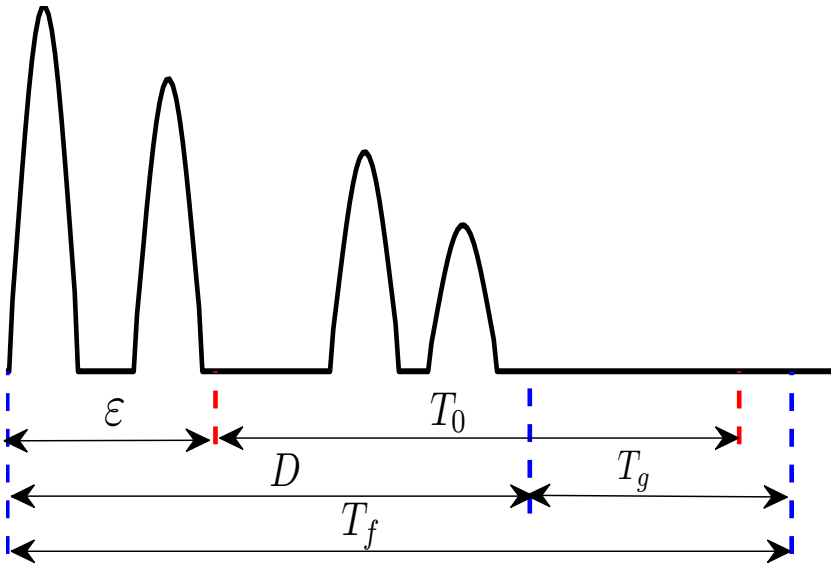

Figure 14: A PWM frame structure in the presence of synchronization errors

is $T_f = T_g + D$, where $T_g = D/2$ as in Section 2.4.1. From Fig. 14, the pdfs of Z are

$$H_0 : Z \sim N(0, 2N_0^2TW + \frac{4}{3}N_0\rho E_b) \tag{2.49}$$

$$H_1 : Z \sim N(\frac{4}{3}\rho E_b, 2N_0^2TW + \frac{8}{3}N_0\rho E_b) \tag{2.50}$$

where ρ denotes the ratio of the captured signal energy in T_0 to the total signal energy of each branch. Using equations (2.28) and (2.29), and following the method in Section 2.2.1, the threshold γ and BER are

$$\gamma = \frac{(\frac{4}{3}\rho E_b)\sqrt{2N_0^2TW + \frac{4}{3}N_0\rho E_b}}{\sqrt{2N_0^2TW + \frac{8}{3}N_0\rho E_b} + \sqrt{2N_0^2TW + \frac{4}{3}N_0\rho E_b}} \tag{2.51}$$

$$P_e = Q(\frac{\frac{4}{3}\rho\frac{E_b}{N_0}}{\sqrt{2TW + \frac{8}{3}\rho\frac{E_b}{N_0}} + \sqrt{2TW + \frac{4}{3}\rho\frac{E_b}{N_0}}}) \tag{2.52}$$

2.5 Numerical Results and Analysis

The BER equations we derived above are based on using Gaussian approximation. Gaussian approximation only works perfectly under large $2TW$ values, so

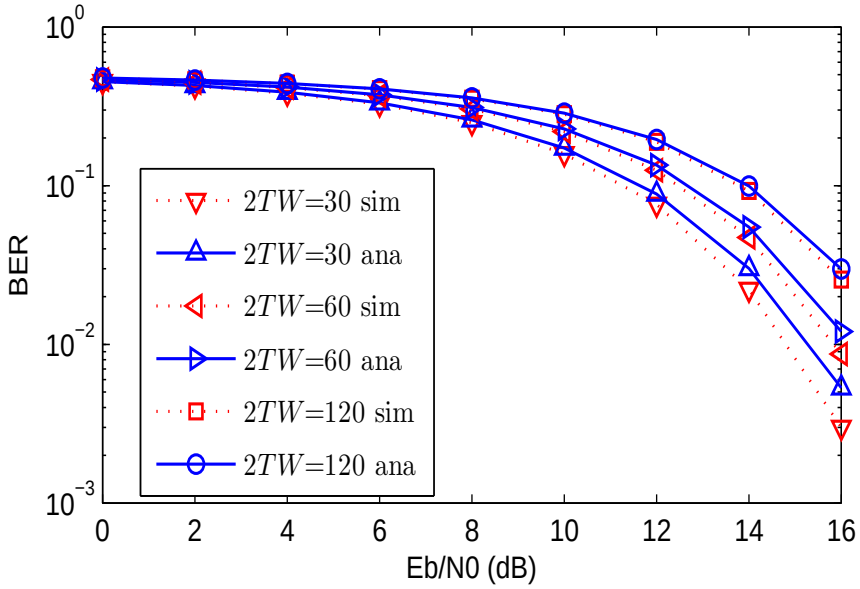

Figure 15: BER performance of PWM for different $2TW$ values in AWGN channels

we run simulations using Matlab to verify the BER equations we derived in the following. Fig. 15 shows the BER curves of PWM for different $2TW$ values. In simulation, the bandwidth of the filters is 3 GHz, the shape factors for bit 0 and 1 are 0.25×10^{-9} and 0.5×10^{-9}, and the corresponding pulse durations are 0.6 ns and 1.2 ns. Analytical BER curves are obtained directly from equation (2.34). When $2TW$ is increased, there is a better match between the simulated and analytical curves, because the Gaussian approximation is more accurate under large $2TW$ values [29]. After the bandwidth W is chosen, the only way to change $2TW$ is to change the length of integration time T. Therefore, when T is increased, the Gaussian approximation is more accurate. However, increasing T degrades BER performance because more noise energy is captured. When a UWB signal passes through a multipath channel, the large number of multipath components result in a very long channel delay. In order to capture the effective signal energy, the integration interval must be very long. This is why Gaussian approximation is commonly used in UWB systems.

Fig. 16 shows the analytical BER curves of PWM and PPM for different $2TW$

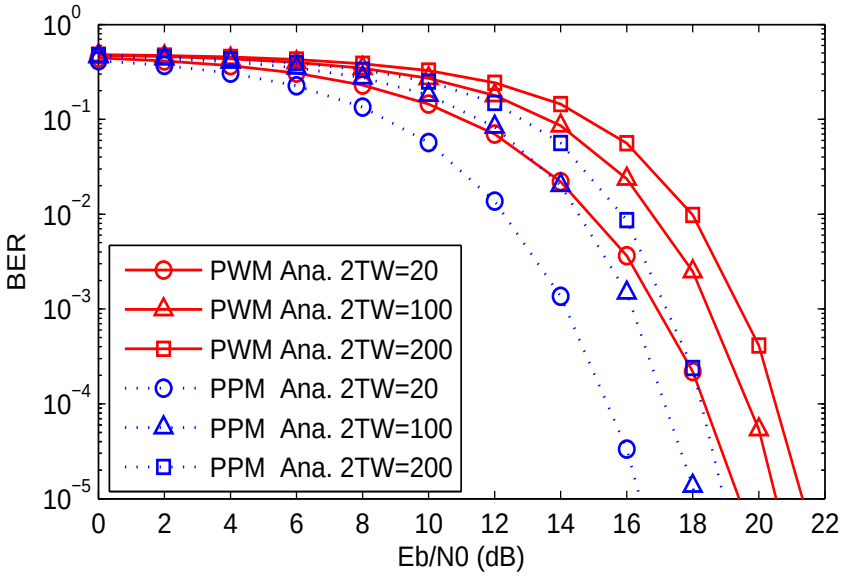

Figure 16: Comparison of BER performance of PWM and PPM for different $2TW$ values

values. Because equation (2.34) has been proved a correct BER equation for PWM above and equation (2.35) was also proved correct for PPM [8], we will use analytical BER curves to compare the BER performances of PWM and PPM in AWGN channels. In Fig. 16, When $2TW = 20$, PPM achieves 2.7 dB improvement over PWM at the BER=10^{-3}. When $2TW = 100$ and 200, the improvement are 2.3 and 2.2 dB, respectively. Fig. 17, Fig. 18, and Fig. 19 show the BER performance comparisons of PWM and PPM in multipath channels. The CM4 model [32] is used in simulation. Synchronization is perfect, and the maximum channel spread D is truncated to 80 ns. The frame length is designed using the method mentioned in Section 2.3, so IFI is avoided in simulation. In this paper, $\delta = T_0 = T_1$ for PPM, and the T_0 of PWM equals the T_0 of PPM. In the following, when a value of δ is given, it implies that T_0 and T_1 also have the same value. The analytical BER curves of PPM and PWM are obtained directly from equations (2.41) and (2.45), respectively. In these two equations, we need to know the values of parameter β_a, β_b and λ. There is no mathematical formula to calculate the captured energy as a function of the length

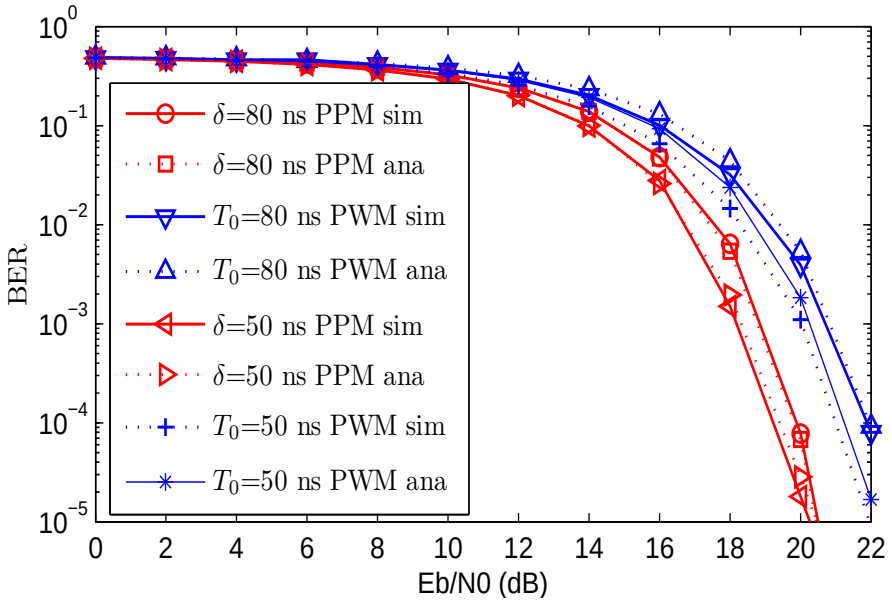

Figure 17: Comparison of BER performance of PWM and PPM in Multipath channels(CM4 model, δ= 80 ns and 50 ns)

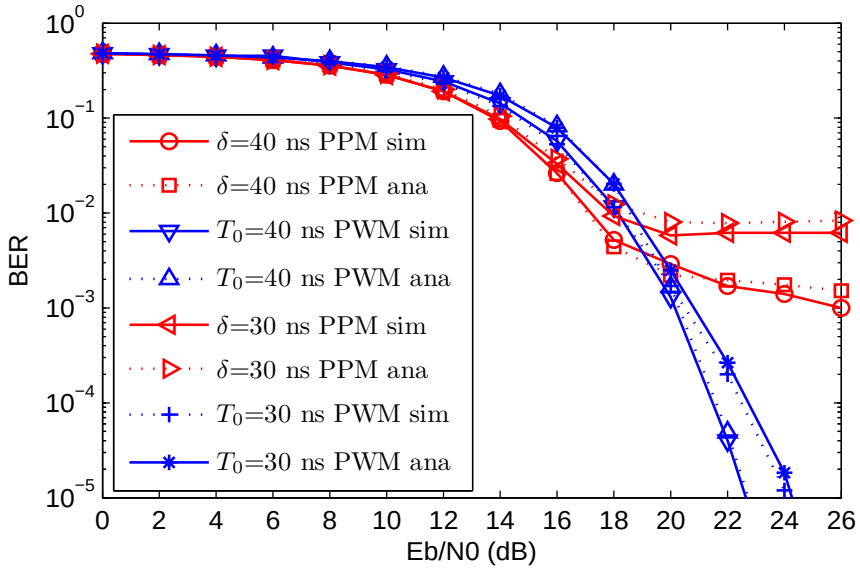

Figure 18: Comparison of BER performance of PWM and PPM in Multipath channels(CM4 model, δ= 40 ns and 30 ns)

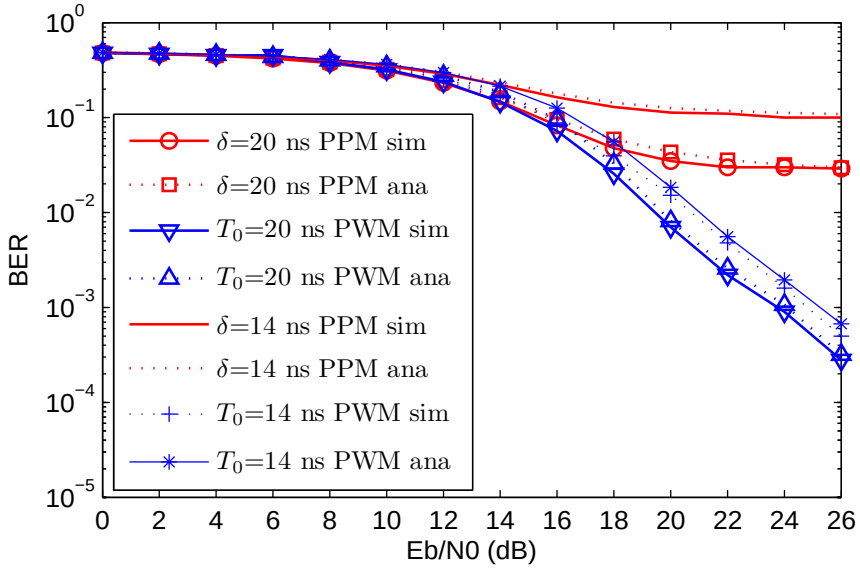

Figure 19: Comparison of BER performance of PWM and PPM in Multipath channels(CM4 model, δ= 20 ns and 14 ns)

of the integration interval for IEEE 802.15.4a channel. We use a statistic method to obtain values for the above parameters. Firstly, we use the MATLAB code in [32] to generate realizations of the channel impulse response $h(t)$. Then we calculate the ratio of energy in a specific time interval to the total energy of a channel realization to obtain values for these parameters. These values are substituted into equations (2.41) and (2.45) to achieve the analytical BER. Both the simulated and the analytical BER are obtained by averaging over 100 channel realizations. In Fig. 17, when $\delta = 80$ ns, no CMI occurs and PPM obtain better BER than PWM. The improvement is 2 dB at BER=10^{-3}. When $\delta = 50$ ns, PPM still obtains better BER performance than PWM in spite of the slight CMI and the improvement is approximately 1.9 dB at BER=10^{-3}. However, we can see from Fig. 17 that the performances of PWM and PPM are improved compared to when $\delta = 80$ ns. This phenomenon can be explained as follows. The multipath components existing in the time interval between 50 ns and 80 ns include low signal energy, so the integrators capture more noise energy than signal energy in this interval. In Fig. 18, when $\delta = 40$ ns, PWM obtains bet-

ter BER performance than PPM and the improvement is approximately 5.8 dB at BER=10^{-3}. When $\delta = 30$ ns, PWM requires an increase of E_b/N_0 approximately 0.5 dB to maintain BER=10^{-3}, but PPM can not achieve this BER level and exhibits BER floor. The phenomena that the BER performance can not be improved is called BER floor [34–37]. In Fig. 19, the δ values are 20 ns and 14 ns. The BER performance of PPM is very bad, and it can not be improved by increasing the signal transmitting power. The reason is that when the signal power is increased, CMI is increased proportionally [33]. Unlike PPM, however, PWM still achieves a good BER performance when the signal transmitting power is increased.

Fig. 20 and Fig.21 are comparisons of BER performance when synchroniza-

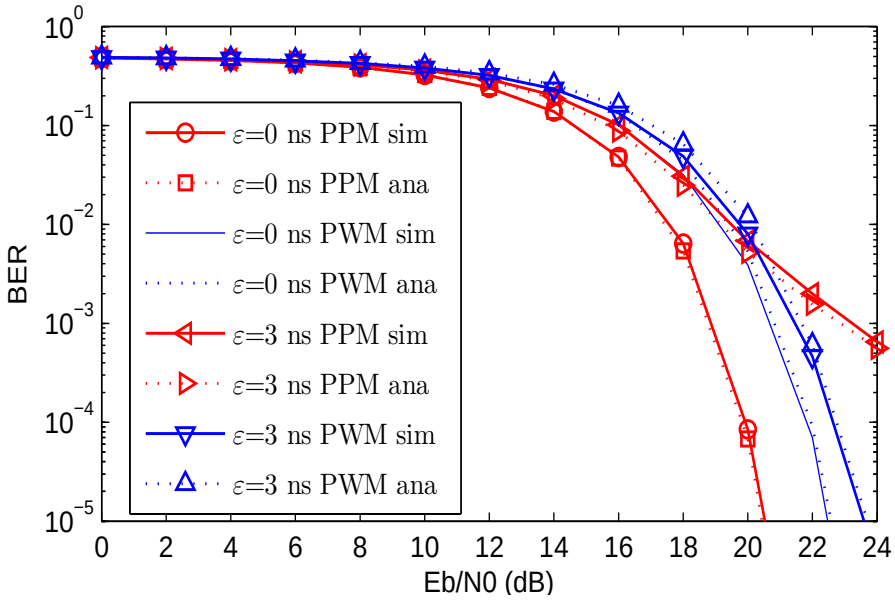

Figure 20: Comparison of BER performance of PWM and PPM in the presence of synchronization errors(CM4 model, $\delta = D = 80$ ns, $\varepsilon = 0$ and 3 ns).

tion errors occur. In simulation, the modulation index δ is set to the maximum channel spread $D = 80$ ns, so no CMI is considered here. The frame structure is designed by following the method mentioned in Section 2.4.2, so IFI are avoided in simulation. The analytical BER curves are obtained directly from equations (2.48) and (2.52), and the values for parameters η and ρ in equations (2.48) and (2.52)

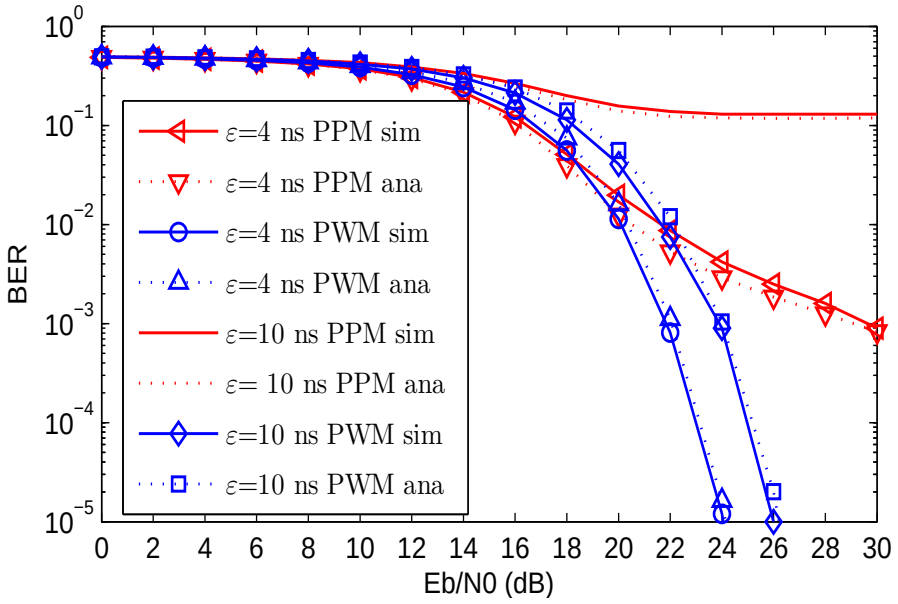

Figure 21: Comparison of BER performance of PWM and PPM in the presence of synchronization errors(CM4 model, $\delta = D = 80$ ns, $\varepsilon = 4$, 10 ns).

are obtained by using the statistic method similar to the one described above. Both the simulated and analytical BERs are obtained by averaging over 100 channel realizations. In Fig. 20, when $\varepsilon = 0$ ns, no synchronization error occurs, and PPM achieve better BER performance than PWM. The improvement is approximately 2 dB at BER= 10^{-3}. When $\varepsilon = 3$ ns, PWM has better BER performance than PPM. The improvement at BER= 10^{-3} is approximately 1.6 dB. In Fig. 21, when $\varepsilon = 4$ ns, PWM obtains approximately 7.5 dB improvement at BER=10^{-3}. When $\varepsilon = 10$ ns, the BER of PPM is extremely bad because of severe synchronization errors, but PWM still achieves a good BER.

The reason the BER performance of PWM is better than PPM in the presence of CMI or synchronization errors can be explained as follows. In a PPM system, modulation is achieved by shifting the pulse position, and the orthogonality of the signals is achieved in time domain. When CMI or synchronization errors occur, this orthogonality is easily destroyed. And this results in the counteraction of the captured signal energy between T_0 and T_1, thereby the absolute values of the mean values

in equations (2.38) and (2.47) are reduced at a higher rate. Because of this effect, the euclidean distance is reduced dramatically and the BER performance is severely degraded. In a PWM system, when bit 0 is transmitted, the mean values in equations (2.42) and (2.49) are always 0. The euclidean distance is not affected by small T_0 values or synchronization errors when bit 0 is transmitted. When bit 1 is transmitted, although the mean values in equations (2.43) and (2.50) are reduced, the phenomena of energy counteraction does not happen in a PWM system.

2.6 Summary

In this chapter, a new energy detection UWB system based on pulse width modulation is proposed. The BER performance of this new system is compared to PPM in AWGN channels, multipath channels and in the presence of synchronization errors. In AWGN channels, the BER performance of PPM is slightly better than PWM. However, in multipath channels, PPM suffers from cross-modulation interference if the integration interval is shorter than maximum channel spread. PWM dose not suffer from cross-modulation interference. This makes PWM a better scheme than PPM for high data rate communications when the integration interval is shorter than the maximum channel spread. Also when synchronization errors occur, PWM is more robust and achieves better BER performance than PPM. In UWB systems, the requirement of synchronization accuracy is much higher than other systems, so this leads to high cost to use accurate synchronizer. If we use PWM other than PPM, it will lower the requirement of synchronization accuracy and we can chose cheap synchronizer to reduce the cost. The complexities of PWM and PPM are in the same level. PWM transmits pulses with different shaping factors, and PPM shifts the position of pulses. At the receiver, PWM uses two energy detection branches. However, this does not increase the complexity of PWM too much. ED receiver has been a

very mature technology for many years and the structure of the receiver is simple and easy to implement. One just adds another simple branch to the receiver and the cost is low.

CHAPTER III

ENERGY DETECTION GAUSSIAN FSK UWB SYSTEMS

In this chapter, a new ultra-wideband system using energy detection is proposed. The transmitter of this system uses two pulses that are different-order derivatives of the Gaussian pulse to transmit bit 0 or 1. These pulses are appropriately chosen to separate their spectra in the frequency domain. The receiver is composed of two energy detection branches. Each branch has a filter which captures the signal energy of either bit 0 or 1. The outputs of the two branches are subtracted from each other to generate the decision statistic. The value of this decision statistic is compared to the threshold to determine the transmitted bit. This new system has the same BER performance as energy detection based pulse position modulation (PPM) system in additive white Gaussian noise channels. In multipath channels, its performance surpasses PPM and it also exhibits better BER performance in the presence of synchronization errors.

The structure of this chaper is as follows: Section 3.1 introduces the system

models, Section 3.2 analyzes the BER performance of systems in AWGN channels, Section 3.3 analyzes the BER performance of systems in multipath channels, Section 3.4 analyzes the BER performance of systems in the presence of synchronization errors. Section 3.5 shows the numerical results. Section 3.6 summarizes this chapter.

3.1 System Models

The design idea of this new system originates from spectral characteristics of the derivatives of the Gaussian pulse. The Fourier transform X_f and center frequency f_c of the kth-order derivative are given by [7]

$$X_f \propto f^k \exp(-\pi f^2 \alpha^2/2) \tag{3.1}$$

$$f_c = \sqrt{k}/(\alpha\sqrt{\pi}) \tag{3.2}$$

where k is the order of the derivative and f is the frequency. The pulse shaping factor is denoted by α. If we assign a constant value to α and change the k value in equation (3.1), we obtain spectral curves for different-order derivatives. It is surprising to find that those curves have similar shapes and bandwidths. The major difference is their center frequencies. The reason that the change of center frequencies can be explained directly from equation (3.2). If the values of k and α are appropriately chosen, it is always possible to separate the spectra of the two pulses. An example of the spectra of two pulses with different-order derivatives is plotted in Fig. 3.1. In this example, the chosen parameters are $\alpha = 0.5 \times 10^{-9}$, k =2 and 24. The spectral curves are amplitude normalized. Exploiting the spectral characteristics of the pulses, the transmitted signal of the mth user of this system is designed as

$$s_{GFSK}^{(m)} = \sum_j \sqrt{E_p}(b_{\lfloor j/N_s \rfloor}^{(m)} p_1(t - jT_f - c_j^{(m)} T_c) + (1 - b_{\lfloor j/N_s \rfloor}^{(m)}) p_2(t - jT_f - c_j^{(m)} T_c)) \tag{3.3}$$

where $p_1(t)$ and $p_2(t)$ denote the waveforms of two different-order derivatives of the Gaussian pulse with normalized energy, and E_p is the signal energy. The transmitted

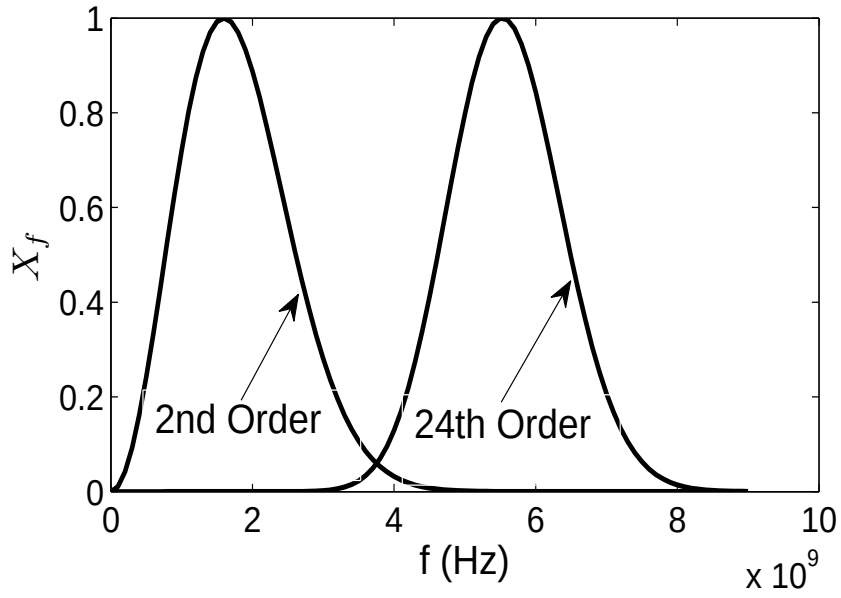

Figure 22: Spectral curves of the 2nd- and 24th-order derivatives of the Gaussian pulse

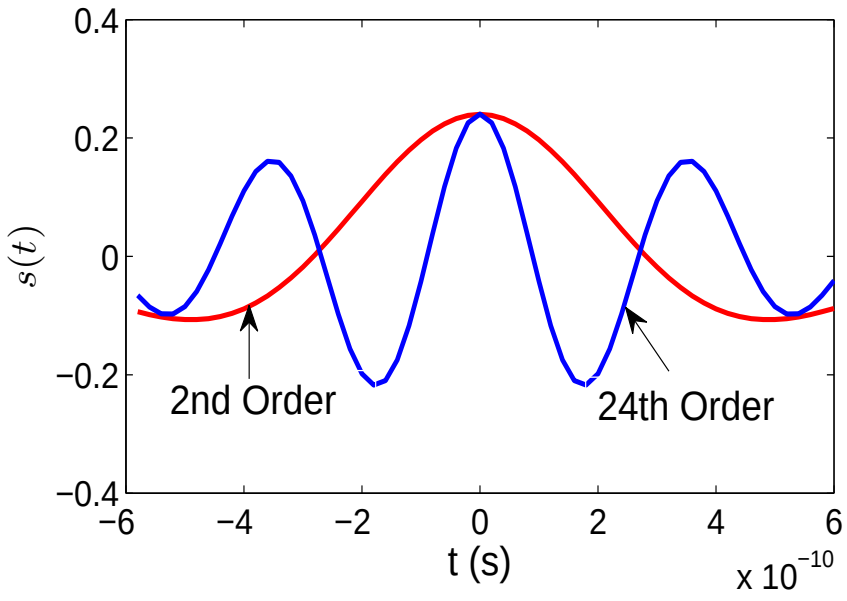

Figure 23: Waveforms of the 2nd- and 24th-order derivatives of the Gaussian pulse

bit of the mth user is denoted by $b^{(m)}_{\lfloor j/N_s \rfloor}$, where $\lfloor j/N_s \rfloor$ means the integer part of j/N_s. Usually, a bit is repeated N_s times and transmitted over N_s frames to improve performance, so the waveforms having the same $\lfloor j/N_s \rfloor$ are generated from the same bit. Without loss of generality, $N_s = 1$ is used in this paper. The chip period is denoted by T_c, and the frame period, which includes multiple chip intervals, is denoted by T_f. The relationship between these two variables is $T_f \geq N_h T_c$, where N_h denotes the number of intervals of length T_c in a frame. The transmitter selects the chip interval using time-hopping (TH) sequence $c^{(m)}_j$ which is generated from pseudo-random sequence. The value of $c^{(m)}_j$ is in the range $0 \leq c^{(m)}_j \leq N_h - 1$. The modulation is carried out as follows. When bit 1 is transmitted, the value of $b^{(m)}_{\lfloor j/N_s \rfloor}$ and $1 - b^{(m)}_{\lfloor j/N_s \rfloor}$ are 1 and 0, respectively, so $p_1(t)$ is transmitted. When bit 0 is transmitted, $b^{(m)}_{\lfloor j/N_s \rfloor}$ and $1 - b^{(m)}_{\lfloor j/N_s \rfloor}$ are 0 and 1, respectively, so the transmitted waveform is $p_2(t)$.

Without loss of generality, we focus on single user communication case, and a bit is transmitted only once. The transmitted signal of this system is reduced to

$$s(t)_{GFSK} = \sum_j \sqrt{E_p}(b_j p_1(t - jT_f) + (1 - b_j)p_2(t - jT_f)) \tag{3.4}$$

where $p_1(t)$ and $p_2(t)$ denote the pulse waveforms of different-order derivatives with normalized energy, and E_p is the signal energy. The jth transmitted bit is denoted by b_j. The frame period is denoted by T_f. The modulation is carried out as follows. When bit 1 is transmitted, the value of b_j and $1 - b_j$ are 1 and 0, respectively, so $p_1(t)$ is transmitted. Similarly, the transmitted waveform for bit 0 is $p_2(t)$.

The receiver is depicted in Fig. 24. It is separated into two branches, and each branch is a conventional energy detection receiver. The only difference between the two branches is the working frequency ranges of Filter 1 and Filter 2. Filter 1 passes the signal energy of $p_1(t)$ and rejects that of $p_2(t)$, and Filter 2 passes the signal energy of $p_2(t)$ and rejects that of $p_1(t)$. So when a bit is transmitted, only one branch can capture its energy. In this system, bits 1 and 0 are transmitted by $p_1(t)$ and $p_2(t)$,

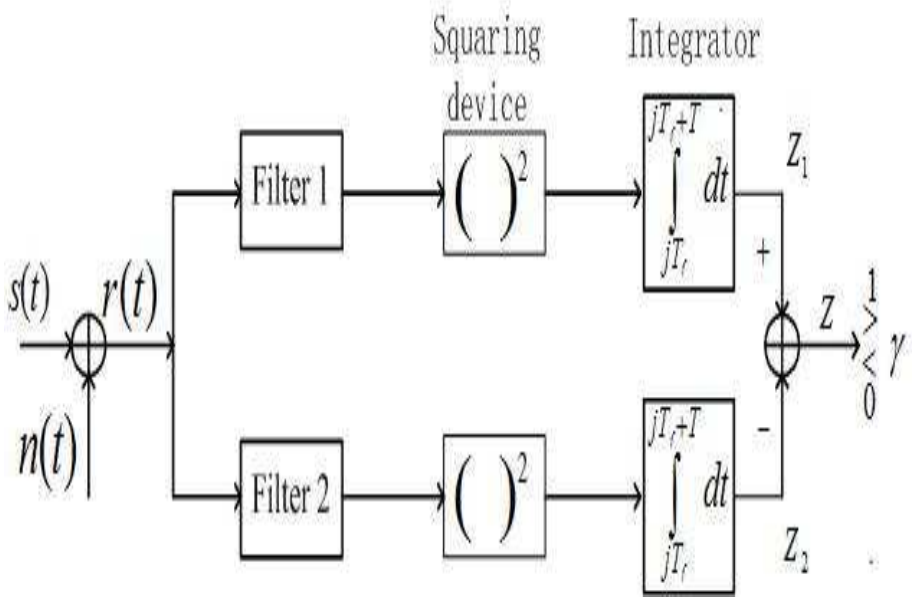

Figure 24: Receiver of GFSK UWB

respectively, so branch 1 captures signal energy of bit 1 and branch 2 captures that of bit 0. The signal arriving at the receiver is denoted by $s(t)$, $n(t)$ is the AWGN, and $r(t)$ denotes the sum of $s(t)$ and $n(t)$. The captured energy of branches 1 and 2 over the integration interval T are denoted by Z_1 and Z_2, respectively. The output of the receiver is given by $Z = Z_1 - Z_2$. Finally, Z is compared with the threshold γ. If $Z \geq \gamma$, the transmitted bit is 1, otherwise it is 0.

In this GFSK system, modulation is carried out by using different-order derivatives of the Gaussian pulse. This type of modulation is entirely different to that used in continuous systems. In continuous FSK systems, modulation is achieved by using sine waveforms with different frequencies as carriers. Our GFSK is a carrier-less technology, and the signal is transmitted in the baseband. The example in Fig. 3.1 uses the 2nd- and 24th-order derivatives of the Gaussian pulse, but this system is not limited to this pair of pulses. The appropriate pulse pair depends on the bandwidth requirement of the system and its allocated frequency range. The bandwidth

of a pulse can be modified by changing the shaping factor α. Increasing the value of α decreases the bandwidth [7]. The bandwidth of the 24th-order derivative pulse in Fig. 3.1 is approximately 3.4 GHz (obtained by numerically calculating the -10 dB bandwidth of the spectral curve of the 24th-order derivative pulse). In Fig. 25, two pulse pairs are generated from $\alpha = 1 \times 10^{-9}$, which gives a narrower bandwidth than $\alpha = 0.5 \times 10^{-9}$. The designer has the flexibility to use either the 2nd- and 20th-order derivatives or the 6th- and 29th-order derivatives depending on the application. They each achieve good spectral separation. The center frequencies of the pulses can be shifted to higher frequencies by increasing the order of the derivatives. Also, the spectral separation of a pulse pair can be increased by increasing the difference of the orders of the derivatives. Although the implementation of this system needs high-order derivatives of the Gaussian pulse, it is already feasible using current technology to generate such pulses. Many papers describing the hardware implementation of pulse generators for high-order derivatives of the Gaussian pulse have been published. In [38], a 7th-order pulse generator is proposed, and the generator in [39] is capable of producing a 13th-order pulse. In [40], the center frequency of the generated pulse is 34 GHz.

In this Chapter, the performance of this new system is compared to a PPM system, and the models of PPM systems has been described in Chapter 2, so it is not repeated here.

Some parameter values are given below, and these values are used later in simulation. The expression for the 2nd-order derivative can be found in [7].

$$s(t) = (1 - 4\pi\frac{t^2}{\alpha^2})e^{-\frac{2\pi t^2}{\alpha^2}} \tag{3.5}$$

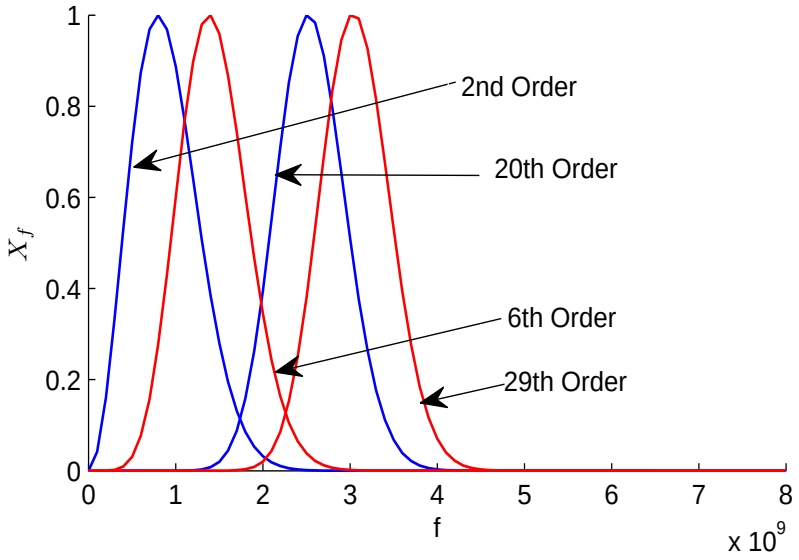

Figure 25: Spectra of two pulse pairs

We can use the symbolic calculation tool MAPLE to perform $\frac{d^{24}}{dt^{24}}(\frac{\sqrt{2}}{\alpha}e^{\frac{-2\pi t^2}{\alpha^2}})$ to obtain the 24th-order derivatives, where $\frac{\sqrt{2}}{\alpha}e^{\frac{-2\pi t^2}{\alpha^2}}$ is the Gaussian pulse [7].

$$
\begin{aligned}
s(t) = (&5305528527460761600 - 2546653693181165568000\pi\frac{t^2}{\alpha^2} \\
&+1867546041666188083200\pi^2\frac{t^4}{\alpha^4} - 498012277777650155520 0\pi^3\frac{t^6}{\alpha^6} \\
&+64030149999983591424 00\pi^4\frac{t^8}{\alpha^8} - 45532551111099442790 40\pi^5\frac{t^{10}}{\alpha^{10}} \\
&+19316839865314915123 20\pi^6\frac{t^{12}}{\alpha^{12}} - 50945511732698677248 0\pi^7\frac{t^{14}}{\alpha^{14}} \\
&+84909186221164462080\pi^8\frac{t^{16}}{\alpha^{16}} - 88793920231283097600\pi^9\frac{t^{18}}{\alpha^{18}} \\
&+56080370672389324 8\pi^{10}\frac{t^{20}}{\alpha^{20}} - 19421773393035264\pi^{11}\frac{t^{22}}{\alpha^{22}} \\
&+281474976710656\pi^{12}\frac{t^{24}}{\alpha^{24}})e^{-\frac{2\pi t^2}{\alpha^2}}
\end{aligned}
\tag{3.6}
$$

Equation (3.6) is the the 24th-order derivative. This is a simplified version of the original one obtained from MAPLE. The common factor of all terms in parentheses is $\sqrt{2}\pi^{12}/\alpha^{25}$. It is a constant and does not affect the waveform shape, so it has been removed to simplify equation. The value of α is set to 0.5×10^{-9} and the width of the pulses are chosen to be $2.4\alpha = 1.2 \times 10^{-9} = 1.2$ ns (the detailed method to

choose pulse width for a shaping factor α can be found from [7]). Fig. 3.1 shows the energy normalized waveforms of the 2nd- and 24th-order derivatives. For GFSK, we use the 2nd-order derivative to transmit bit 1, and the 24th-order to transmit bit 0. For PPM, the pulse is the 2nd-order derivative.

The BER performance of a GFSK system in AWGN and multipath channels and in the presence of synchronization errors will be analyzed in the following. The BER performance of a PPM system has been analyzed in Chapter 2, please see equations (2.35), (5.10), and (5.15).

3.2 GFSK Performance in AWGN Channels

In Fig. 24, Z_1 and Z_2 are the outputs of conventional energy detectors, and they are defined as chi-square variables with approximately a degree of $2TW$ [28], where T is the integration time and W is the bandwidth of the filtered signal. A popular method for energy detection, called Gaussian approximation, has been developed to simplify the derivation of the BER formula. When $2TW$ is large enough, a chi-square variable can be approximated as a Gaussian variable. This method is commonly used in energy detection communication systems [8, 27, 29, 30]. The mean value and variance of this approximated Gaussian variable are [31]

$$\mu = N_0 TW + E \tag{3.7}$$

$$\sigma^2 = N_0^2 TW + 2N_0 E \tag{3.8}$$

where μ and σ^2 are the mean value and variance, respectively. The double-sided power spectral density of AWGN is $N_0/2$, where N_0 is the single-sided power spectral density. The signal energy which passes through the filter is denoted by E. If the filter rejects all of the signal energy, then $E = 0$. In Fig. 24, when bit 1 is transmitted, the signal energy passes through Filter 1 and is rejected by Filter 2. The probability density

function (pdf) of Z_1 and Z_2 can be expressed as $Z_1 \sim N(N_0TW+E_b, N_0^2TW+2N_0E_b)$ and $Z_2 \sim N(N_0TW, N_0^2TW)$, where E_b denotes the bit energy. In this paper, the same bit is not transmitted repeatedly, so E_b is used to replace E here. Since $Z = Z_1 - Z_2$, the pdf of Z is

$$H_1 : Z \sim N(E_b, 2N_0^2TW + 2N_0E_b) \tag{3.9}$$

Using the same method, the pdf of Z when bit 0 is transmitted is

$$H_0 : Z \sim N(-E_b, 2N_0^2TW + 2N_0E_b) \tag{3.10}$$

After obtaining the pdf of Z, we follow the method in [29] to derive the BER formula. Firstly, we calculate the BER when bits 0 and 1 are transmitted as follows:

$$P_0 = \int_{\gamma}^{\infty} f_0(x)dx = \int_{\gamma}^{\infty} \frac{1}{\sqrt{2\pi}\sigma_0} e^{-\frac{(x-\mu_0)^2}{2\sigma_0^2}} dx \tag{3.11}$$

$$P_1 = \int_{-\infty}^{\gamma} f_1(x)dx = \int_{-\infty}^{\gamma} \frac{1}{\sqrt{2\pi}\sigma_1} e^{-\frac{(x-\mu_1)^2}{2\sigma_1^2}} dx \tag{3.12}$$

where $f_0(x)$ and $f_1(x)$ denote the probability density functions, and γ denotes the decision threshold. From equation (3.9) and (3.10), it is straightforward to obtain $\mu_0 = -E_b$, $\sigma_0^2 = 2N_0^2TW + 2N_0E_b$, $\mu_1 = E_b$, $\sigma_1^2 = 2N_0^2TW + 2N_0E_b$. Substituting these parameter values into equations (3.11) and (3.12), and then expressing P_0 and P_1 in terms of the complementary error function $Q(\cdot)$, we obtain

$$P_0 = Q((E_b + \gamma)/\sqrt{2N_0^2TW + 2N_0E_b}) \tag{3.13}$$

$$P_1 = Q((E_b - \gamma)/\sqrt{2N_0^2TW + 2N_0E_b}) \tag{3.14}$$

The optimal threshold is obtained by setting $P_0 = P_1$ [8, 29]

$$(E_b + \gamma)/\sqrt{2N_0^2TW + 2N_0E_b} = (E_b - \gamma)/\sqrt{2N_0^2TW + 2N_0E_b} \tag{3.15}$$

Solving equation (3.15), the optimal threshold is obtained as

$$\gamma = 0 \tag{3.16}$$

The total BER is $P_e = 0.5(P_0 + P_1)$. Since $P_0 = P_1$, it follows that $P_e = P_0$. Substituting equation (3.16) into (3.13), the total BER of GSFK in AWGN channels is

$$P_e = Q(\frac{E_b/N_0}{\sqrt{2TW + 2E_b/N_0}}) \tag{3.17}$$

3.3 GFSK Performance in Multipath Channels

In this Chapter, the BER performances of GFSK in multipath channels are researched. The channel model of the IEEE 802.15.4a standard [32] is used. The details about this channel model has been stated in Chapter 2.

Fig. 26 is the frame structure of GFSK in multipath channels. CMI does not

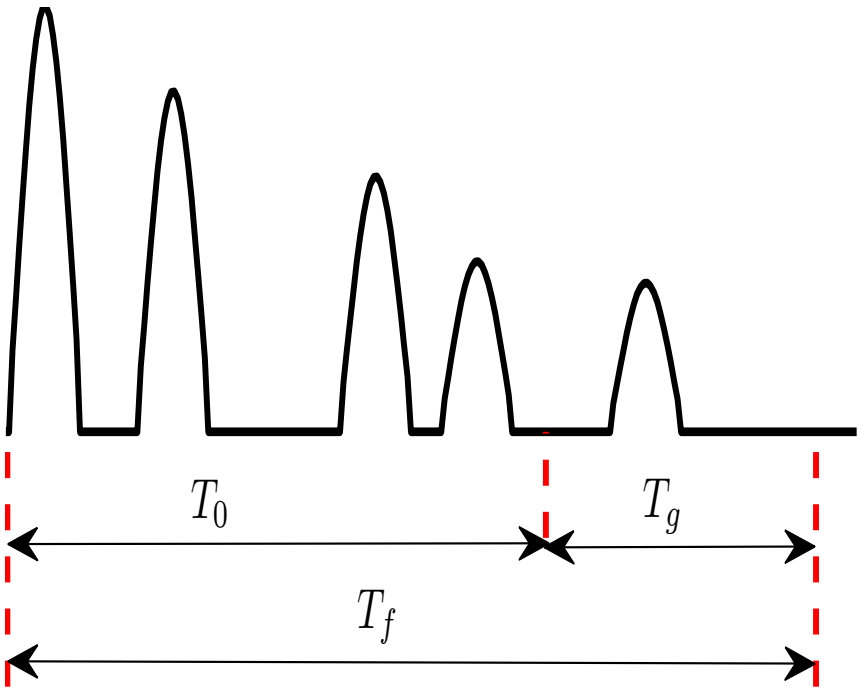

Figure 26: A GFSK frame structure in multipath channels

occur in GFSK systems as it does in PPM systems. In order to compare GFSK to

PPM under the same energy capture condition, the integration interval T_0 of GFSK has the same length as the T_0 of PPM. Also synchronization is assumed to be perfect as in PPM. The guard interval is T_g, and the frame period is set to $T_f = T_0 + T_g = D$. This will achieve the maximum data rate and prevent IFI simultaneously. This frame structure is applied to both bits 0 and 1. From Fig. 26, it is straightforward to obtain the pdfs of Z when bits 1 and 0 are transmitted as follows:

$$H_1 : Z \sim N(\lambda E_b, 2N_0^2 TW + 2N_0 \lambda E_b) \tag{3.18}$$

$$H_0 : Z \sim N(-\lambda E_b, 2N_0^2 TW + 2N_0 \lambda E_b) \tag{3.19}$$

where $\lambda = E_{T_0}/E_b$. Using equations (3.11) and (3.12), and following the method in Section 3.2, we obtain the BER

$$P_e = Q(\frac{\lambda E_b/N_0}{\sqrt{2TW + 2\lambda E_b/N_0}}) \tag{3.20}$$

3.4 GFSK Performance in The Presence of Synchronization Errors

Fig. 27 depicts the GFSK frame structure in the presence of synchronization errors. The integration interval $T_0 = D$ is the same as that of PPM. The frame length is $T_f = T_g + D$, where $T_g = D/2$ as in Section 2.4.1. From Fig. 27, the pdfs of Z are

$$H_1 : Z \sim N(\rho E_b, 2N_0^2 TW + 2N_0 \rho E_b) \tag{3.21}$$

$$H_0 : Z \sim N(-\rho E_b, 2N_0^2 TW + 2N_0 \rho E_b) \tag{3.22}$$

where $\rho = E_{T_0}/E_b$. Using equations (3.11) and (3.12), and following the method in Section 3.2, the total BER is

$$P_e = Q(\frac{\rho E_b/N_0}{\sqrt{2TW + 2\rho E_b/N_0}}) \tag{3.23}$$

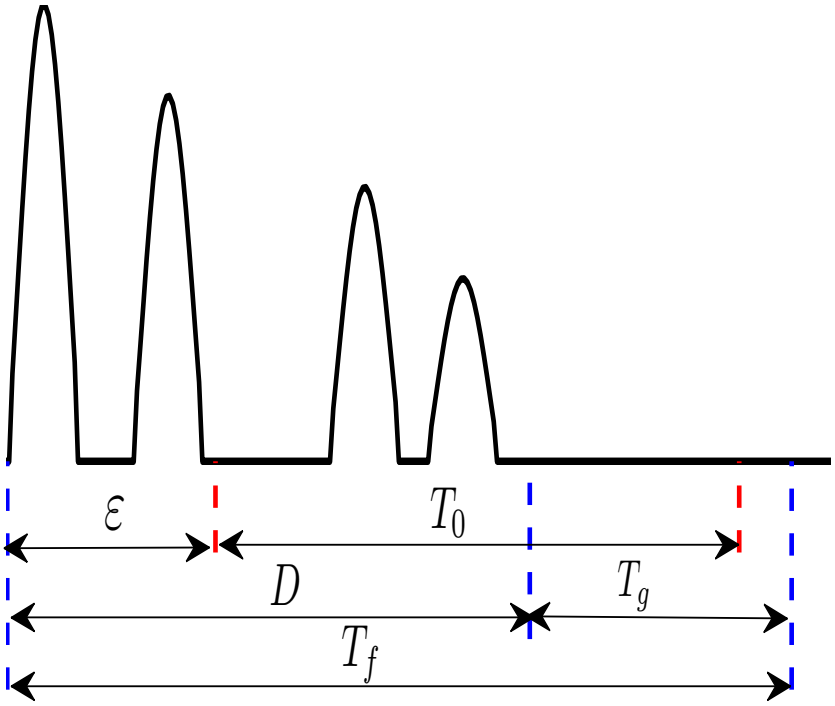

Figure 27: A GFSK frame structure in the presence of synchronization errors

3.5 Numerical Results and Analysis

Fig. 28 shows the BER curves for different $2TW$ values. In simulation, the bandwidth of the filters is 3.4 GHz, and the pulse duration is 1.2 ns. Analytical BER curves are obtained directly from equation (3.17). When $2TW$ is increased, there is a better match between the simulated and analytical curves, because the Gaussian approximation is more accurate under large $2TW$ values [29]. After the bandwidth W is chosen, the only way to change $2TW$ is to change the length of integration time T. Therefore, when T is increased, the Gaussian approximation is more accurate. However, increasing T degrades BER performance because more noise energy is captured. When a UWB signal passes through a multipath channel, the large number of multipath components result in a very long channel delay. In order

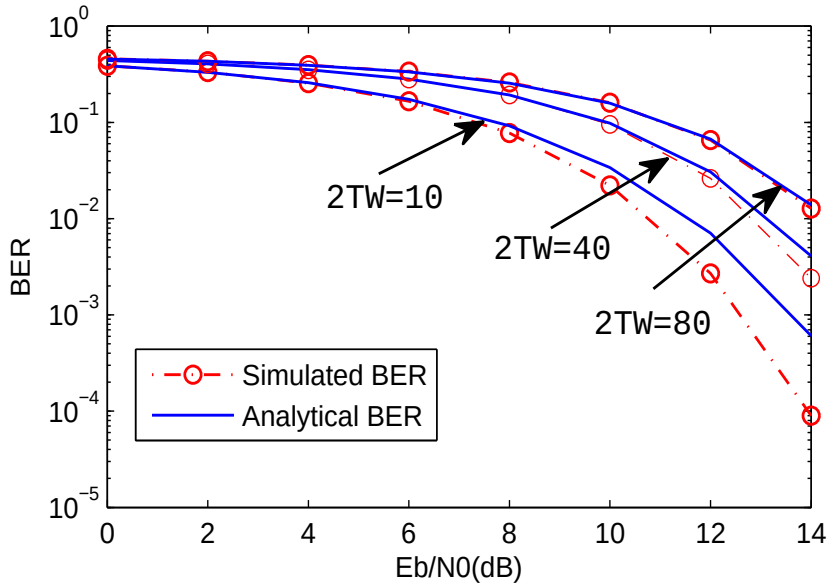

Figure 28: BER performance of GFSK for different $2TW$ values in AWGN channels

to capture the effective signal energy, the integration interval must be very long. This is why Gaussian approximation is commonly used in UWB systems.

Fig. 29, Fig. 30, and Fig. 31 show the BER performance comparisons of GFSK and PPM in multipath channels. The CM4 model [32] is used in simulation. Synchronization is perfect, and the maximum channel spread D is truncated to 80 ns. The frame length of PPM and GFSK are designed using the method mentioned in Section 2.3.1 and Section 3.3, respectively, so IFI is avoided in simulation. In this paper, $\delta = T_0 = T_1$ for PPM, and the T_0 of GFSK equals the T_0 of PPM. In the following, when a value of δ is given, it implies that T_0 and T_1 also have the same value. The analytical BER curves of PPM and GFSK are obtained directly from equations (2.41) and (3.20), respectively. In these two equations, we need to know the values of parameter β_a, β_b and λ. There is no mathematical formula to calculate the captured energy as a function of the length of the integration interval for IEEE 802.15.4a channel. We use a statistic method to obtain values for the

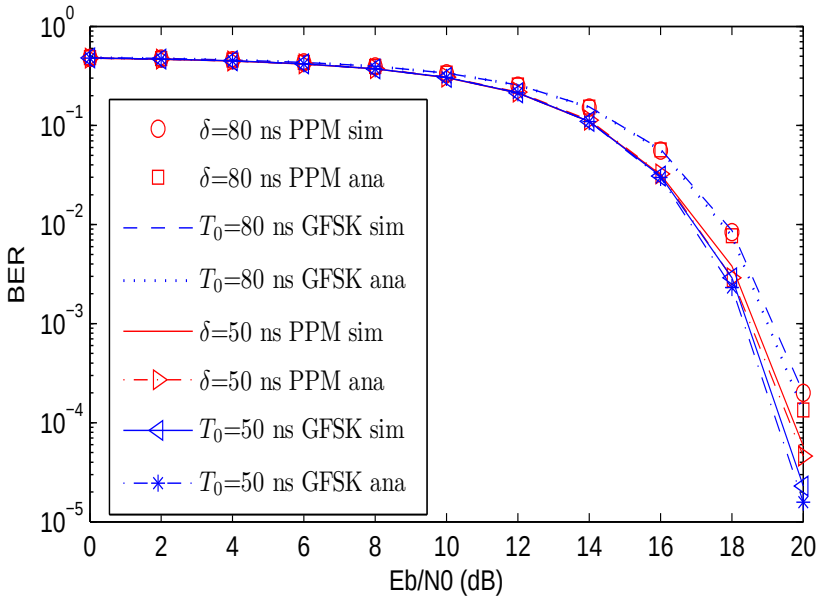

Figure 29: Comparisons of BER performance of GFSK and PPM in multipath channels (CM4 model, $D = 80$ ns, $\delta = 80$ and 50 ns).

above parameters. Firstly, we use the MATLAB code in [32] to generate realizations of the channel impulse response $h(t)$. Then we calculate the ratio of energy in a specific time interval to the total energy of a channel realization to obtain values for these parameters. These values are substituted into equations (2.41) and (3.20) to achieve the analytical BER. Both the simulated and the analytical BER are obtained by averaging over 100 channel realizations. In Fig. 29, when $\delta = 80$ ns, no CMI occurs and GFSK and PPM obtain the same BER. The analytical curves of GFSK and PPM match very well, as do the simulated curves. When $\delta = 50$ ns, GFSK obtains better BER performance than PPM, and the improvement is approximately 0.2 dB at BER=10^{-3}. The reason is that δ is less than D, CMI occurs, and PPM performance is degraded. However, we can see from Fig. 29 that the performances of GFSK and PPM are improved compared to when $\delta = 80$ ns. This phenomenon can be explained as follows. The multipath components existing in the time interval between 50 ns and 80 ns include low signal energy, so the integrators capture more

noise energy than signal energy in this interval. In Fig. 30, when $\delta = 40$ ns, GFSK obtains approximately 7.5 dB improvement at BER=10^{-3}. When $\delta = 30$ ns, GFSK requires an increase of E_b/N_0 approximately 0.6 dB to maintain BER=10^{-3}, but PPM can not achieve this BER level. In Fig. 31, the δ values are 20 ns and 14 ns. The BER performance of PPM is very bad, and it can not be improved by increasing the signal transmitting power. The reason is that when the signal power is increased, CMI is increased proportionally [33]. Unlike PPM, however, GFSK still achieves a good BER performance when the signal transmitting power is increased.

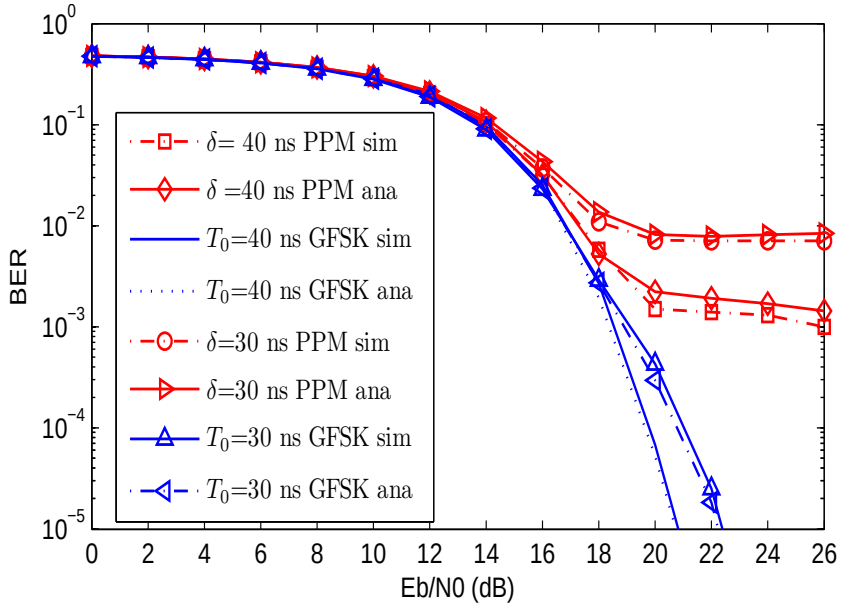

Figure 30: Comparisons of BER performance of GFSK and PPM in multipath channels (CM4 model, $D = 80$ ns, $\delta = 40$ and 30 ns)

Fig. 32 and Fig. 33 are comparisons of BER performance when synchronization errors occur. In simulation, the modulation index δ is set to the maximum channel spread $D = 80$ ns, so no CMI is considered here. The frame structures of PPM and GFSK are designed by following the method mentioned in Section 2.4.1 and Section 3.4, respectively, so IFI are avoided in simulation. The analytical BER curves are obtained directly from equations (2.48) and (3.23), and the values for parameters η

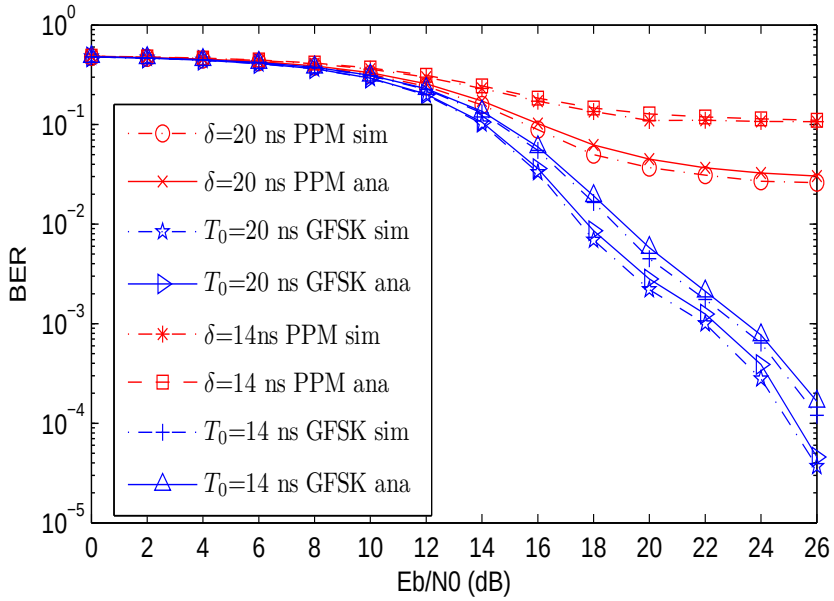

Figure 31: Comparisons of BER performance of GFSK and PPM in multipath channels (CM4 model, $D = 80$ ns, $\delta = 20$ and 14 ns)

and ρ in equations (2.48) and (3.23) are obtained by using the statistic method similar to the one described above. Both the simulated and analytical BERs are obtained by averaging over 100 channel realizations. In Fig. 32, when $\varepsilon = 0$ ns, no synchronization error occurs, and GFSK and PPM achieve the same BER performance. When $\varepsilon = 2$ ns, GFSK has better BER performance than PPM. The improvement at BER= 10^{-3} is approximately 1 dB. In Fig. 33, when $\varepsilon = 3$ ns, GFSK obtains approximately 3.2 dB improvement at BER=10^{-3}. When $\varepsilon = 10$ ns and $\varepsilon = 15$ ns, the BER of PPM is extremely bad because of severe synchronization errors, but GFSK still achieves an acceptable BER.

3.6 Summary

In this chapter, a new energy detection UWB system GFSK UWB system is proposed and the system performance of this system is compared to an ED PPM

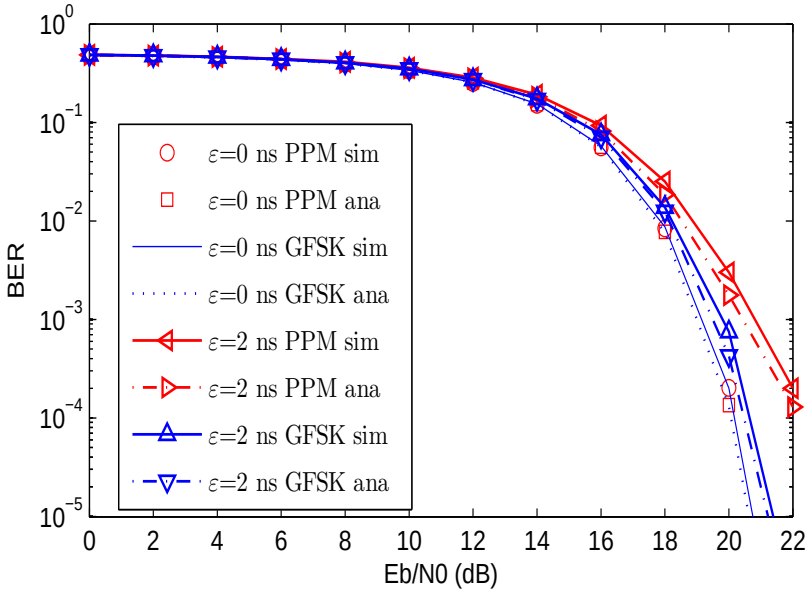

Figure 32: Comparisons of BER performance of GFSK and PPM in the presence of synchronization errors (CM4 model, $\delta = D = 80$ ns, $\varepsilon = 0$ and 2 ns).

UWB system. This ED GFSK system achieves the same BER performance as PPM in AWGN channels. However, after the signals pass through multipath channels, GFSK achieves better performance than PPM because it is not affected by CMI. Also when synchronization errors occur, GFSK achieves better BER performance than PPM. In PPM, modulation is achieved by shifting the pulse position, and the orthogonality of the signals is achieved in time domain. When CMI or synchronization errors occur, this orthogonality is easily destroyed. The orthogonality of GFSK is achieved in the frequency domain. Although the integration interval and synchronization error also affect performance of GFSK, its orthogonality is not affected by these two factors. This is why GFSK has better BER performance than PPM in the presence of CMI and synchronization errors. The cost of this advantage of GFSK is that it occupies more frequency resources than PPM. For low data rate UWB systems, the usable frequency range is much larger than the signal bandwidth. This makes GFSK more flexible because we can use different-order pulse pairs to shift signal center frequency

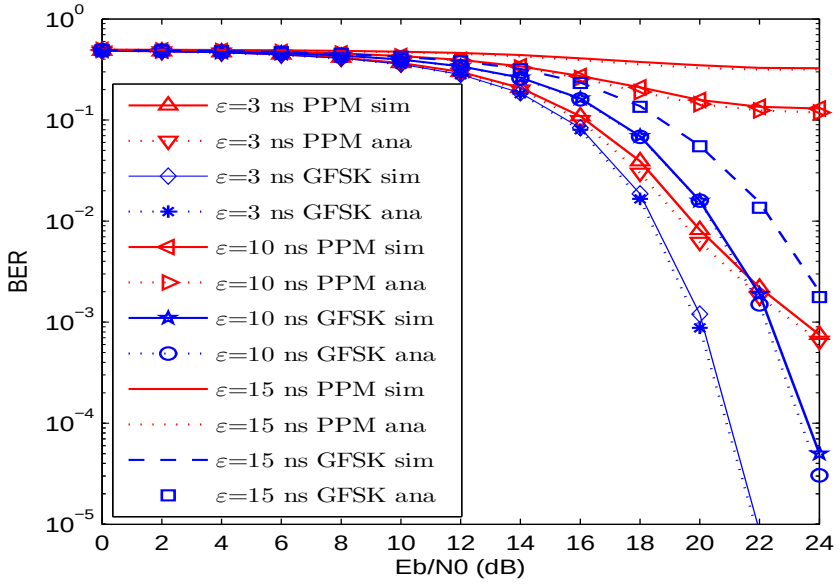

Figure 33: Comparisons of performance of GFSK and PPM in the presence of synchronization errors (CM4 model, $\delta = D = 80$ ns, $\varepsilon = 3$, 10 and 15 ns).

to suitable locations. But for high data rate UWB systems, it is impossible to increase the signal bandwidth without restrictions because the usable frequency is constrained by many possible institutional regulations. The maximum possible signal bandwidth of a single pulse in GFSK is at most one half of that of PPM. But this does not mean that the maximum possible data rate of GFSK is one half of that of PPM. If only AWGN channels are considered, the modulation index δ of PPM can be chosen to be the duration of one pulse. And the frame period of PPM is twice as long as the pulse duration assuming the guard interval is zero. In GFSK, the frame period is equal to one pulse duration, but the shortest possible pulse duration of GFSK is twice that of PPM. This results in the same frame period as PPM, so the maximum possible data rates of GFSK and PPM will be the same in AWGN channels. But when the signals pass through multipath channels, the maximum channel spread of GFSK may not be twice that of PPM. If it is less than twice that of PPM, the maximum data rate of GFSK is greater than PPM. Son it is possible that the spectral efficiency of

GFSK is higher than PPM. In this chapter, we have not investigated this topic, and it will be discussed later in Chapter 6. The complexities of these two systems are also discussed here. GFSK needs two pulse generators at the transmitter and two branches at the receiver. However, this does not increase the complexity of GFSK too much. As mentioned above, many methods to generate different-order derivatives of the Gaussian pulse have been proposed and the cost of using two pulse generators is not expensive. Other components at the transmitter can be shared by these two pulse generators, such as the power amplifier and other baseband components. At the receiver side, the system needs two ED receiver branches which have filters with different frequency range. ED receiver has been a very mature technology for many years and the structure of the receiver is simple and easy to implement. Two branches in GFSK system do not increase the complexity of the receiver too much. One just adds another simple branch to the receiver and the cost is low. Although PPM only needs one energy detection branch, its implementation needs more accurate synchronizer at the receiver and accurate design of modulation index at the transmitter. These factors will greatly increase the cost of the system.

CHAPTER IV

COMPARISON OF PWM AND GFSK SYSTEMS

In the previous two chapters, two new ED UWB systems, PWM and GFSK, are proposed and their performances have been compared with PPM systems. In multipath channels and in the presence of synchronization errors, performances of these two systems surpass that of a PPM system. In this chapter, the performance of PWM and GFSK systems will be compared.

4.1 Comparison of BER performance of PWM and GFSK system

Because the BER equations of ED PWM and GFSK systems are already derived and verified in the previous chapters, we will use the analytical BER curves to compare system performance directly.

In Fig. 34, Fig. 35, Fig. 36, and Fig. 37, the comparison of BER performance of

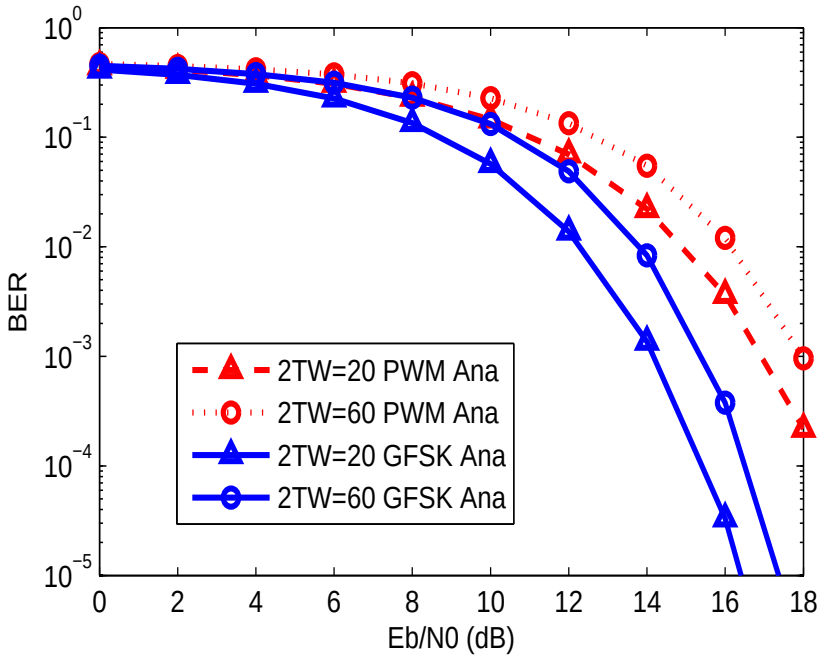

Figure 34: Comparisons of Analytical BER performance of PWM and GFSK in AWGN channels(2TW=20 and 60)

PWM and GFSK systems in AWGN channels are shown. In Fig. 34, when $2TW = 20$, GFSK achieves approximately 2.8 dB improvement over PWM at the BER= 10^{-3}. When $2TW = 60$, GFSK achieves approximately 2.7 dB improvement at the BER= 10^{-3}. In Fig. 35, when $2TW = 80$, GFSK achieves approximately 2.3 dB improvement at the BER= 10^{-3}. When $2TW = 120$, GFSK achieves approximately 2.25 dB improvement at the BER= 10^{-3}. In Fig. 36, when $2TW = 160$, GFSK achieves approximately 2.2 dB improvement at the BER= 10^{-3}. When $2TW = 220$, GFSK achieves approximately 2.2 dB improvement at the BER= 10^{-3}. In Fig. 37, when $2TW = 240$, GFSK achieves approximately 2.2 dB improvement at the BER= 10^{-3}. When $2TW = 300$, GFSK achieves approximately 2.14 dB improvement at the BER= 10^{-3}.

In Fig. 38, 39, 40, and 41, the analytical BER curves of PWM and GFSK

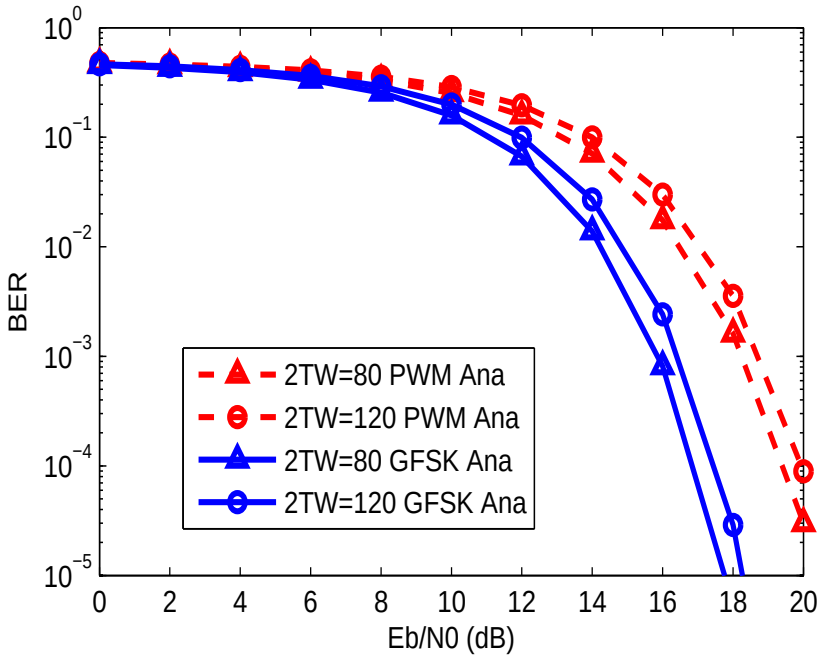

Figure 35: Comparisons of Analytical BER performance of PWM and GFSK in AWGN channels(2TW=80 and 120)

systems are shown. In Fig. 38, when $T_0 = 80$ ns, GFSK achieves approximately 2.1 dB improvement over PWM at the BER= 10^{-3}. When $T_0 = 50$ ns, GFSK achieves approximately 2.1 dB improvement at the BER= 10^{-3}. In Fig. 39, when $T_0 = 40$ ns, GFSK achieves approximately 2.1 dB improvement at the BER= 10^{-3}. When $T_0 = 30$ ns, GFSK achieves approximately 2.1 dB improvement at the BER= 10^{-3}. In Fig. 40, when T_0=25 ns, GFSK achieves approximately 2.1 dB improvement at the BER= 10^{-3}. When T_0=20 ns, GFSK achieves approximately 2.1 dB improvement at the BER= 10^{-3}. In Fig. 41, when $T_0 = 18$ ns, GFSK achieves approximately 2.1 dB improvement at the BER= 10^{-3}. When $T_0 = 14$ ns, GFSK achieves approximately 2.1 dB improvement at the BER= 10^{-3}.

In Fig. 42, Fig. 43, Fig. 44, and Fig. 45, the analytical BER curves of PWM and GFSK systems in the presence of synchronization errors are shown. In Fig. 42,

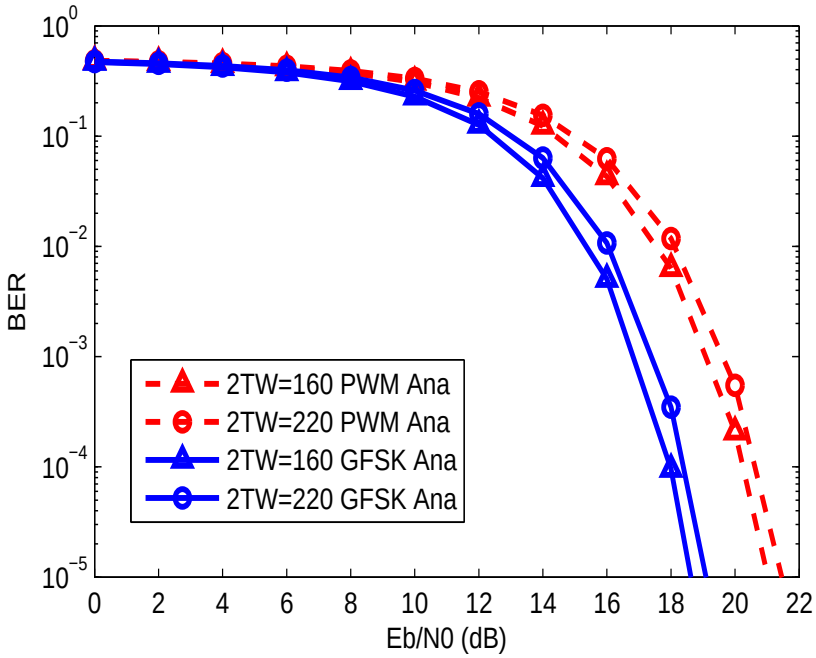

Figure 36: Comparisons of Analytical BER performance of PWM and GFSK in AWGN channels(2TW=160 and 220)

when $\varepsilon = 0$ ns, there is no synchronization error and GFSK achieves approximately 2.1 dB improvement over PWM at the BER= 10^{-3}. When $\varepsilon = 2$ ns, GFSK achieves approximately 2.1 dB improvement at the BER= 10^{-3}. In Fig. 43, when $\varepsilon = 3$ ns, GFSK achieves approximately 2.1 dB improvement at the BER= 10^{-3}. When $\varepsilon = 4$ ns, GFSK achieves approximately 2.1 dB improvement at the BER= 10^{-3}. In Fig. 44, when ε =5 ns, GFSK achieves approximately 2.1 dB improvement at the BER= 10^{-3}. When ε =10 ns, GFSK achieves approximately 2.1 dB improvement at the BER= 10^{-3}. In Fig. 45, when $\varepsilon = 15$ ns, GFSK achieves approximately 2.1 dB improvement at the BER= 10^{-3}. When $\varepsilon = 20$ ns, GFSK achieves approximately 2.1 dB improvement at the BER= 10^{-3}.

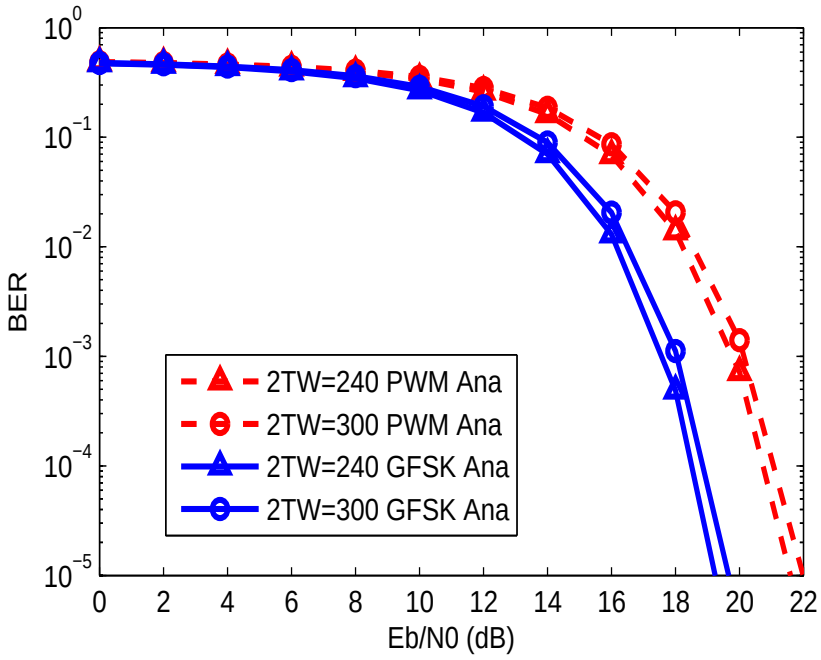

Figure 37: Comparisons of Analytical BER performance of PWM and GFSK in AWGN channels(2TW=240 and 300)

4.2 Comparison of System Complexity

GFSK systems all exhibit better BER performance in AWGN channels, multi-path channels, and in the presence of synchronization errors. However, PWM systems are more easy to implement than GFSK systems. The modulation of PWM can be obtained by assigning different α values for bits 0 and 1. In GFSK systems, the transmitter needs two different pulse generators to transmit the signal and this will increase the complexity and expense of the system. The high-order derivative pulse generators are especially more complicated than low-order generators.

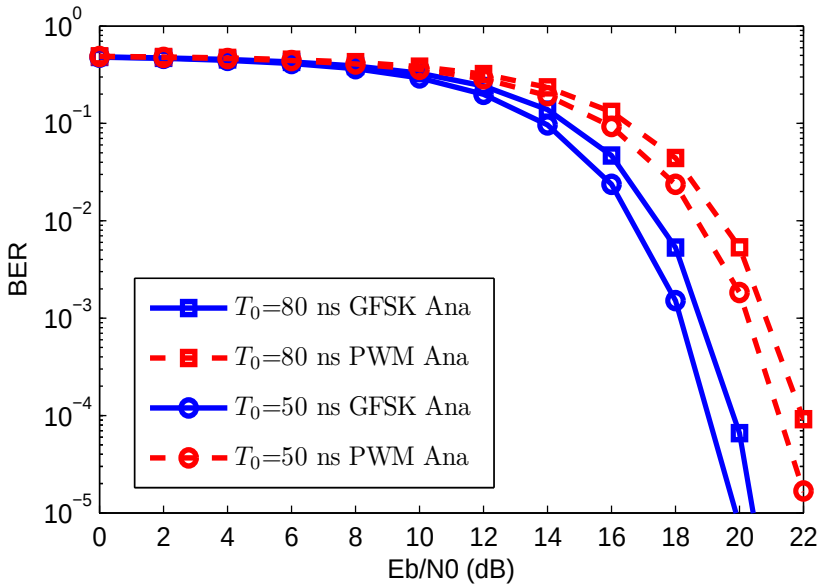

Figure 38: Comparisons of Analytical BER performance of PWM and GFSK in multipath channels(T_0=80 ns and 50 ns)

4.3 Summary

GFSK systems exhibit better BER performance than PWM systems in AWGN channels, multipath channels, and in the presence of synchronization errors. However, PWM systems have simpler structures than GFSK systems. When choosing a system, both of theses factors must be considered to decide which system is more appropriate. If performance is the most important factor to be considered, GFSK is the better candidate. If the requirement of system performance is not so stringent, then PWM can be a better candidate because the pulse generator is not so complicate and the price is lower.

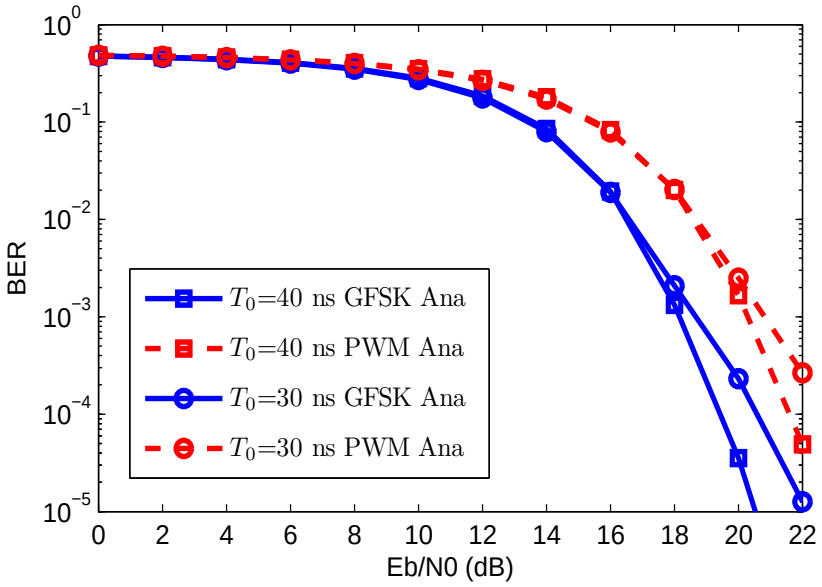

Figure 39: Comparisons of Analytical BER performance of PWM and GFSK in multipath channels(T_0=40 ns and 30 ns)

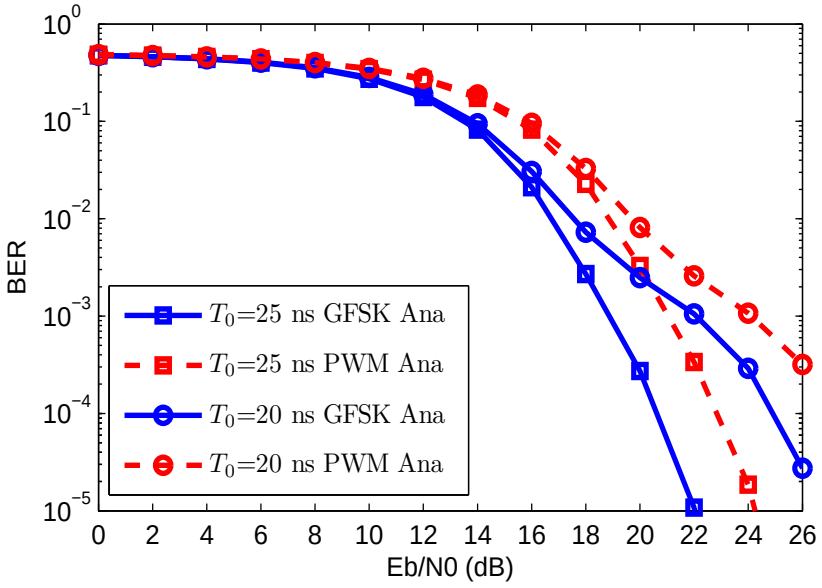

Figure 40: Comparisons of Analytical BER performance of PWM and GFSK in multipath channels(T_0=25 ns and 20 ns)

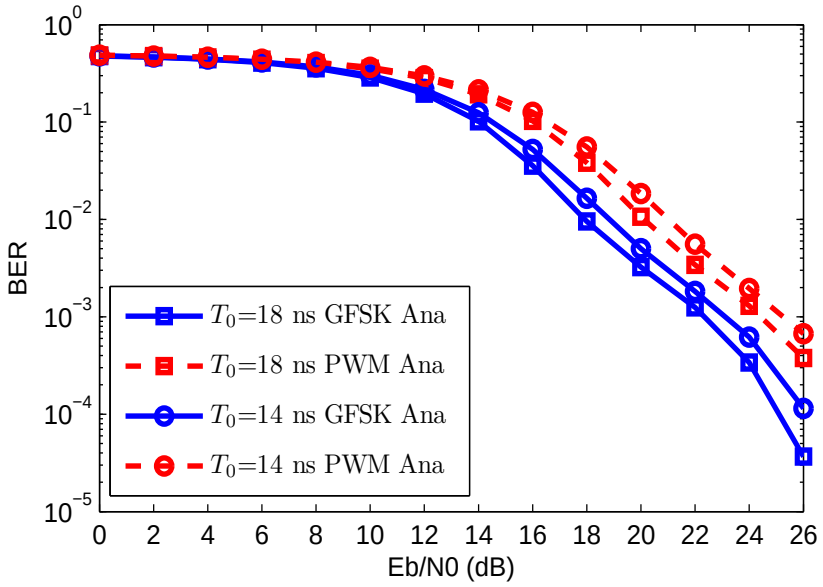

Figure 41: Comparisons of Analytical BER performance of PWM and GFSK in multipath channels(T_0=18 ns and 14 ns)

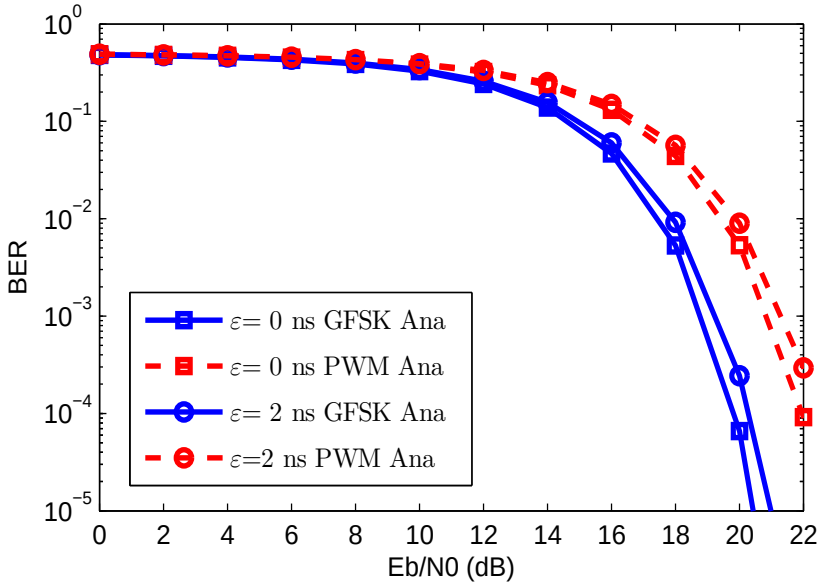

Figure 42: Comparisons of Analytical BER performance of PWM and GFSK in the presence of synchronization errors(ε =0 ns and 2 ns)

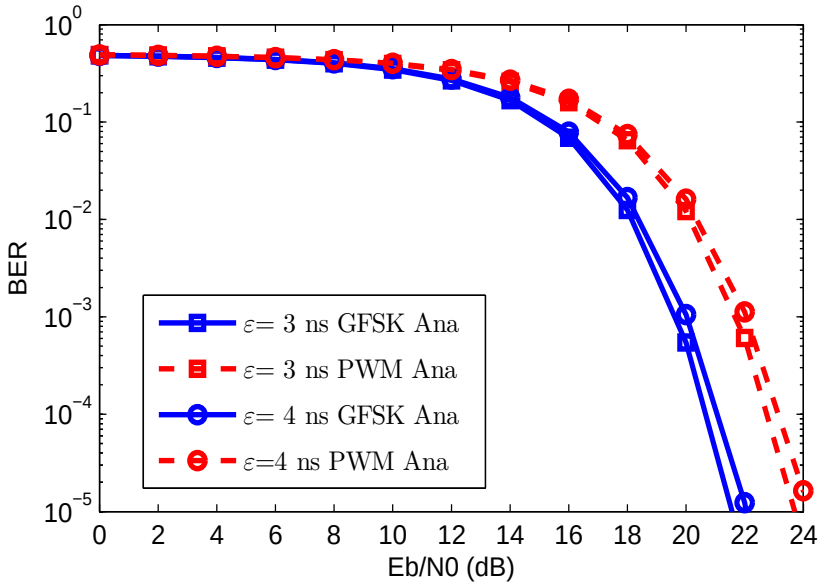

Figure 43: Comparisons of Analytical BER performance of PWM and GFSK in the presence of synchronization errors(ε =3 ns and 4 ns)

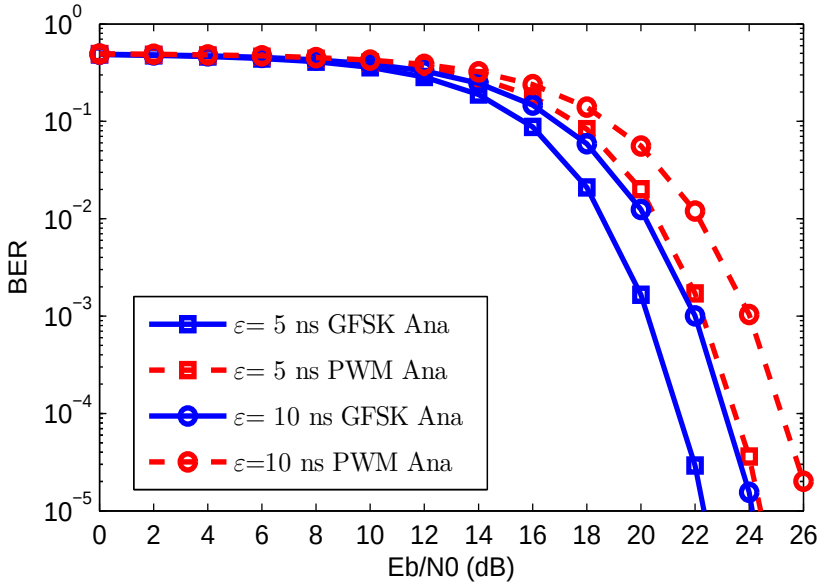

Figure 44: Comparisons of Analytical BER performance of PWM and GFSK in the presence of synchronization errors(ε =5 ns and 10 ns)

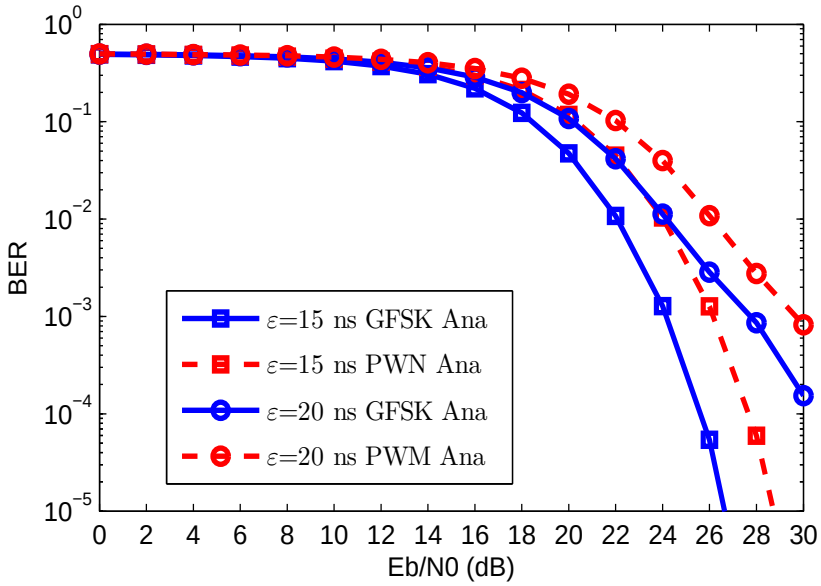

Figure 45: Comparisons of Analytical BER performance of PWM and GFSK in the presence of synchronization errors(ε =15 ns and 20 ns)

CHAPTER V

THE OPTIMAL THRESHOLD TO MITIGATE THE EFFECT OF CROSS-MODULATION INTERFERENCE AND SYNCHRONIZATION ERRORS IN ED PPM UWB SYSTEMS

In conventional energy detection PPM systems, the optimal decision threshold is 0. However, when CMI or synchronization errors occur, the optimal threshold deviates from 0 and the BER performance is degraded greatly. The optimal threshold is used to replace the 0 threshold in this chapter. The research results show that this optimal threshold effectively mitigates the effect of CMI or synchronization errors and achieves BER improvement.

The structure of this chapter is as follows: Section 5.1 analyzes the system performance in multipath channels. Section 5.2 analyzes the system performance in the presence of synchronization errors. Section 5.3 shows the simulation results and analysis. Section 5.4 summarizes this chapter.

5.1 BER Performance Analysis in Multipath Channels

In PPM systems, the modulation index δ in equation (2.18) must be chosen appropriately. If it is chosen to be too large, it will waste the transmission time and reduce the data rate. However, if it is designed to be less than the maximum channel spread D, CMI will occur [27, 30, 33]. When CMI occurs, the system performance will be degraded greatly. Even increasing the transmitting power will not improve the performance because of the proportional increase of interference [33]. When we design a system, we always want to achieve maximum transmission rate and maintain an acceptable BER performance simultaneously. The choice of an appropriate value for δ is not easy because we can not guarantee the δ value will always match the actual channel circumstance. So the effect of CMI on system performance can not be neglected. The effect of CMI on BER performance of PPM has been analysed in [30]. But the BER equation in [30] is not expressed with respect to E_b/N_0. In our previous work in Chapter 2, the BER equation is expressed in terms of E_b/N_0. However, both the works in [30] and Chapter 2 are based on $\gamma = 0$. In this chapter, the BER equation of optimal threshold PPM systems will be analyzed. To analyse the BER performance in multipath channels, we follow the method in Chapter 2 to design the frame structure. The frame structures of PPM in the presence of CMI is shown in Fig. 11 , where T_0 and T_1 are the time intervals reserved for multipath

components of bits 0 and 1, respectively. The modulation index δ is set to $\delta = T_0 = T_1$. Synchronization error is assumed to be 0. When δ is less than the maximum channel spread D, some multipath components of bit 0 extend into the interval T_1 and cause CMI. But the multipath components of bit 1 do not cause CMI and some of them just extend into the guard interval T_g, which is designed to prevent IFI. The frame period is $T_f = T_0 + T_1 + T_g$. If T_g is chosen to be too large, it will waste transmission time. So it is set $T_f = \delta + D$. This will always achieve as high a data rate as possible and prevent IFI simultaneously [27].

When bit 0 is transmitted, the pdfs of Z_1 and Z_2 are $Z_1 \sim N(N_0TW + \beta_a E_b, N_0^2TW + 2N_0\beta_a E_b)$, $Z_2 \sim N(N_0TW + \beta_b E_b, N_0^2TW + 2N_0\beta_b E_b)$, where $\beta_a = E_{T_0}/E_b$ and $\beta_b = E_{T_1}/E_b$. The meanings of E_{T_0} and E_{T_1} are the captured signal energies in integration interval T_0 and T_1, respectively. Under these conversions, E_{T_0} and E_{T_1} are expressed as $\beta_a E_b$ and $\beta_b E_b$, respectively. The values of β_a and β_b are in the range $[0, 1]$. Since $Z = Z_1 - Z_2$, we obtain

$$H_{0:}\ \ Z \sim N((\beta_a - \beta_b)E_b, 2N_0^2TW + 2N_0(\beta_a + \beta_b)E_b) \tag{5.1}$$

When bit 1 is transmitted, $E_{T_0} = 0$, the pdfs become $Z_1 \sim N(N_0TW, N_0^2TW)$ and $Z_2 \sim N(N_0TW + \beta_a E_b, N_0^2TW + 2N_0\beta_a E_b)$. The pdf of Z is

$$H_{1:}\ \ Z \sim N(-\beta_a E_b, 2N_0^2TW + 2N_0\beta_a E_b) \tag{5.2}$$

where the β_a in equation (5.2) has the same value as that in equation (5.1), but their meaning are different. In equation (5.2), $\beta_a = E_{T_1}/E_b$. After obtaining the pdf of Z, we follow the method in [29] to derive the BER formula. Firstly, we calculate the BER when bits 0 and 1 are transmitted as follows:

$$P_0 = \int_{-\infty}^{\gamma} f_0(x)dx = \int_{-\infty}^{\gamma} \frac{1}{\sqrt{2\pi}\sigma_0} e^{-\frac{(x-\mu_0)^2}{2\sigma_0^2}} dx \tag{5.3}$$

$$P_1 = \int_{\gamma}^{\infty} f_1(x)dx = \int_{\gamma}^{\infty} \frac{1}{\sqrt{2\pi}\sigma_1} e^{-\frac{(x-\mu_1)^2}{2\sigma_1^2}} dx \tag{5.4}$$

where $f_0(x)$ and $f_1(x)$ are probability density functions corresponding to equations (5.1) and (5.2), respectively. From equations (5.1) and (5.2), it is straightforward to obtain $\mu_0 = (\beta_a - \beta_b)E_b$, $\sigma_0^2 = 2N_0^2TW + 2N_0(\beta_a + \beta_b)E_b$, $\mu_1 = -\beta_a E_b$, $\sigma_1^2 = 2N_0^2TW + 2N_0\beta_a E_b$. Substituting these parameter values into equations (5.3) and (5.4) and then expressing P_0 and P_1 in terms of the complementary error function $Q(\cdot)$, we obtain

$$P_0 = Q(\frac{\mu_0 - \gamma}{\sigma_0}) = Q(\frac{(\beta_a - \beta_b)E_b - \gamma}{\sqrt{2N_0^2TW + 2N_0(\beta_a + \beta_b)E_b}}) \tag{5.5}$$

$$P_1 = Q(\frac{\gamma - \mu_1}{\sigma_1}) = Q(\frac{\gamma + \beta_a E_b}{\sqrt{2N_0^2TW + 2N_0\beta_a E_b}}) \tag{5.6}$$

The optimal threshold is obtained by setting $P_0 = P_1$ [29], and then we obtain

$$\frac{(\beta_a - \beta_b)E_b - \gamma}{\sqrt{2N_0^2TW + 2N_0(\beta_a + \beta_b)E_b}} = \frac{\gamma + \beta_a E_b}{\sqrt{2N_0^2TW + 2N_0\beta_a E_b}} \tag{5.7}$$

Solving equation (5.7), the optimal threshold is obtained as

$$\gamma = \frac{(\beta_a - \beta_b)E_b\sqrt{2TW + 2\beta_a E_b/N_0} - \beta_a E_b\sqrt{2TW + 2(\beta_a + \beta_b)E_b/N_0}}{\sqrt{2TW + 2(\beta_a + \beta_b)E_b/N_0} + \sqrt{2TW + 2\beta_a E_b/N_0}} \tag{5.8}$$

This optimal threshold depends on the captured energy in intervals T_0, T_1, and E_b/N_0. The total BER is $P_e = 0.5(P_0 + P_1)$ [29]. Since $P_0 = P_1$, it is straightforward to obtain $P_e = P_0 = P_1$. Substituting equation (5.8) into (5.6), the total BER of PPM systems using optimal threshold is obtained as

$$\begin{aligned} P_e = Q(&\frac{(\beta_a-\beta_b)(E_b/N_0)\sqrt{2TW+2\beta_a(E_b/N_0)}-\beta_a(E_b/N_0)\sqrt{2TW+2(\beta_a+\beta_b)(E_b/N_0)}}{\sqrt{2TW+2\beta_a(E_b/N_0)}(\sqrt{2TW+2(\beta_a+\beta_b)(E_b/N_0)}+\sqrt{2TW+2\beta_a(E_b/N_0)})} \\ &+\frac{\beta_a(E_b/N_0)}{\sqrt{2TW+2\beta_a(E_b/N_0)}}) \end{aligned} \tag{5.9}$$

The total BER of PPM systems using $\gamma = 0$ has been derived in Chapter 2

$$P_e = \frac{1}{2}Q(\frac{(\beta_a - \beta_b)(E_b/N_0)}{\sqrt{2TW + 2(\beta_a + \beta_b)(E_b/N_0)}}) + \frac{1}{2}Q(\frac{\beta_a(E_b/N_0)}{\sqrt{2TW + 2\beta_a(E_b/N_0)}}) \quad (5.10)$$

When no CMI occurs, $\beta_a = 1$ and $\beta_b = 0$. Substituting the values of β_a and β_b into equation (5.8), we have $\gamma = 0$. And equations (5.9) and (5.10) will obtain the same BER $P_e = Q(\frac{E_b/N_0}{\sqrt{2TW+2(E_b/N_0)}})$, when $\beta_a = 1$ and $\beta_b = 0$.

5.2 Performance Analysis in The Presence of Synchronization Errors

Fig. 13 depicts PPM frame structures when synchronization errors ε occur. And we follow the frame structure in Chapter 2 as follows: because only the effect of synchronization errors is analysed in this section, so the modulation index is set to $\delta = D = T_0 = T_1$ to avoid CMI. Assuming that coarse synchronization has been achieved, the BER performance of PPM is analyzed in the range $\varepsilon \in [0, D/2]$. To prevent IFI, the frame length is set to $T_f = 2D + T_g$, where the guard interval T_g equals to $D/2$, the maximum synchronization error used in this paper. When bit 0 is transmitted, we have $Z_1 \sim N(N_0TW + \eta E_b, N_0^2TW + 2\eta E_bN_0)$ and $Z_2 \sim N(N_0TW, N_0^2TW)$. The pdf of Z is

$$H_0 : \quad Z \sim N(\eta E_b, 2N_0^2TW + 2\eta E_bN_0) \quad (5.11)$$

where $\eta = E_{T_0}/E_b$, and $E_{T_1} = 0$. When bit 1 is transmitted, we have $Z_1 \sim N(N_0TW + (1-\eta)E_b, N_0^2TW + 2(1-\eta)E_bN_0)$ and $Z_2 \sim N(N_0TW + \eta E_b, N_0^2TW + 2\eta E_bN_0)$. And then we obtain

$$H_1 : \quad Z \sim N((1 - 2\eta)E_b, 2N_0^2TW + 2E_bN_0) \quad (5.12)$$

where η in equation (5.12) has the same value as that in equation (5.11), but in equation (5.12), $\eta = E_{T_1}/E_b$, and $E_{T_0} = (1 - \eta)E_b$. Following the method in Section 5.1,

the optimal threshold is obtained as

$$\gamma = \frac{\eta E_b\sqrt{2TW + 2E_b/N_0} + (1-2\eta)E_b\sqrt{2TW + 2\eta E_b/N_0}}{\sqrt{2TW + 2\eta E_b/N_0} + \sqrt{2TW + 2E_b/N_0}} \tag{5.13}$$

This optimal threshold depends on the captured energy in intervals T_0, T_1, and E_b/N_0. As mentioned in Section 2.3.1, $P_e = P_0 = P_1$, so we use $P_e = P_0 = Q(\frac{\mu_0-\gamma}{\sigma_0})$ to calculate the BER and obtain

$$\begin{aligned} P_e = Q(&\frac{\eta(E_b/N_0)}{\sqrt{2TW+2\eta(E_b/N_0)}} \\ &-\frac{\eta(E_b/N_0)\sqrt{2TW+2(E_b/N_0)}+(1-2\eta)(E_b/N_0)\sqrt{2TW+2\eta(E_b/N_0)}}{\sqrt{2TW+2\eta(E_b/N_0)}(\sqrt{2TW+2\eta(E_b/N_0)}+\sqrt{2TW+2(E_b/N_0)})}) \end{aligned} \tag{5.14}$$

The BER equation based on $\gamma = 0$ is given in Chapter 2

$$P_e = \frac{1}{2}Q(\frac{\eta E_b/N_0}{\sqrt{2TW + 2\eta E_b/N_0}}) + \frac{1}{2}Q(\frac{(2\eta-1)E_b/N_0}{\sqrt{2TW + 2E_b/N_0}}) \tag{5.15}$$

When no synchronization errors occur, $\eta = 1$. If we substitute $\eta = 1$ into equation (5.13), the threshold will be $\gamma = 0$. Also equations (5.14) and (5.15) will obtain the same BER value, $P_e = Q(\frac{E_b/N_0}{\sqrt{2TW+2(E_b/N_0)}})$, when $\eta = 1$.

5.3 Numerical Results and Analysis

In simulation, the bandwidth of the filters is 6 GHz and the second-order derivative of the Gaussian pulse $s(t) = (1 - 4\pi\frac{t^2}{\alpha^2})e^{-\frac{2\pi t^2}{\alpha^2}}$ is used. The shape factors α for the pulse is 0.25×10^{-9} and the corresponding pulse durations are 0.6 ns (the detail to chose a pulse width for a specific shape factor can be found in [7]). The CM4 model [32] is used in simulation and the maximum channel spread D is truncated to 80 ns.

Fig. 46, Fig. 47, and Fig. 48 show the BER performance comparisons of 0 threshold and the optimal threshold PPM systems in multipath channels. In simulation, the frame length is designed using the method mentioned in Section 5.1, so IFI

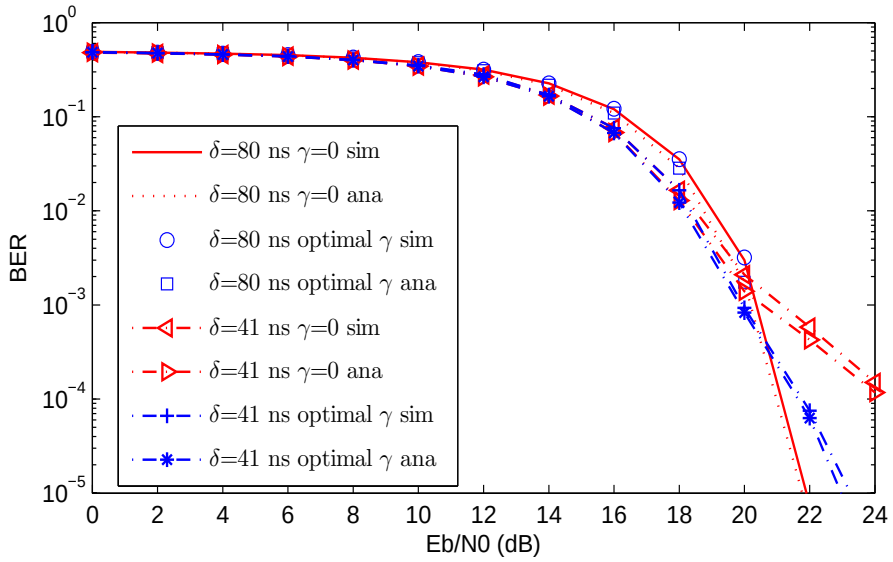

Figure 46: Comparison of BER performance of the 0 and optimal threshold PPM systems in multipath channels(CM4 model, D=80 ns, δ =80 and 41 ns)

is avoided in simulation. And synchronization is perfect. The analytical BER curves are obtained directly from equations (5.9) and (5.10), respectively. In these two equations, we need to know the values of parameters β_a and β_b . There is no mathematical formula to calculate the captured energy as a function of the length of the integration interval for IEEE 802.15.4a channel. So we follow the statistic method in Chapter 2 to obtain values for the above parameters. Firstly, we use the MATLAB code in [32] to generate realizations of the channel impulse response $h(t)$. Then we calculate the ratio of energy in a specific time interval to the total energy of a channel realization to obtain the values for these parameters. These values are substituted into (5.9) and (5.10) to achieve the analytical BER. Both the simulated and the analytical BER are obtained by averaging over 100 channel realizations. In Fig. 46, when $\delta = 80$ ns, no CMI occurs and the 0 threshold and the optimal PPM systems achieve the same BER performance. When $\delta = 41$ ns, the optimal threshold PPM achieves better BER performance than the 0 threshold PPM, and the improvement is approximately 0.7

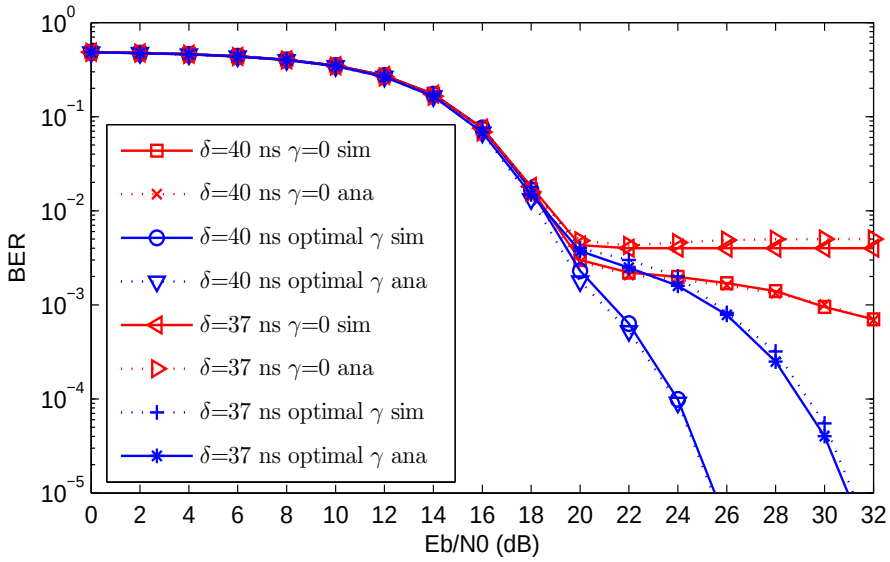

Figure 47: Comparison of BER performance of 0 and optimal threshold PPM systems in multipath channels(CM4 model, D=80 ns, δ =40 and 37 ns)

dB at BER=10^{-3}. In Fig. 47, when δ = 40 ns, the optimal threshold PPM achieves better BER performance than the 0 threshold PPM and the improvement is approximately 9 dB at BER=10^{-3}. When δ = 37 ns, the optimal threshold PPM requires an increase of E_b/N_0 approximately 4.5 dB to maintain BER=10^{-3}. However, the 0 threshold PPM can not achieve this BER level and the BER performance can not be improved by increasing the transmitted power due to the proportional increase of CMI [33]. This phenomena is called BER floor. In Fig. 48, the δ values are 35 and 30 ns, respectively. The BER curves of the 0 threshold PPM all exhibit BER floors. Unlike the 0 threshold PPM, however, the optimal threshold PPM still achieves a good BER performance when the signal transmitting power is increased.

Fig. 49, Fig. 50, and Fig. 51 show comparisons of BER performance in the presence of synchronization errors. In simulation, the modulation index δ is set to the maximum channel spread D = 80 ns to avoid CMI. The frame structure is designed by following the method mentioned in Section 5.2, so IFI is avoided in simulation.

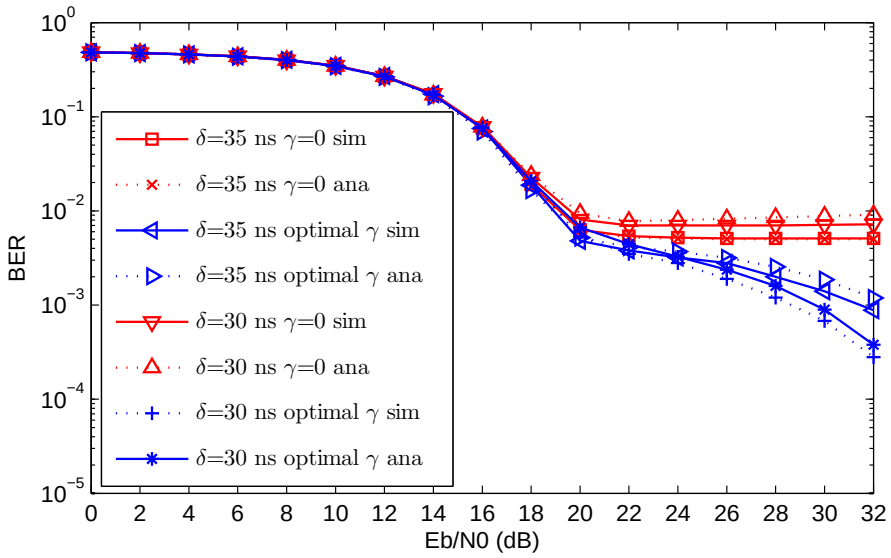

Figure 48: Comparison of BER performance of 0 and optimal threshold PPM systems in multipath channels(CM4 model, D=80 ns, δ =35 and 30 ns)

The analytical BER curves are obtained directly from equations (5.14) and (5.15), and the values for parameters η in equations (5.14) and (5.15) are obtained by using the statistic method in Chapter 2. Both the simulated and analytical BERs are obtained by averaging over 100 channel realizations. In Fig. 49, when $\varepsilon = 0$ ns, no synchronization error occurs, and the 0 threshold and the optimal threshold PPM achieve the same BER performance. When $\varepsilon = 2$ ns, the optimal threshold PPM achieves better BER performance than the 0 threshold PPM. The improvement at BER= 10^{-3} is approximately 0.4 dB. In Fig. 50, when $\varepsilon = 3$ ns, the optimal threshold PPM achieves approximately 2 dB improvement at BER=10^{-3}. When $\varepsilon = 4$ ns, the optimal threshold PPM achieves approximately 7 dB improvement at BER=10^{-3}. In Fig. 51, the values of ε are 5 and 7 ns, respectively. The BER curves of the 0 threshold PPM are extremely bad and exhibit BER floors because of severe synchronization errors, but the optimal threshold PPM still achieves a good BER performance when transmitting power is increased.

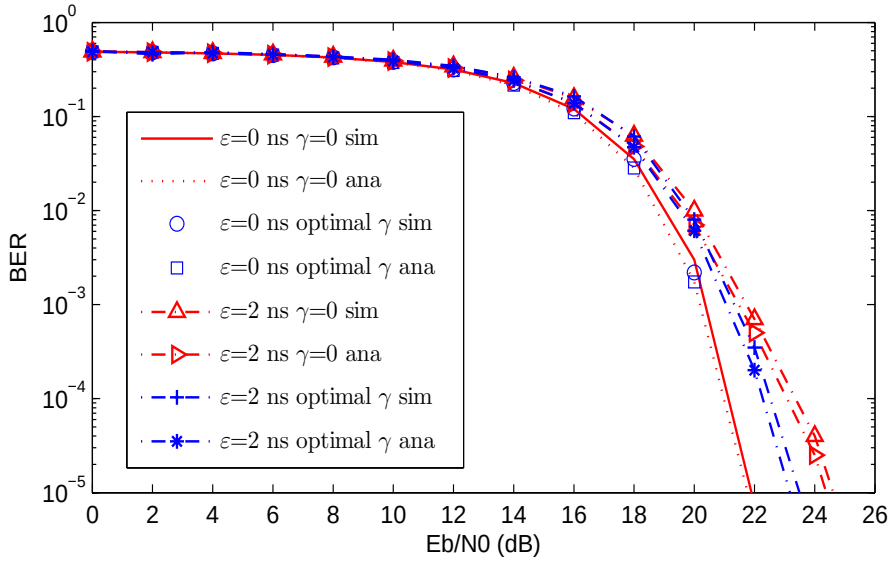

Figure 49: Comparison of BER performance of 0 and optimal threshold PPM systems in the presence of synchronization errors(CM4 model, D=80 ns, ε =0 and 2 ns)

The reason that the optimal threshold PPM systems achieve better BER performance in the presence of CMI and synchronization can be explained as follows. The orthogonality of PPM systems is achieved in time domain. When CMI and synchronization errors occur, this orthogonality is easy to be destroyed. After loss of the orthogonality, the signal energy counteraction occurs between T_0 and T_1, and then this will lead to a great reduction of euclidean distance. Consequently, the system performance is degraded severely. This can be verified by observing the mean values of equations (5.1) and (5.12). Also CMI and synchronization errors can cause the unsymmetrical pdfs between bit 0 and 1. When we observe the mean values and variance of equations (5.1) and (5.2), we will find that their mean values are not symmetrical to 0 point and their variance are different. Similarly, equations (5.11) and (5.12) also exhibit the same phenomena. Fig. 52 show the pdf curves of bit 0 and 1 in the absence and presence CMI. When there is no CMI, the pdf curves of bit 0 and 1 are symmetrical to 0 point. However, when CMI occurs, this symmetry is

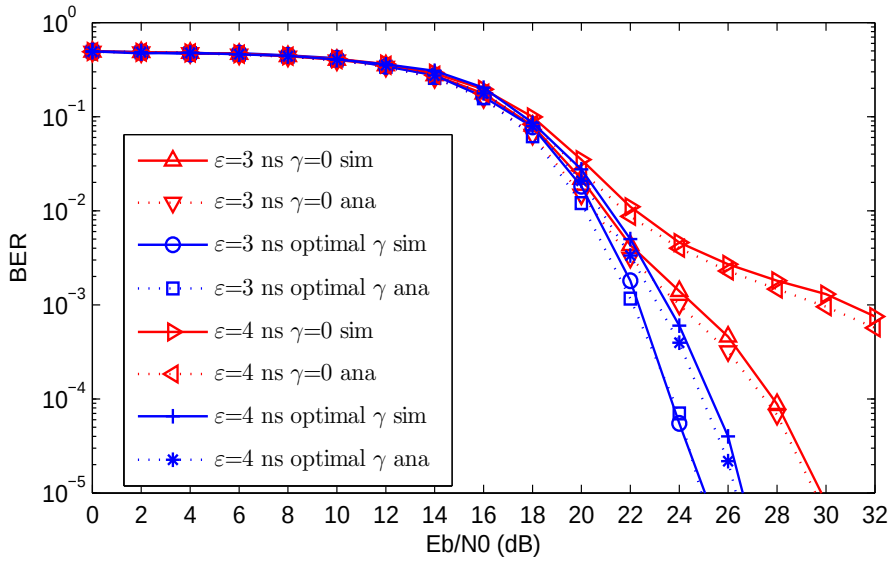

Figure 50: Comparison of BER performance of 0 and optimal threshold PPM systems in the presence of synchronization errors(CM4 model, D=80 ns, ε =3 and 4 ns)

destroyed. The mean values in equations (5.1) and (5.2) are $(\beta_a - \beta_b)E_b$ and $-\beta_a E_b$. In the presence of CMI, if we still chose 0 as the decision threshold, it will deviate from the optimal threshold and cause a large number of decision errors. In the optimal threshold system, the receiver always use the optimal threshold to determine the transmitted signal. And this will achieve better BER performance. Similarly, when synchronization errors occur, the optimal threshold system exhibit better BER performance than the 0 threshold system because of the use of optimal threshold.

In the following, we will use the analytical BER to compare the BER performances of GFSK and PWM with the optimal threshold PPM, respectively.

In Fig. 53, Fig. 54, and Fig. 55, the BER performance of GFSK and the optimal threshold PPM systems are compared in multipath channel. we will use the same parameters as Chapter 3 to compare these two systems. In Fig. 53, the values of δ are 80 ns and 50 ns, respectively. When δ =80 ns, GFSK and the optimal threshold PPM achieves the same BER performance. When δ =50 ns, GFSK achieves approxi-

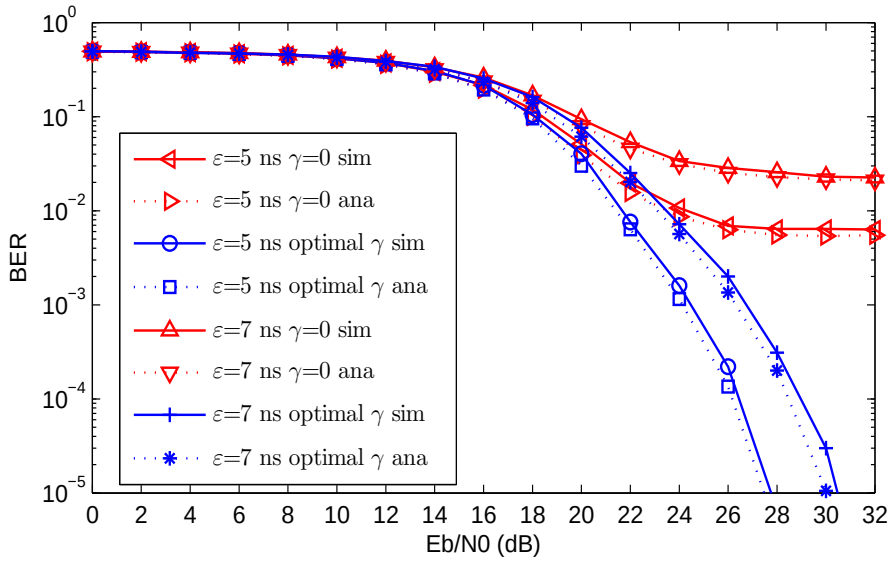

Figure 51: Comparison of BER performance of 0 and optimal threshold PPM systems in the presence of synchronization errors(CM4 model, D=80 ns, ε =5 and 7 ns)

mately 0.1 dB improvement at BER= 10^{-3}. In Fig. 29 of Chapter 3, GFSK achieves approximately 0.2 dB improvement over 0 threshold PPM. It seems that the optimal threshold can improve BER performance in the presence of CMI. In Fig. 54, when δ =40 ns and 30 ns, GFSK achieves approximately 1.5 dB and 9.8 dB improvement over the optimal threshold PPM at BER= 10^{-3}, respectively. However, in Fig. 30 of Chapter 3, when δ =40 ns, GFSK achieves 7.5 dB improvement over the 0 threshold PPM at BER= 10^{-3}. And when δ =30 ns, the BER curve in Fig. 30 exhibit a BER floor. We can see that the performance improvement of the optimal threshold PPM system is great when CMI increases. In Fig. 55, δ =20 ns and 14 ns, the optimal threshold PPM system still exhibit BER floors.

Fig. 56 and Fig. 57 show the comparison of BER performance of GFSK and the optimal threshold PPM in the presence of synchronization error. In Fig. 56, when ε =0 ns, GFSK and the optimal threshold PPM achieve the same BER performance. When ε =2 ns, GFSK achieves approximately 0.6 dB improvement at BER= 10^{-3}.

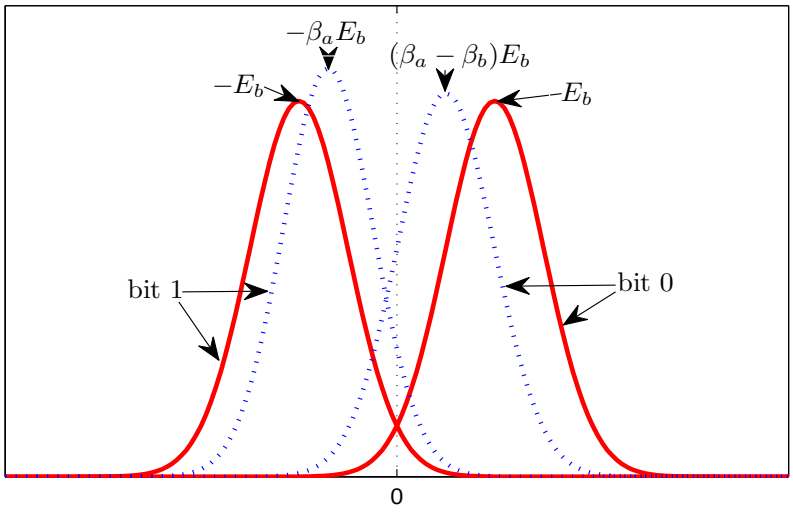

Figure 52: the curves of pdf of bit 0 and 1 in the absence and presence CMI

In Fig. 32 of Chapter 3, GFSK achieves approximately 1 dB improvement over 0 threshold PPM at BER= 10^{-3}. In Fig. 57, ε =3, 10, and 15 ns, respectively. When δ =3 ns, GFSK achieves approximately 1.2 dB improvement at BER= 10^{-3}. However, in Fig. 33 of Chapter 3, GFSK achieves approximately 3.2 dB improvement. When ε =, the optimal threshold PPM still exhibit BER floors.

Fig. 58, Fig. 59, and Fig. 60 show the comparison of BER performance of PWM and the optimal threshold PPM in multipath channels. In Fig. 58, when δ =80 ns, the optimal threshold PPM achieves approximately 2 dB improvement at BER= 10^{-3}. It is the same as the 0 threshold PPM because no CMI occurs when δ =80 ns. When δ =50 ns, the optimal threshold PPM achieves approximately 2 dB improvement at BER= 10^{-3}. In Fig. 59, when δ =40 ns, the optimal threshold PPM still achieves approximately 0.5 dB improvement at BER= 10^{-3}. But in Fig. 18 of Chapter 2, PWM has achieved 5.8 dB improvement over the 0 threshold PPM at BER= 10^{-3}. In Fig. 59, when δ =30 ns, PWM achieves approximately 8.1 dB improvement at

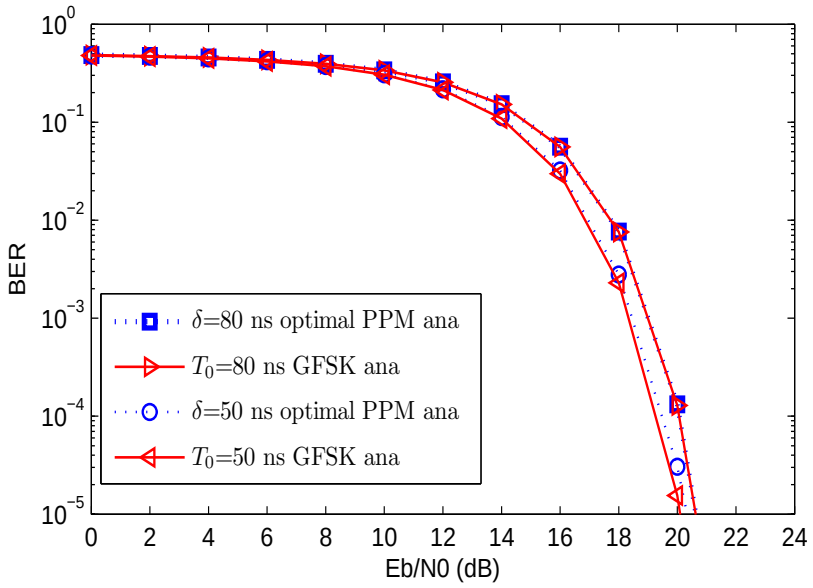

Figure 53: Comparison of BER performance of GFSK and optimal threshold PPM systems in multipath channels(CM4 model, D=80 ns, δ =80 and 50 ns)

BER= 10^{-3}. However, in Fig. 18 of Chapter 2, the 0 threshold PPM has exhibit a BER floor. In Fig. 60, the optimal threshold PPM still exhibit BER floors.

Fig. 61 and Fig. 62 show the comparison of BER performance of PWM and the optimal threshold PPM in the presence of synchronization errors. In Fig. 61, when ε =0 ns, no synchronization errors occur and the optimal threshold PPM achieves 2 dB improvement at BER= 10^{-3}. When ε =3 ns, the optimal threshold PPM achieves 0.9 dB improvement at BER= 10^{-3}. In Fig. 20 of Chapter 2, PWM has achieved better BER performance than the 0 threshold PPM when ε =3 ns. The improvement is approximately 1.6 dB at BER= 10^{-3}. In Fig. 62, when ε =4 ns, PWM and the optimal threshold PPM need the same value of E_b/N_0 to achieve BER= 10^{-3}. When ε =10 ns, PWM still achieves a good BER performance , however, the optimal threshold PPM can not arrive to this BER level.

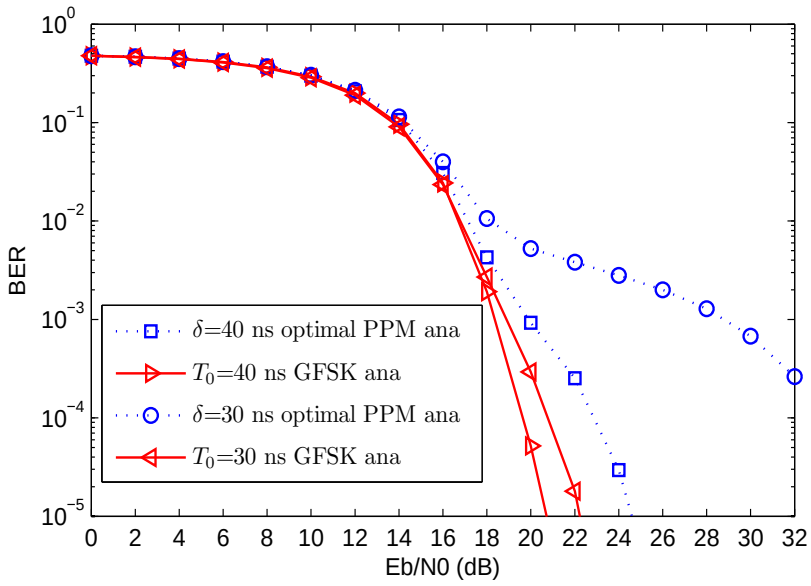

Figure 54: Comparison of BER performance of GFSK and optimal threshold PPM systems in multipath channels(CM4 model, D=80 ns, δ =40 and 30 ns)

5.4 Summary

In this chapter, the optimal threshold is used to replace the 0 threshold conventional ED PPM UWB systems. The BER performance of PPM system with the optimal threshold is analyzed and compared to the 0 threshold PPM systems. In the presence of CMI or synchronization errors, the 0 threshold is no longer the optimal threshold and leads to the degradation of system BER performance in ED PPM systems. The application of optimal threshold can improve the system performance because the optimal threshold always achieves the optimal decision threshold. Especially, when severe CMI or synchronization errors occur, the system achieves great performance improvement. Also we compare the BER performance of the optimal threshold PPM to PWM and GFSK in multipath channels and in the presence of synchronization errors. The research results show that the performance improvements of PWM and GFSK over PPM are reduced when an optimal threshold is applied to

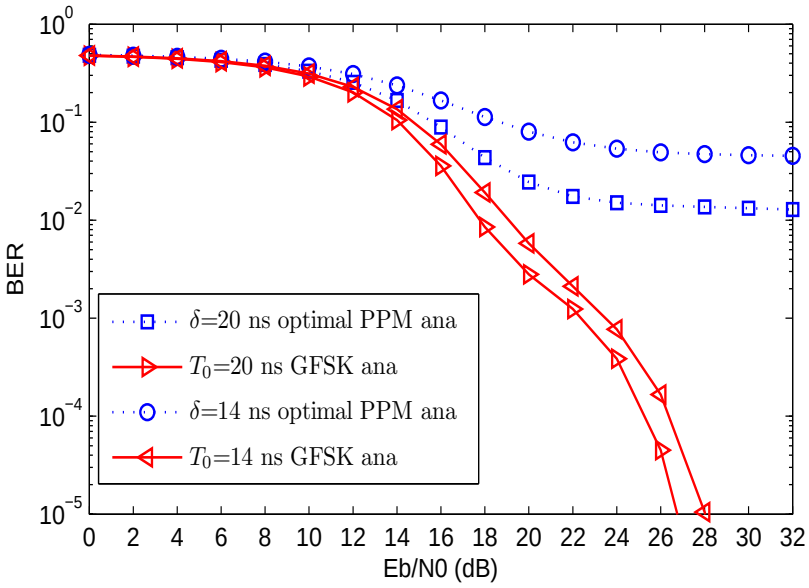

Figure 55: Comparison of BER performance of GFSK and optimal threshold PPM systems in multipath channels(CM4 model, D=80 ns, δ =20 and 14 ns)

PPM. Although the BER performance of PPM is improved after the application of an optimal threshold, the system performance is still worse than PWM and GFSK because this optimal threshold can not entirely remove the effect of energy counteraction between interval T_0 and T_1, which leads to a greater reduction of euclidian distance. However, the optimal threshold has brought great performance improvement, and it is still very significant.

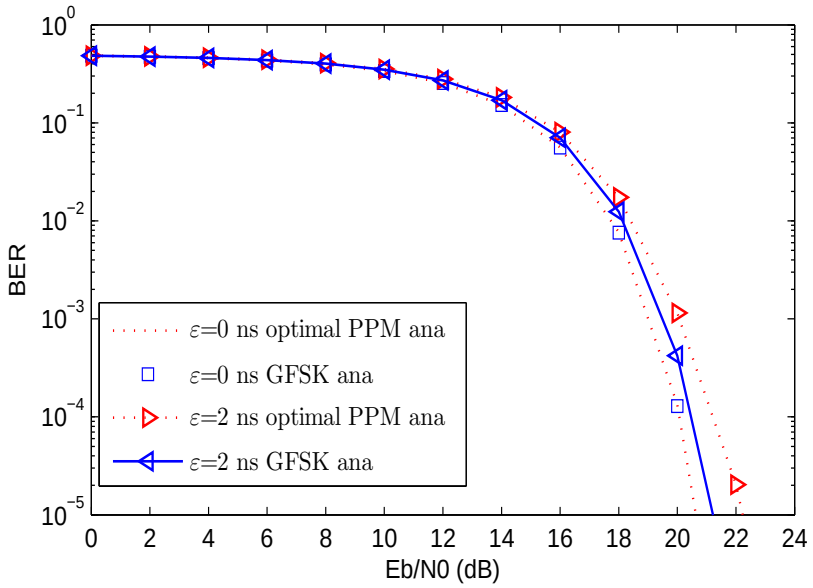

Figure 56: Comparison of BER performance of GFSK and optimal threshold PPM systems in multipath channels(CM4 model, D=80 ns, ε =0 and 2 ns)

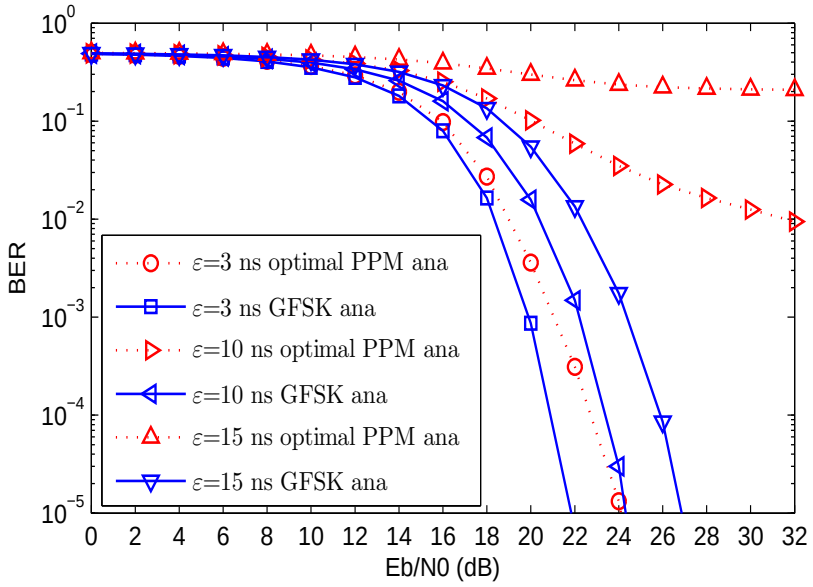

Figure 57: Comparison of BER performance of GFSK and optimal threshold PPM systems in multipath channels(CM4 model, D=80 ns, ε =3, 10, and 15 ns)

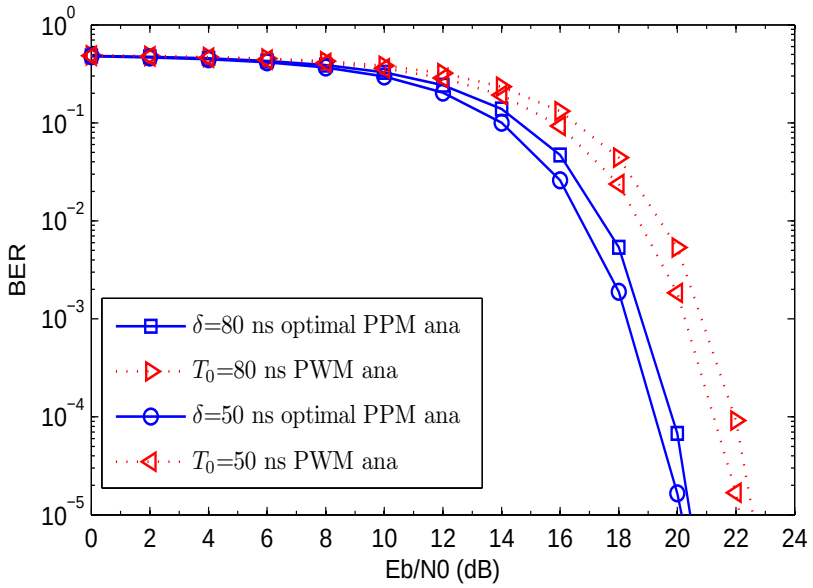

Figure 58: Comparison of BER performance of PWM and optimal threshold PPM systems in multipath channels(CM4 model, D=80 ns, δ =80 and 50 ns)

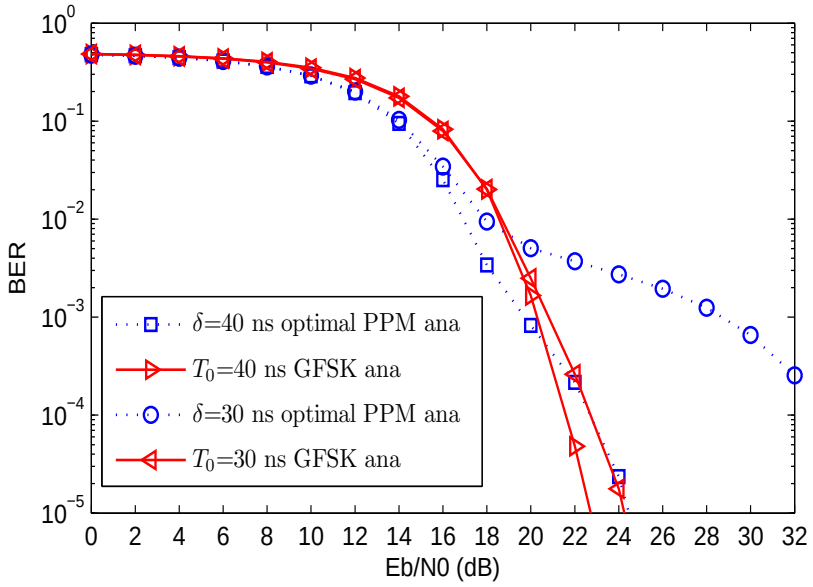

Figure 59: Comparison of BER performance of PWM and optimal threshold PPM systems in multipath channels(CM4 model, D=80 ns, δ =40 and 30 ns)

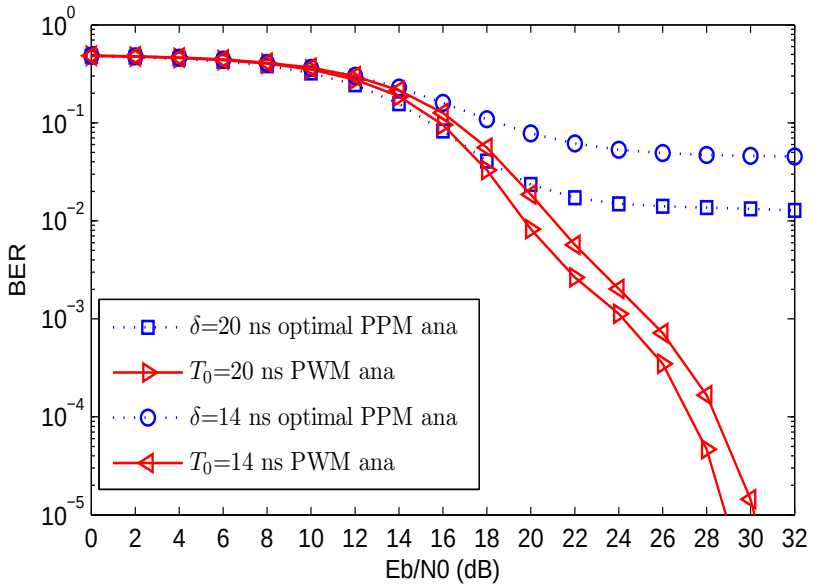

Figure 60: Comparison of BER performance of PWM and optimal threshold PPM systems in multipath channels(CM4 model, D=80 ns, δ =20 and 14 ns)

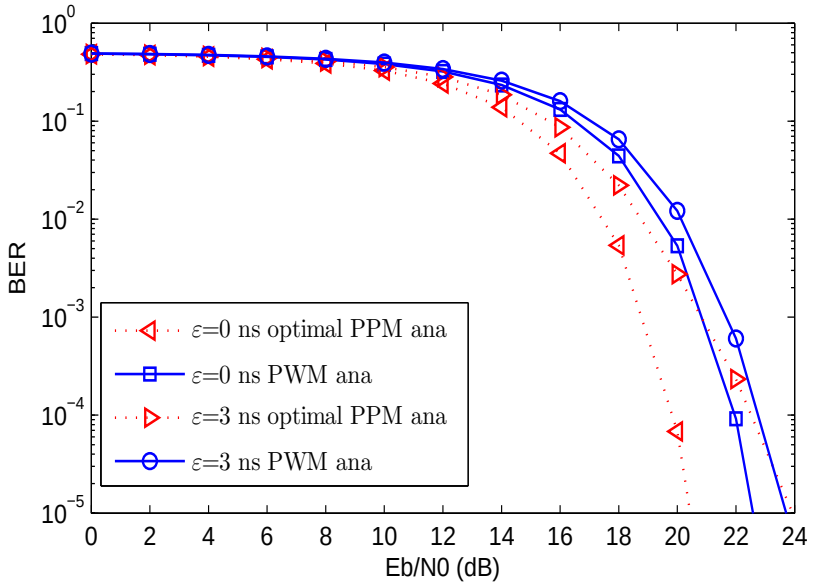

Figure 61: Comparison of BER performance of PWM and optimal threshold PPM systems in multipath channels(CM4 model, D=80 ns, ε =0 and 3 ns)

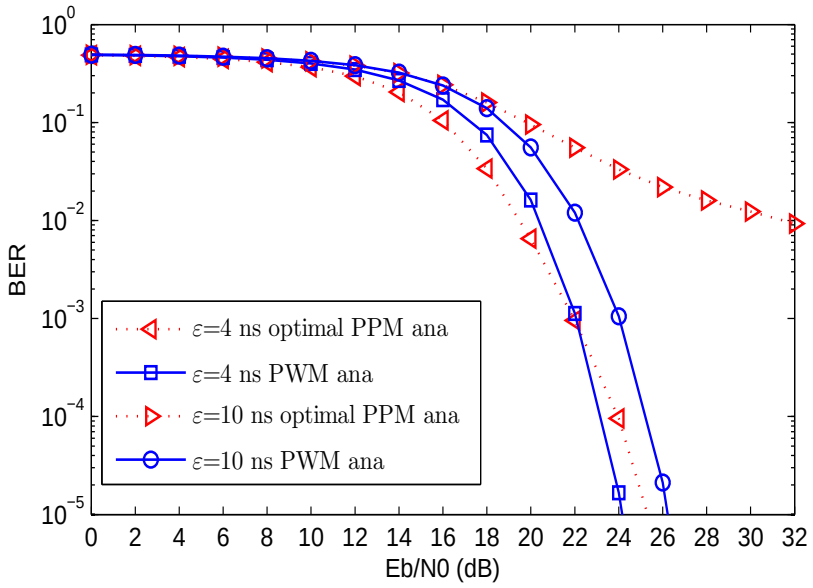

Figure 62: Comparison of BER performance of PWM and optimal threshold PPM systems in multipath channels(CM4 model, D=80 ns, ε =4 and 10 ns)

CHAPTER VI

PWM AND GFSK SYSTEM VERSUS UWB POWER MASK

In Chapter 2 and 3, the PWM and GFSK are analyzed and researched without considering the emission power limit. Because UWB systems occupy super wide frequency ranges, the FCC has set a strict emission mask to avoid the possible interference of UWB to other systems. Table I is the emission mask at different frequencies set by the FCC [1]. Usually, UWB system use -10dB bandwidth, so we at least guarantee the -10 dB bandwith point of signal spectra falls under the emission mask. That is the -10 dB bandwidth point is in the range of 3.1-10.6 GHz [1]. Because the signal spectra of PWM occupy different width and that of GFSK locate at different center frequency, it is necessary that we analyze whether the signal spectra of these two systems matches the requirement of the FCC mask. If it is not a good match, we must find some method to remedy our systems.

Table I: UWB Emission Mask Set by Federal Communication Commission (FCC)

Frequency in MHz	Emission Mask in dBm
0-960	-41.3
960-1610	-75.3
1610-1990	-53.3
1990-3100	-51.3
3100-10600	-41.3
Above 10600	-51.3

6.1 Signal Spectra of PWM Systems Versus FCC Emission Mask

In Chapter 2, when we analyze the performance of PWM systems, the 2nd-order derivative of the Gaussian pulse is used, Fig. 63, Fig. 64 and Fig. 65 show the spectra of PWM signals with different α values versus FFC emission mask. In Fig. 63, the shape factor $\alpha = 0.25 \times 10^{-9}$ and 0.5×10^{-9} are used for pulses to transmit bits 0 and 1, respectively. We can see from Fig. 63 that both spectral curves do not match the requirement of FCC emission mask. Even the center frequency of the pulse with a shape factor $\alpha = 0.5 \times 10^{-9}$ is not in the range of 3.10-10.6 GHz. From equation (2.9) and (2.8), we can establish that when the value of α is decreased, the center frequency of the signal spectra will move to higher frequency and the bandwidth is also increased, so we will try smaller α values to move the center frequency of signal spectra into the range of 3.1-10.6 GHz. In Fig. 64, the values of the shape factor are $\alpha = 0.25 \times 10^{-9}$ and 0.125×10^{-9}, respectively. Although the center frequencies of both spectral curves are moved to higher frequencies, the curves of $\alpha = 0.25 \times 10^{-9}$ still do not match the FCC mask. In Fig. 65, the values of $\alpha = 0.1 \times 10^{-9}$ and $\alpha = 0.2 \times 10^{-9}$ are used. The spectral curve of $\alpha = 0.2 \times 10^{-9}$ still does not match the requirement. Moreover, the spectral curve of $\alpha = 0.1 \times 10^{-9}$ surpasses the FCC mask due to the larger bandwidth generated from small α value.

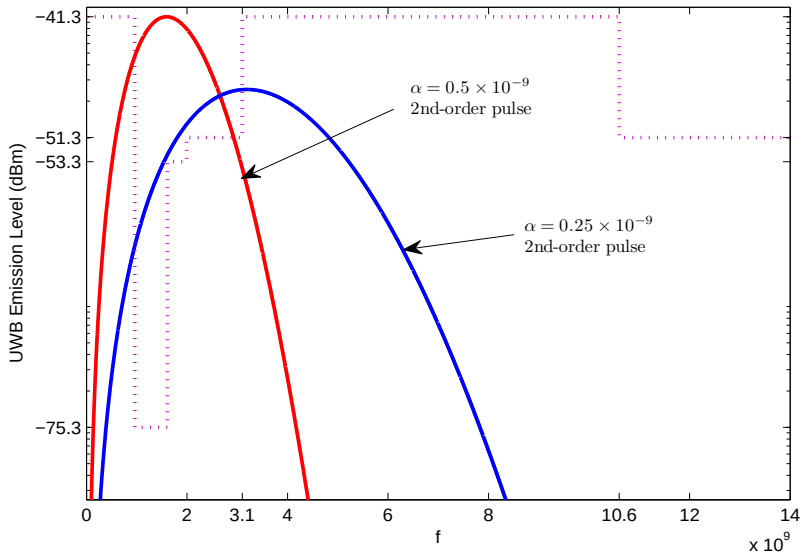

Figure 63: Spectra of PWM signals versus FCC emission mask, 2nd-order derivative of the Gaussian pulse , shape factor $\alpha = 0.25 \times 10^{-9}$ and 0.5×10^{-9}

Based on the above analysis, it is apparent that it is difficult to find appropriate α values for PWM systems using the second-order derivative of the Gaussian pulse.

To solve the problem of PWM systems, we will pick appropriate α values to obtain an acceptable bandwidth and simultaneously use a higher-order derivative pulse to move signal spectra to match the FCC mask. When we try to use high-order derivative pulses, we found that the bandwidth of the pulse generated from 2α is still half of that of the pulse generated from α. However, the center frequencies of these two pulses do not maintain the characteristics as the second-order pulse. Consequently, if we still use two filters like that in Chapter 2, the energy of pulse generated from 2α will not fall into the passband of Filter 1. So we will use different-order derivatives for pulses generated from shape factors α and 2α, respectively. Fig. 66, Fig. 67 and Fig. 68 show the spectral curves of pulses with different-order derivatives and α values. In Fig. 66, the spectral curves are those of pulses of 16th-order with $\alpha = 0.5 \times 10^{-9}$ and 8th-order with $\alpha = 0.25 \times 10^{-9}$. In Fig. 67, the spectral curves are those of pulses

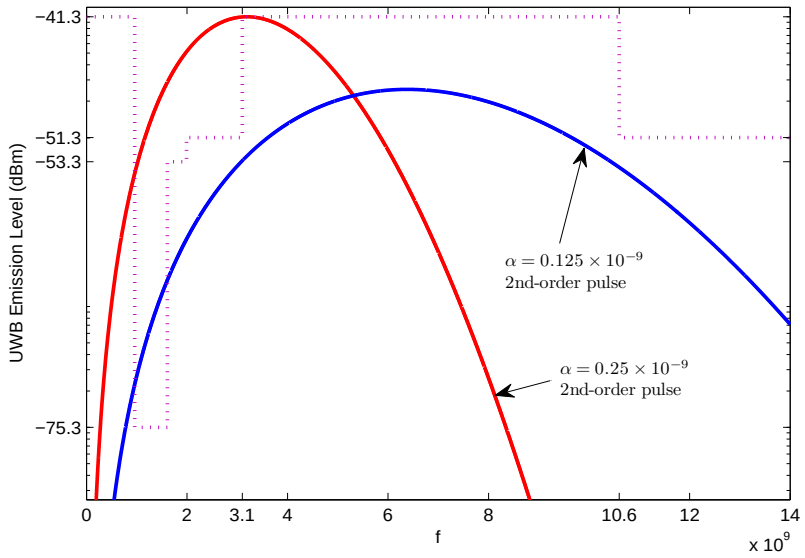

Figure 64: Spectra of PWM signals versus FCC emission mask, 2nd-order derivative of the Gaussian pulse, shape factor $\alpha = 0.125 \times 10^{-9}$ and 0.25×10^{-9}

of 11th-order with $\alpha = 0.4 \times 10^{-9}$ and 5th-order with $\alpha = 0.2 \times 10^{-9}$. In Fig. 68, the spectral curves are those of pulses of 11th-order with $\alpha = 0.35 \times 10^{-9}$ and 5th-order with $\alpha = 0.175 \times 10^{-9}$. These combinations all match the FCC mask and maintain the characteristics of PWM systems. In these three figures, the scale of Y coordinate is logarithmic, and the signal energy below -10 dB point (-51.3 dBm in these three figures) is very low. For convenience, a linear-scale version of Fig. 67 is shown in Fig. 69. Two bandpass filters are shown in in Fig. 69.

To verify whether the previous results in Chapter 2 are still effective after we apply different-order derivatives to our PWM system, we will run the simulation again. In Chapter 2, $p_0(t)$ and $p_1(t)$ are 2nd-order derivative pulses with the same amplitude but different widths, and we have proven that $E_1 = 2E_0$. Now, we are using different-order derivative pulses, and we still set the energy relationship of $p_0(t)$ and $p_1(t)$ to $E_1 = 2E_0$. However, it is not necessary to maintain the same amplitudes because their waveforms are different. The shape factors of $p_0(t)$ and $p_1(t)$ are still α

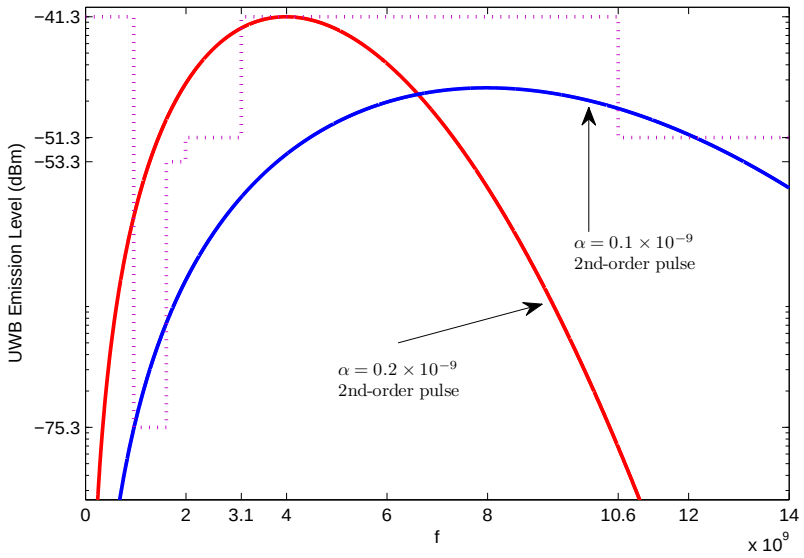

Figure 65: Spectra of PWM signals versus FCC emission mask, 2nd-order derivative of the Gaussian pulse , shape factor $\alpha = 0.1 \times 10^{-9}$ and $\alpha = 0.2 \times 10^{-9}$

and 2α. Under these assumptions, the energy and spectral relationship of $p_0(t)$ and $p_1(t)$ are still the same as that in Chapter 2. In Fig. 69, the spectral curves of $p_1(t)$ are generated from the 11th-order derivative pulse with a shape factor $\alpha = 0.4 \times 10^{-9}$, and that of $p_0(t)$ are generated from the 5th-order derivative pulse with a shape factor $\alpha = 0.2 \times 10^{-9}$. The bandwidths of the filters are 3.2 GHz. In the following simulation, we will analyze a PWM system with different-order derivative pulses in AWGN channels, multipath channels and in the presence of synchronization errors. The analytical BER curves are generated from equations (2.34), (2.45) and (2.52), respectively. The equations of the 5th- and 11th-order derivatives of the Gaussian pulse are obtained by performing $\frac{d^5}{dt^5}(\frac{\sqrt{2}}{\alpha}e^{\frac{-2\pi t^2}{\alpha^2}})$ and $\frac{d^{11}}{dt^{11}}(\frac{\sqrt{2}}{\alpha}e^{\frac{-2\pi t^2}{\alpha^2}})$ using Maple.

$$s(t)_5 = (-960t + \frac{2560\pi t^2}{\alpha^2} - \frac{1024\pi^2 t^5}{\alpha^4})e^{-\frac{2\pi t^2}{\alpha^2}} \tag{6.1}$$

$$\begin{aligned} s(t)_{11} = (&42577920t - \frac{283852800\pi t^3}{\alpha^2} + \frac{454164480\pi^2 t^5}{\alpha^4} \\ &- \frac{259522560\pi^3 t^7}{\alpha^6} + \frac{57671680\pi^4 t^9}{\alpha^8} - \frac{4194304\pi^5 t^{11}}{\alpha^{10}})e^{-\frac{2\pi t^2}{\alpha^2}} \end{aligned} \tag{6.2}$$

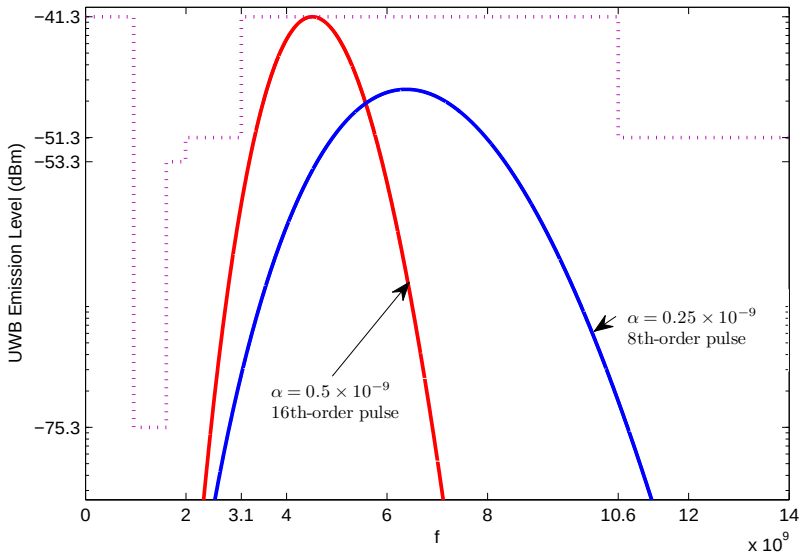

Figure 66: Spectra of PWM signals versus FCC emission mask, 16th-order pulse with $\alpha = 0.5 \times 10^{-9}$ and 8th-order pulse with $\alpha = 0.25 \times 10^{-9}$

Equation (6.1) and (6.2) have the common term $\frac{\sqrt{2}\pi^3}{\alpha^7}$ and $\frac{\sqrt{2}\pi^6}{\alpha^{13}}$, respectively. They are both constant and do not affect the waveform, so they are removed. In Fig. 70, the waveforms of the 5th- and 11th-order pulses are shown.

In Fig. 71 and Fig. 72, the BER curves of PWM with different-order derivative pulses in AWGN channels are shown. The analytical curves are directly generated from equations (2.34). In Fig. 71, the values of $2TW$ are 7, 30 and 50, respectively. In Fig. 72, the values of $2TW$ are 70, 120 and 170, respectively. When the values of $2TW$ increase, the analytical curves match the simulated curves better. Also, the BER performance is degraded when $2TW$ increases because more noise energy is captured. These results are similar to that in Chapter 2. This proves that the BER equation (2.34) of a PWM system in AWGN channels is still effective after we use different-order derivative pulses. Equation (2.34) does not depend on the waveforms used. When two waveforms satisfy two conditions, equation (2.34) is effective. The first condition is that the bandwidth of the spectrum of bit 0 is half of that of bit 1

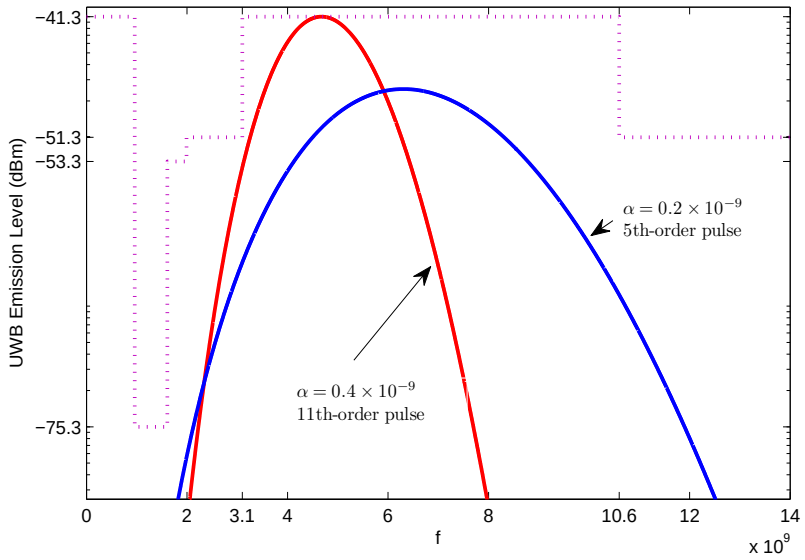

Figure 67: Spectra of PWM signals versus FCC emission mask, 11th-order pulse with $\alpha = 0.4 \times 10^{-9}$ and 5th-order pulse with $\alpha = 0.2 \times 10^{-9}$

and the spectrum of bit 0 falls in the left half range of the spectrum of bit 1. Secondly, the transmitting energy of bit 1 is controlled to be twice of that of bit 0.

In Fig. 73, Fig. 74 and Fig. 75, the BER curves of PWM systems with different-order derivative pulses in multipath channels are shown. The CM4 model of the IEEE 802.15.4a channel model is used in simulation. The maximum channel spread D is truncated to 80 ns. The analytical BER curves are generated from equation (2.45). The values of parameter λ in equation (2.45) is obtained by using the same method in Chapter 2. In Fig. 73, the integration time T_0 is 80 and 50 ns, respectively. When $T_0 = 80$ ns, the integrator captures almost all of the signal energy. When $T_0 = 50$ ns, the integrator misses some of the signal energy but it captures less noise energy. Therefore the BER performance is improved. In Fig. 74, the integration time T_0 =40 and 30 ns. In Fig. 75, the integration time T_0 =25 and 20 ns. In all of these three figures, all simulated curves match analytical curves very well. This proves that the equation (2.45) is also effective to PWM systems with different-order derivative

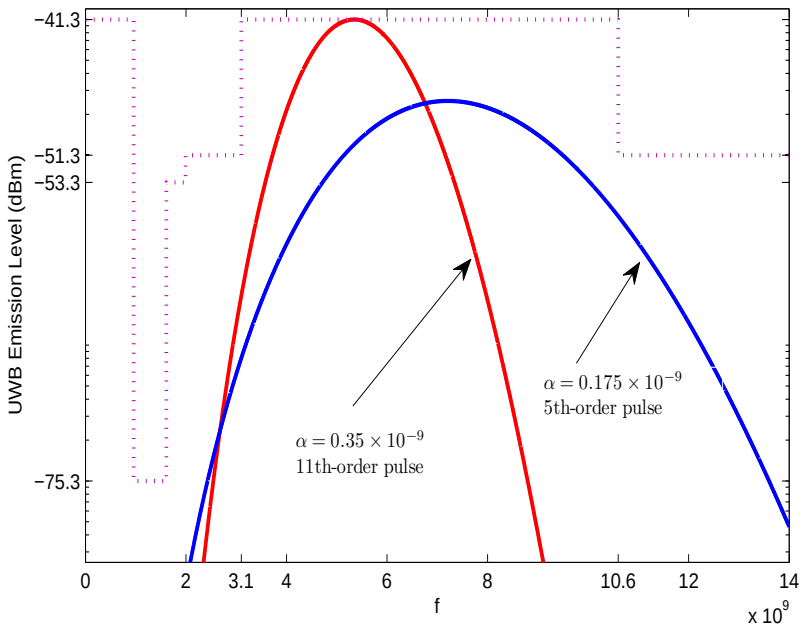

Figure 68: Spectra of PWM signals versus FCC emission mask, 11th-order pulse with $\alpha = 0.35 \times 10^{-9}$ and 5th-order pulse with $\alpha = 0.175 \times 10^{-9}$

pulses. When the two waveforms to transmit bit 0 and 1 satisfy the two conditions we state above, equation (2.45) is always effective no matter which waveforms are used.

In Fig. 76, Fig. 77, Fig. 78 and Fig. 79, the BER curves in the presence of synchronization errors are shown. In simulation, the maximum channel spread D is truncated to 80 ns. The analytical BER curves are generated from equation (2.52), and the same method as that in Chapter 2 is used to obtain parameter values for ρ in equation (2.52). In Fig. 76, the synchronization error values are ε=0 and 2 ns. When ε=0, no synchronization error occurs and the system achieves best BER performance. When ε=2 ns, the system BER performance is degraded. In Fig. 77, the values of ε are 3 and 5 ns. In Fig. 78,the values of ε are 10 and 15 ns. In Fig. 79, the values of ε are 20 and 30 ns. All simulated and analytical BER curves match very

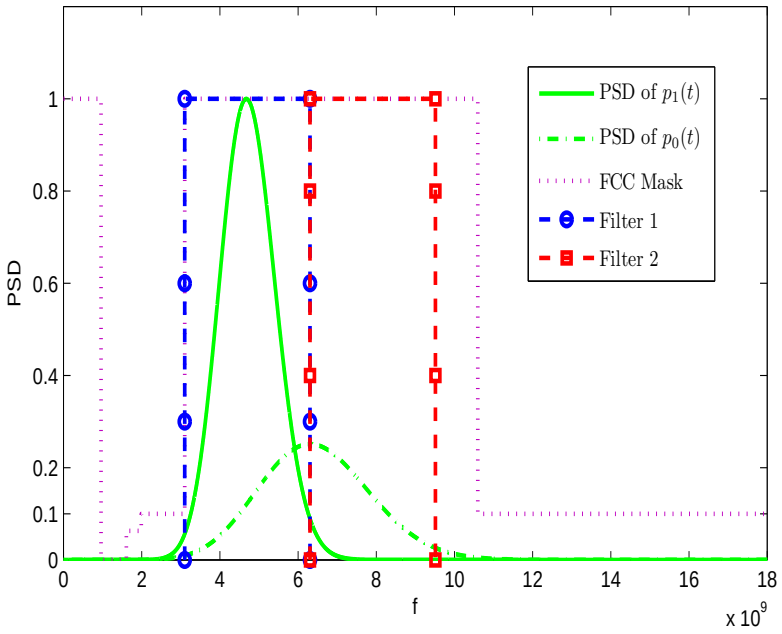

Figure 69: UWB Power Mask, Filter

well. This proves that equation (2.52) is effective for PWM systems with different-order derivative pulses. As we state above, when the two waveforms satisfy the two conditions, equation (2.52) is always effective.

6.2 Signal Spectra of GFSK Systems Versus FCC Emission Mask

In Chapter 3, we research and analyze GFSK systems without considering FCC power mask. In this section, we will find appropriate pulse-pairs which satisfy the FCC mask. In Fig. 80, the spectral curves are generated from the 9th-order and 27th-order derivatives of the Gaussian pulse, respectively. The shape factor is $\alpha = 0.34 \times 10^{-9}$. Both of these two spectral curves satisfy the FCC emission mask. It appears in Fig. 80 that the two spectral curves intersect at a very high point. This is

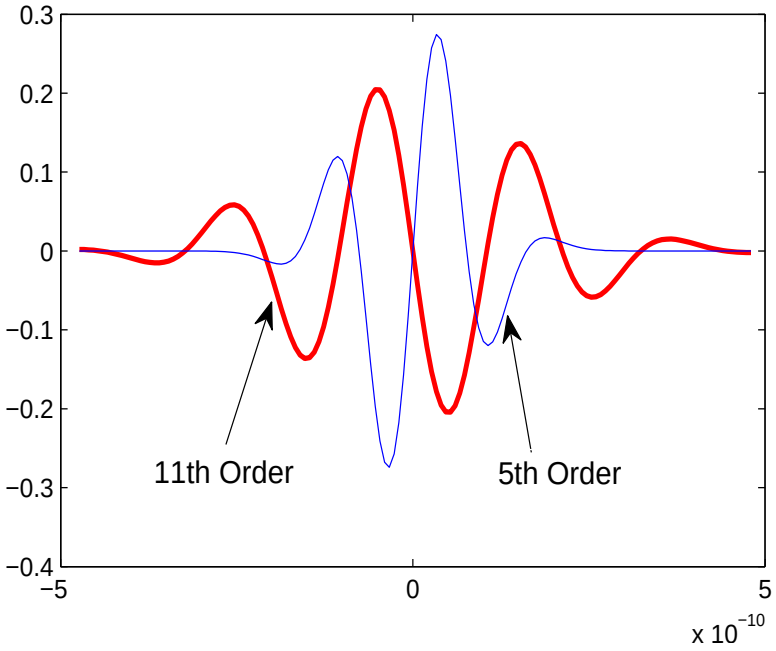

Figure 70: Waveform of the 5th- and 11th-order derivatives of the Gaussian pulse, $\alpha = 0.2 \times 10^{-9}$ for 5th-order and $\alpha = 0.4 \times 10^{-9}$ for 11th-order

caused by the logorithmic scale of the y axis. In fact, the intersected point is 10 dB below the maximum (-51.3 dB in Fig. 80). For a clearer observation of the spectral separation, we plot these two curves in Fig. 81 which is based on a linear scale.

In the following, we will run the simulation for GFSK with pulses which satisfy FCC emission mask. The 10th- and 30th-order derivatives pulses in Fig. 83 are used. We can obtain the equations of the 10th- and 30th-order derivatives by using MAPLE to perform $\frac{d^{10}}{dt^{10}}(\frac{\sqrt{2}}{\alpha}e^{\frac{-2\pi t^2}{\alpha^2}})$ and $\frac{d^{30}}{dt^{30}}(\frac{\sqrt{2}}{\alpha}e^{\frac{-2\pi t^2}{\alpha^2}})$, respectively.

$$\begin{aligned} s(t)_{10} = (&-967680 + \frac{19353600\pi t^2}{\alpha^2} \\ &- \frac{51609600\pi^2 t^4}{\alpha^4} + \frac{41287680\pi^3 t^6}{\alpha^6} \\ &- \frac{11796480\pi^4 t^8}{\alpha^8} + \frac{1048576\pi^5 t^{10}}{\alpha^{10}})e^{\frac{-2\pi t^2}{\alpha^2}} \end{aligned} \tag{6.3}$$

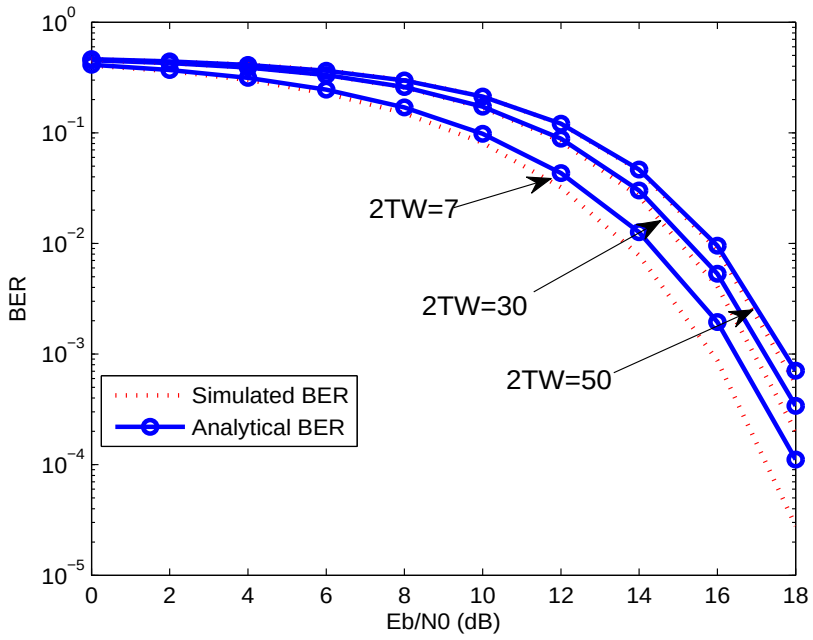

Figure 71: BER performance of PWM with different=order derivative pulses in AWGN channels, $2TW = 7$, 30, and 50

$$
\begin{aligned}
s(t)_{30} = (&-664676613920284213248000 + \frac{3988059683521705279488000000\pi t^2}{\alpha^2} \\
&- \frac{37221890379535915941888000000\pi^2 t^4}{\alpha^4} + \frac{1290358866490578419318784000\pi^3 t^6}{\alpha^6} \\
&- \frac{22120437711267058616893440000\pi^4 t^8}{\alpha^8} + \frac{216288724287944573142958080000\pi^5 t^{10}}{\alpha^{10}} \\
&- \frac{13108407532602701402603520000\pi^6 t^{12}}{\alpha^{12}} + \frac{518574363927139835707392000\pi^7 t^{14}}{\alpha^{14}} \\
&- \frac{13828649704723728952197120000\pi^8 t^{16}}{\alpha^{16}} + \frac{2530733279295845821317120000\pi^9 t^{18}}{\alpha^{18}} \\
&- \frac{319671572121580524797952000\pi^{10} t^{20}}{\alpha^{20}} + \frac{27677192391478833315840000\pi^{11} t^{22}}{\alpha^{22}} \\
&- \frac{1604474921245149757440000\pi^{12} t^{24}}{\alpha^{24}} + \frac{5924215093828245258240\pi^{13} t^{26}}{\alpha^{26}} \\
&- \frac{1253802136259946086400\pi^{14} t^{28}}{\alpha^{28}} + \frac{11529215046068469760\pi^{15} t^{30}}{\alpha^{30}}) e^{\frac{-2\pi t^2}{\alpha^2}}
\end{aligned}
\tag{6.4}
$$

where equations (6.3) and (6.4) are the 10th- and 30th-order derivatives pulses, respectively. These two equations are the simplified versions of the original ones obtained from MAPLE. The common factors of the terms in parentheses of equations (6.3) and (6.4)are $\frac{\sqrt{2}\pi^5}{\alpha^{11}}$ and $\frac{\sqrt{2}\pi^{15}}{\alpha^{31}}$, respectively. They are constants and do not affect the waveform shapes, so they been removed to simplify equation. The value of α is set to

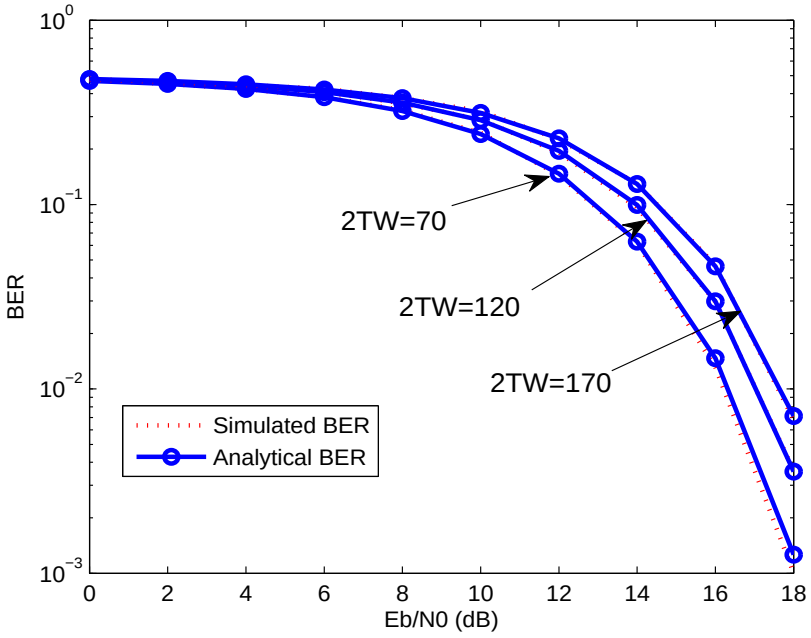

Figure 72: BER performance of PWM with different-order derivative pulses in AWGN channels, $2TW = 70$, 120, and 170

0.365×10^{-9} and the width of the pulses are chosen to be $2.4\alpha = 0.876 \times 10^{-9} = 0.876$ ns. For GFSK, we use the 10th-order derivative to transmit bit 1, and the 30th-order to transmit bit 0. The waveforms of the 10th- and 30th-order derivatives of the Gaussian pulse is in Fig. 85.

Fig. 86 shows the BER curves of GFSK systems in AWGN channels. In simulation, the bandwidth of the filters is 3.52 GHz and the pulse duration is 0.876 ns. Analytical BER curves are obtained directly from equation (3.17). When $2TW$ is increased, there is a better match between the simulated and analytical curves, because the Gaussian approximation is more accurate under large $2TW$ values [29].

Fig. 87 and Fig. 88 show the BER performance comparisons of GFSK and PPM (0 threshold) in multipath channels. The CM4 model [32] is used in simulation. Synchronization is perfect, and the maximum channel spread D is truncated to 80 ns. The frame length is designed using the method mentioned in Chapeter 3, so IFI is avoided in simulation. The analytical BER curves of PPM and GFSK are obtained

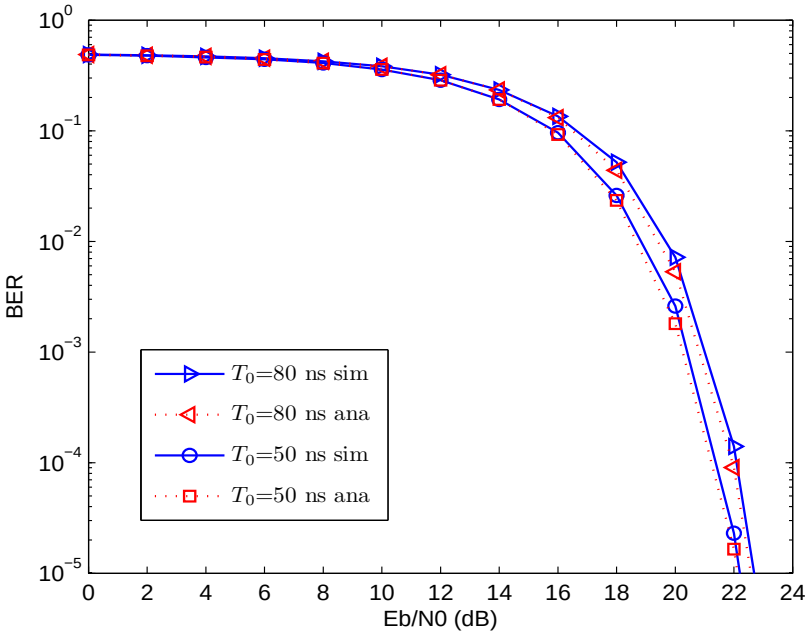

Figure 73: BER performance of PWM in multipath channels (CM4 model, $D = 80$ ns, $T_0 = 80$ and 50 ns)

directly from equation (5.10) and (3.20), respectively. In these two equations, we need to know the values of parameters β_a, β_b and λ. We use the similar statistic method in Chapter 3 to obtain values for the above parameters. Firstly, we use the MATLAB code in [32] to generate realizations of the channel impulse response $h(t)$. Then, we calculate the ratio of energy in a specific time interval to the total energy of a channel realization to obtain values for these parameters. These values are substituted into equation (5.10) and (3.20) to achieve the analytical BER. Both the simulated and the analytical BER are obtained by averaging over 100 channel realizations. In Fig. 87, when $\delta = 80$ ns, no CMI occurs and GFSK and PPM obtain the same BER. The analytical curves of GFSK and PPM match very well, as do the simulated curves. When $\delta = 50$ ns, GFSK obtains better BER performance than PPM, and the improvement is approximately 0.2 dB at BER=10^{-3}. The reason is that when δ is less than D, CMI occurs and PPM performance is degraded. However, we can see from

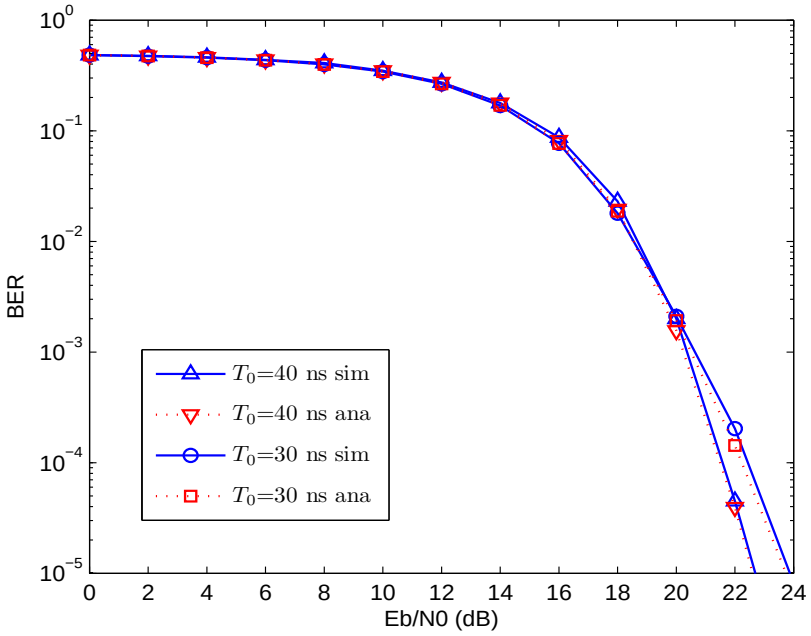

Figure 74: BER performance of PWM in multipath channels (CM4 model, $D = 80$ ns, $T_0 = 40$ and 30 ns)

Fig. 87 that the performances of GFSK and PPM are improved compared to when $\delta = 80$ ns. The reason is that the multipath components existing in the time interval between 50 ns and 80 ns include low signal energy, so the integrators capture more noise energy than signal energy in this interval. In Fig. 88, when $\delta = 42$ ns, GFSK obtains approximately 1.2 dB improvement at BER=10^{-3}. When $\delta = 30$ ns, GFSK requires an increase of E_b/N_0 approximately by 0.7 dB to maintain BER=10^{-3}, but PPM can not achieve this BER level and exhibit a BER floor. The BER performance of PPM can not be improved by increasing the signal transmitting power.

Fig. 89 and Fig. 90 show comparisons of BER performance when synchronization errors occur. In simulation, the modulation index δ is set to the maximum channel spread $D = 80$ ns, so no CMI is in simulation. The frame structure is designed by following the method mentioned in Chapter 3, so IFI is avoided in simulation. The analytical BER curves are obtained directly from equations (5.15) and (3.23), and

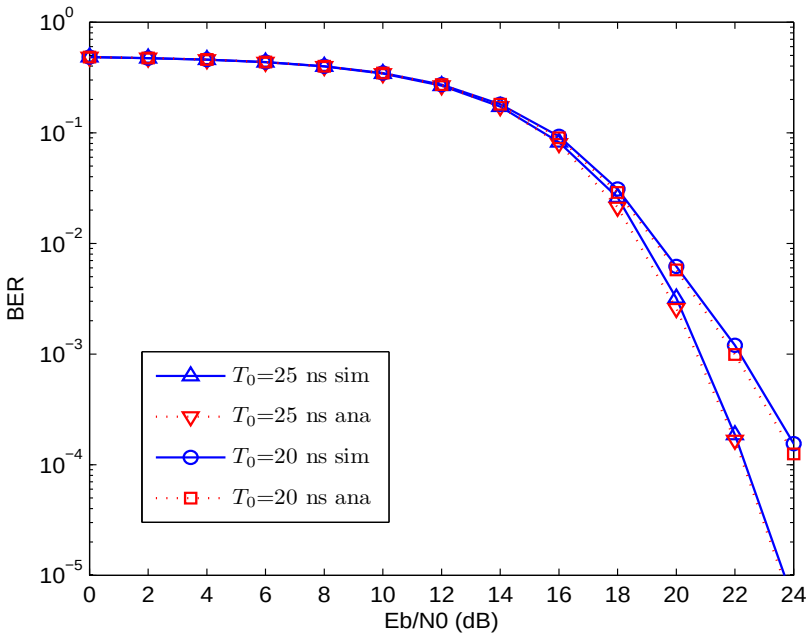

Figure 75: BER performance of PWM in multipath channels (CM4 model, $D = 80$ ns, $T_0 = 25$ and 20 ns)

the values for parameters η and ρ in equations (5.15) and (3.23) are obtained by using the statistic method similar to the one described above. Both the simulated and analytical BERs are obtained by averaging over 100 channel realizations. In Fig. 89, when $\varepsilon = 0$ ns, no synchronization error occurs and GFSK and PPM achieve the same BER performance. When $\varepsilon = 2$ ns, GFSK has a better BER performance than PPM. The improvement at BER= 10^{-3} is approximately 1 dB. In Fig. 90, when $\varepsilon = 3$ ns, GFSK obtains approximately 2.5 dB improvement at BER=10^{-3}. When $\varepsilon = 10$ ns, the BER of PPM is extremely bad and exhibits a BER floor because of severe synchronization errors, but GFSK still achieves a good BER.

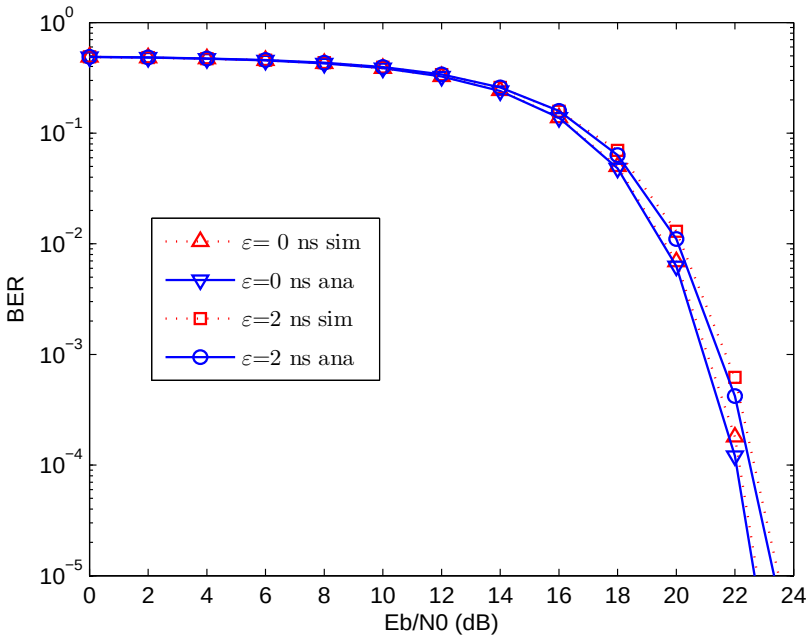

Figure 76: BER performance of PWM in multipath channels (CM4 model, $\delta = D =$ 80 ns, $\varepsilon = 0$ and 2 ns)

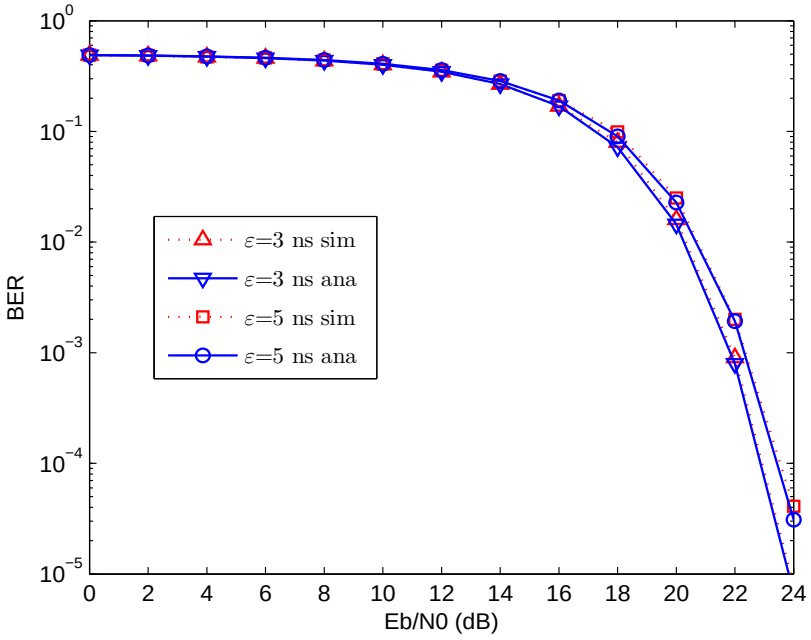

Figure 77: BER performance of PWM in multipath channels (CM4 model, $\delta = D =$ 80 ns, $\varepsilon = 3$ and 5 ns)

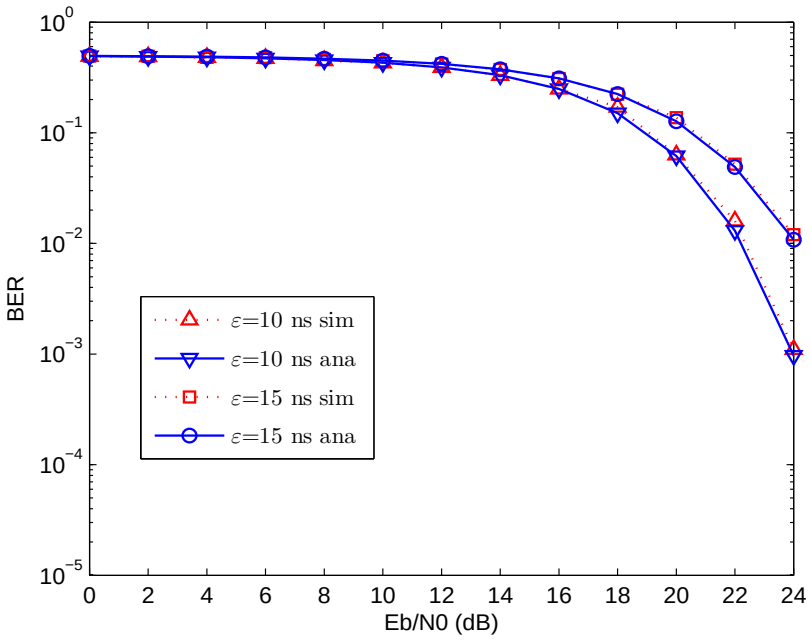

Figure 78: BER performance of PWM in multipath channels (CM4 model, $\delta = D =$ 80 ns, $\varepsilon = 10$ and 15 ns)

6.3 Maximum Transmission Rate under The Limit of FCC Power Mask

In Chapter 3, we have mentioned the topic about the comparison of the maximum possible transmission rate of GFSK and PPM system under the limit of institute regulations. In this chapter, we will use the FCC emission mask as an example to compare these two systems. Since the usable frequency is constrained by FCC regulations, we can not increase the signal bandwidth to infinity. The maximum possible signal bandwidth of a single pulse in a GFSK system is at most one half of that of a PPM system. But this does not mean that the maximum possible data rate of a GFSK system is one half of that of a PPM system. In UWB channels, the multipath components are resolvable and not overlapped due to the extremely short pulse duration. Each pulse will generate many multipath components and the arriving time of

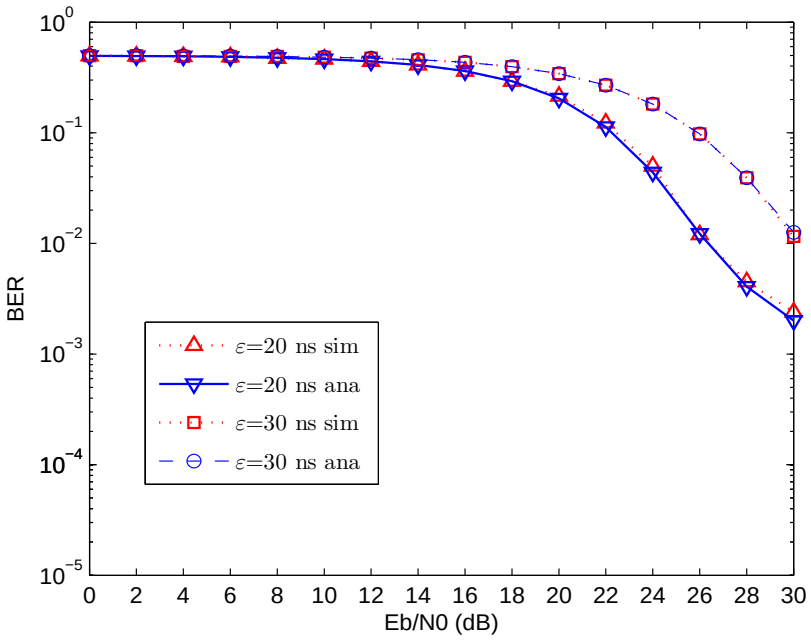

Figure 79: BER performance of PWM in multipath channels (CM4 model, $\delta = D =$ 80 ns, $\varepsilon = 20$ and 30 ns)

each multipath component is not decided by the pulse but the channel environment. Usually, the maximum channel spread D is very long when compared to a single pulse duration. Although the single pulse duration of a GFSK system is twice that of a PPM system, but the values of D are almost the same because the multipath components in these two systems arrive at the same time and the only difference is the duration of the pulses in these two systems. But the difference of the durations of the pulses in these two systems is very small when compared to maximum channel spread. If we choose the value of D from either a GFSK system or a PPM system as a common reference value, the signal energies of these two systems in the time interval $[0, D]$ will be almost the same. The tiny difference is no more than half of the energy of the last multipath component in this range. Usually, this multipath component includes very low signal energy, so the energy difference can be neglected. So we can obtain the same maximum channel spread for GFSK and PPM systems despite

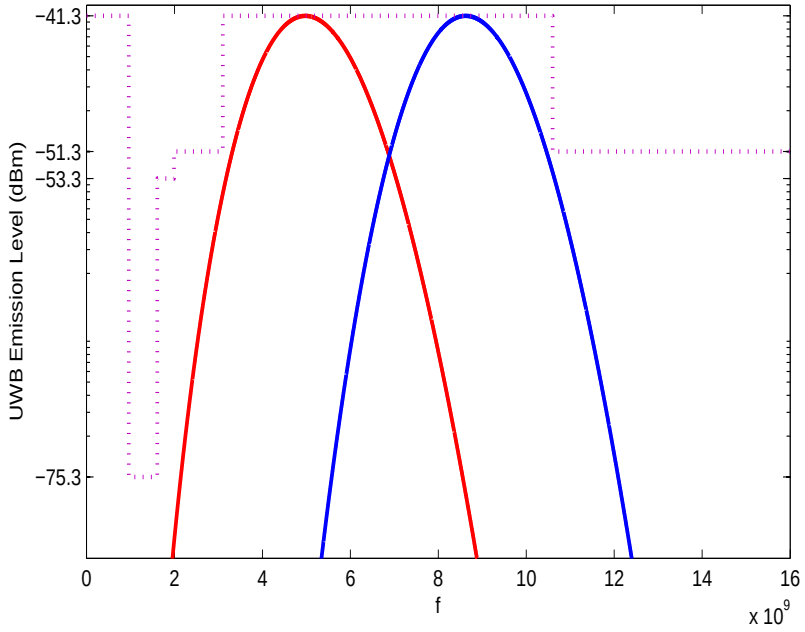

Figure 80: Spectra of GFSK signals versus FCC emission mask, the 9th- and 27th-order derivative pulses with $\alpha = 0.34 \times 10^{-9}$

the pulse duration of the GFSK system being twice that of a PPM system. We also verify our conclusion by using the Matlab code in [32] and these two systems both obtain the same values of D=80 ns. However, the frame of a PPM system include two intervals (T_0 and T_1), so its frame period is twice that of a GFSK system. This leads to the data rate in a PPM system will be half of that of a GFSK system. Also, we can conclude that the spectral efficiency of GFSK is higher than PPM.

Similarly, the maximum possible data rate of PWM is higher than PPM. If we assume the bandwidth of the pulse to transmit bit 0 is the same as the pulse of PPM, it means these two systems will occupy the same frequency range under FCC emission mask limit. The bandwidth of pulse to transmit bit 1 in PWM is half that of the pulse to transmit bit 0 and half that of the pulse used in PPM. As mentioned above, the maximum channel spread D will not be affected by the pulse duration. We also use Matlab code to verify that both PPM and PWM achieve the same value $D = 80$ ns. Also, PWM only has one interval T_0 in its frame structure, so it has a

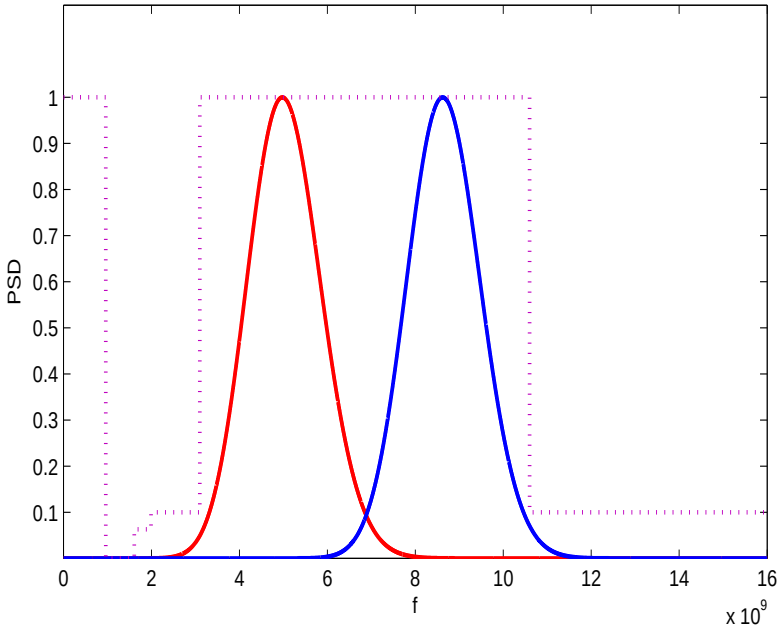

Figure 81: GFSK UWB Mask normal scale, 9 and 27 order α =0.34 ns

higher data rate and spectral efficiency than PPM.

6.4 Summary

In this chapter, we research the spectral characteristics of PWM and GFSK signals versus the FCC emission mask, and find suitable parameters which can make the spectra match the FCC emission mask for these two systems. To match the FCC emission mask, PWM will use two different-order pulses to transmit signals and the order of each pulse is higher than that in Chaper 2. Also, GFSK uses higher order pulses to move signal center frequency to suitable location to match the FCC emission mask. Although the two systems both use higher order pulses, the order of pulses in PWM is still lower than GFSK. Therefore, the pulse generator of PWM is still simpler than that of GFSK. Also, the maximum possible data rate of PWM, GFSK, and PPM are analyzed when the usable frequency is limited by institute regulation

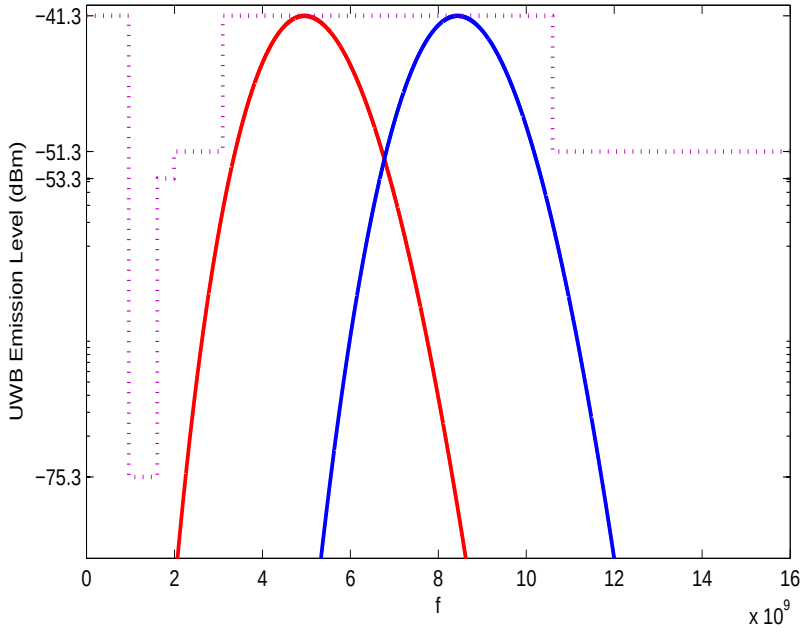

Figure 82: GFSK UWB Mask normal scale, 10 and 29 order α =0.36 ns

such as the FCC emission mask. The analysis shows that PWM and GFSK both achieve higher data rate and spectral efficiency than PPM when the usable frequency range is limited.

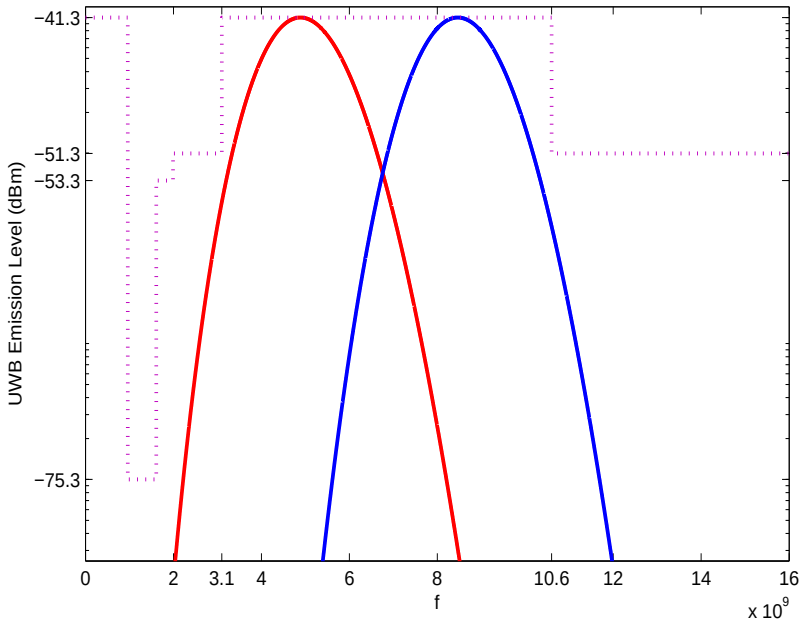

Figure 83: GFSK UWB Mask normal scale, 10 and 30 order α =0.365 ns

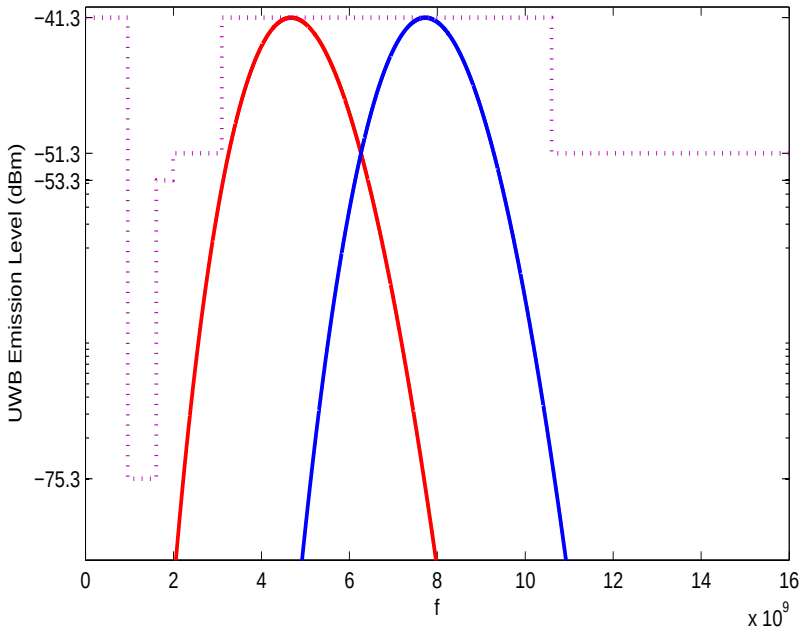

Figure 84: GFSK UWB Mask normal scale, 11 and 30 order α =0.4 ns

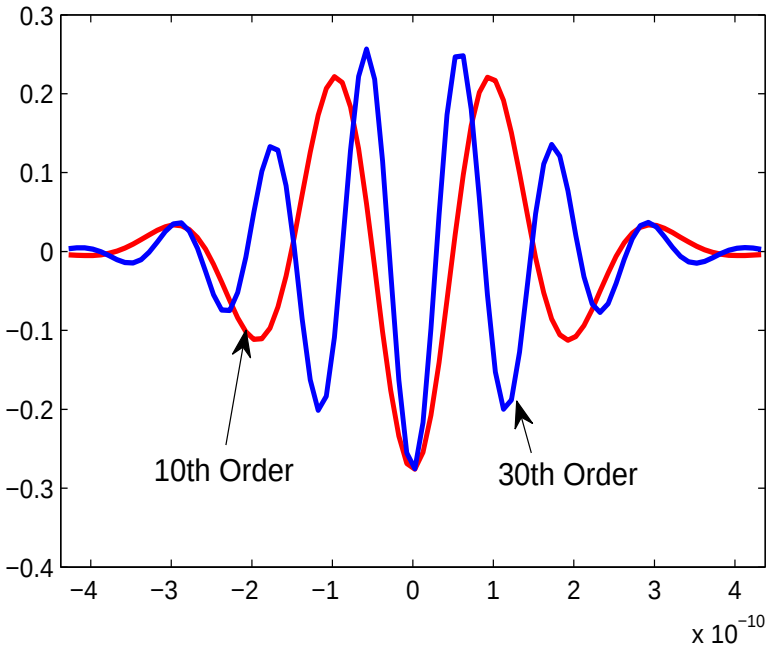

Figure 85: Waveforms of the 10th- and 30th-order derivatives of the Gaussian pulse

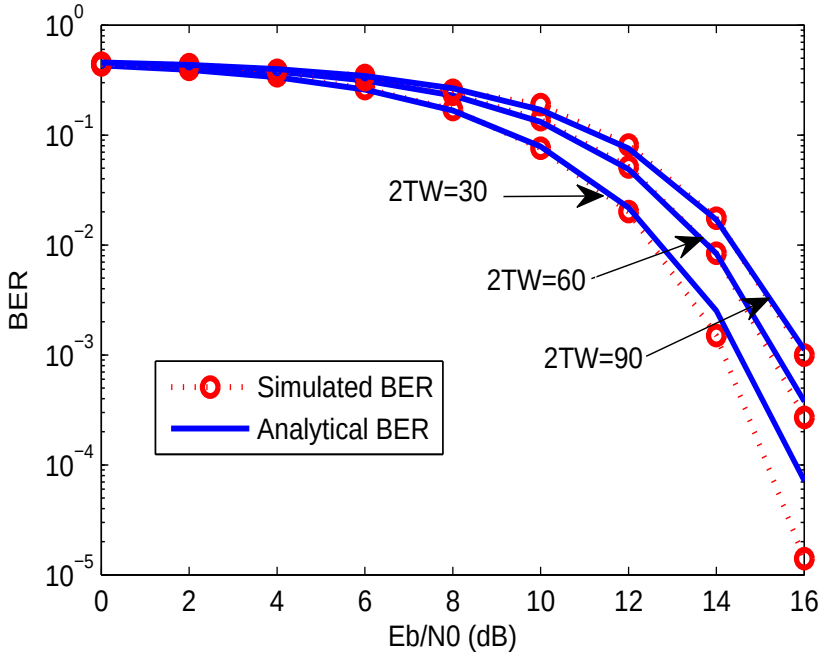

Figure 86: BER performance of GFSK for different $2TW$ values in AWGN channels

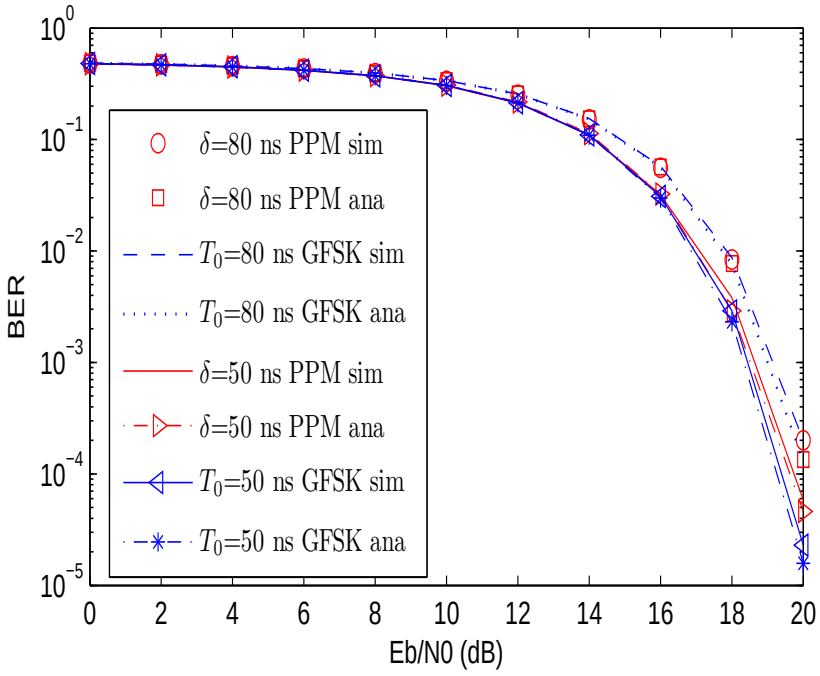

Figure 87: Comparison of BER performance of GFSK and PPM in multipath channels (CM4 model, $D = 80$ ns, $\delta = 80$ and 50 ns)

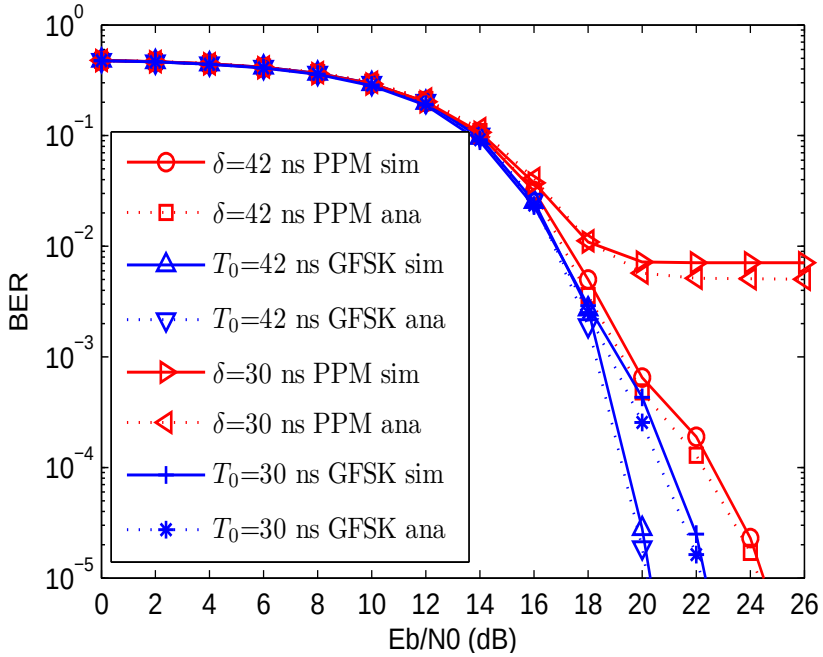

Figure 88: Comparison of BER performance of GFSK and PPM in multipath channels (CM4 model, $D = 80$ ns, $\delta = 42$ and 30 ns)

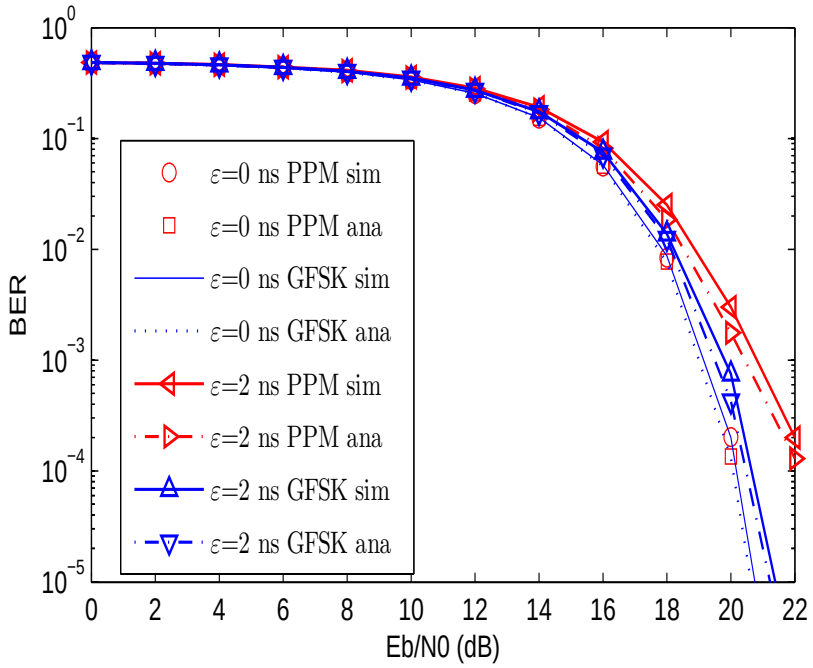

Figure 89: Comparison of BER performance of GFSK and PPM in multipath channels (CM4 model, $D = 80$ ns, $\varepsilon = 0$ and 2 ns)

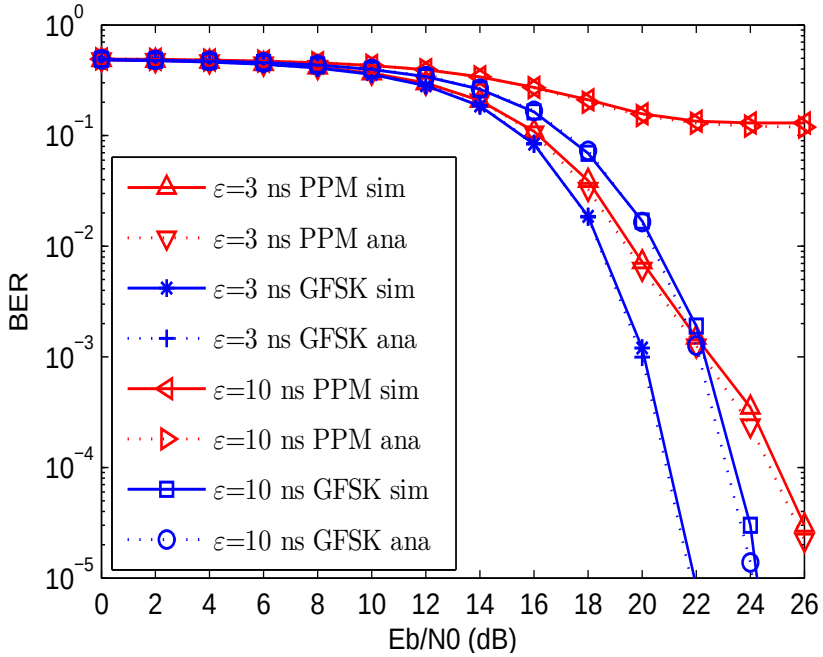

Figure 90: Comparison of BER performance of GFSK and PPM in multipath channels (CM4 model, $D = 80$ ns, $\varepsilon = 3$ and 10 ns)

CHAPTER VII

MULTIPLE ACCESS SCHEMES FOR PWM AND GFSK SYSTEMS

In communication systems, different users often share the same physical medium to transmit and receive data. It is possible to distinguish different users when the users share the transmission resource under a coordinated manner [7]. How to manage these different users to maximize the efficiency of limited spectrum resource is a very important research topic. The development of wireless communication has experienced from the first generation to the third generation [41–83], and now the forth generation communication protocol has entered the theory research stage [84–106]. Almost every generation of the communication systems is accompanied by a new multiple access scheme. In the first generation communication system, frequency division multiple access (FDMA) was used. To increase the number of users, time division multiple access (TDMA) is induced in the second generation communication systems. In the third generation communication system, code division multiple access (CDMA) was used. We will introduce some popular multiple access schemes in

this chapter. Then we will compare and analyze the characteristics of these multiple access schemes. After the consideration of characteristics of UWB systems, we will pick an optimum multiple access scheme for our UWB and GFSK systems. Although in Chapter 2 and 3, we have presented the equations of transmission including multiple access schemes, we will further analyze why we use time hopping as the multiple access scheme for PWM and GFSK systems.

7.1 FDMA

In a FDMA system, the frequency is divided into multiple sub-bands, and every sub-band occupies different frequency range. These sub-bands are called channels and are allocated for different users. FDMA has some inherent advantage due to the frequency separation among users. For example, the interference among users is very low when the frequency ranges of users are adequately separated and the guard band is wide enough. The front-end filters can entirely distinguish the different users. However, a channel is only allocated for a specific user and other users are not allowed to share the same frequency resource. Even when the channel is idle, the other users still can not use this user's channel. Therefore, the spectral efficiency is very low. In early stage of communication systems, FDMA has wide range of applications. All countries at that time adopted the FDMA system as their mobile phone standard technology. FDMA was a very hot research topic in the past, and we can see many research related to this technology [107–118]. The allowable number of users was difficult to satisfy the booming market of wireless communications, and only a few people can enjoy this luxury service in those days. When the demand of the market is continuously increased, this access scheme became gradually obsolete due to the limited user number.

7.2 TDMA

TDMA allows users to share the same frequency band by dividing the frame time into fixed length intervals called time slots. The channel in TDMA system is defined according to time slots, so different users will occupy different channels and multiple access is achieved. When a transmitting/receiving pair is allowed to communicate, the system will assign a specific time slot for them to communicate during the whole procedure. In each frame, each transmitting/receiving pair can transmit a signal in their slot, and all users are allowed to transmit once in a frame. Compared to FDMA, TDMA can provide larger capacity of users. In FDMA, a user does not use the allocated channel all the time, so system will have some idle time. However, the channel is allocated to a specific user and other users are not allowed to occupy the channel even when the channel is idle. And this leads to great waste of transmission time. Unlike FDMA, TDMA can adequately exploit transmission time to maximize the number of the users. TDMA is widely used in the second generation mobile communication systems, such as GSM [119–124], PDC (used in Japan) [125–129], and iDEN [130, 131]. Also, TDMA is applied to satellite communication systems [132–136]. The application of TDMA to wireless communication greatly increases the number of users and lowers the expense of each user. The service fee of mobile users is not as expensive as that of the first generation communication systems. When FDMA was used, the limited frequency resource could provide only a few users, so the license fee to occupy the frequency band is very expensive. During that time, mobile telephone service was a luxury consumption for only a few rich people. TDMA changed this situation and initiated the revolution of wireless communication. The service fee to use a frequency band can be shared by a large number of users, so it can be affordable by more and more people. Likewise, since TDMA systems use digital technology, the fast development of semiconductors has lowered

the price of mobile terminals. The market for wireless communication was expanded quickly and the use of mobile telephones has pervaded and is no longer a luxury consumption. This booming market of wireless communication has also brought a good development opportunity to many companies, such as Motorola, Nokia, and Ericsson, and these companies have achieved great progress. The history of wireless communication has entered a new time after TDMA has been successfully applied to commercial applications. The TDMA scheme is continuously developed in technologies, such as general packet radio service (GPRS) and enhanced data rates for GSM evolution (EDGE), which was developed to compete with the new technology CDMA.

7.3 CDMA

In CDMA systems, the multiple access can be achieved by two schemes, direct sequence spread and frequency hopping. In the direct sequence CDMA (DS-CDMA) system, the signals of different users are spread using orthogonal spreading codes. At the receiver, only the user with the correct spreading code can recover the data. Different users can share the same bandwidth and time to transmit signals in DS-CDMA system, so it increases the user capacity and data rate. In frequency hopping CDMA (FH-CDMA) systems, the carrier frequency is periodically changed over some predetermined bandwidth. The center frequency of carrier hops to N non-overlapping frequency band, so the total spectrum is increased to N times of a single band. The hopping position is controlled by pseudo-random codes. In military applications, FH-CDMA is very immune to interception and jamming because the acquisition of center frequency of carrier is difficult to obtain. DS-CDMA is more popular in commercial applications. For example, IS-95 is the commercial standard of the 2.5G communication system, and this standard uses DS-CDMA as multiple access tech-

nology [137–146]. As one of the candidates of 3G mobile communications, wideband CDMA (WCDMA) is evolved from IS-95, the only difference is a higher chip rate of spreading codes, and it generates a larger bandwidth of 5 MHz. WCDMA is very popular in 3G systems and its multiple access scheme is also DS-CDMA [147–156]. High speed packet access (HSPA) is evolved from WCDMA to provide packet data uplink and downlink services [157–168], and it also maintain the multiple access method DS-CDMA. In commercial communication field, CDMA technology has dominated the market for more than ten years. The first commercial standard of CDMA was proposed by Qualcomm, and this technology become popular due to its inherent characteristics. Also, Qualccomm obtained great profit from sale of its CDMA products and technology, and it became a big company in communication field. The application of CDMA technology will continue to dominate the market before a new technology appears. Although in 3G and 4G mobile communication systems, the data rate is higher and higher by using high order modulation like 64 quadrature amplitude modulation (QAM), the multiple access scheme is always CDMA.

7.4 Multiple Access Scheme Discussion of GFSK and PWM Systems

In Chapters 2 and 3, we have proposed time hopping (TH) multiple access scheme for these two systems. In this chapter, we will further analyze the reason why we choose this multiple access scheme rather than other schemes. TH is a commonly used multiple access scheme in PPM [169–180] and PAM [181–192] UWB systems. Due to the ultra-fast transmission speed of UWB signal, usually the transmission of data is finished in a very short time. Therefore, there exists a great length of idle time during the transmission. We will analyze different multiple access schemes under the

characteristics of UWB transmission.

If we use FDMA as multiple access scheme for PWM and GFSK systems, what is the accommodated number of users? The minimum bandwidth of an UWB pulse is 500 MHz and this will lead to the system bandwidth of GFSK and PWM to be 1 GHz. The available bandwidth is 7.5 GHz (3.1-10.6 GHz) under the FCC emission mask, so the maximum number of users is no more than seven. It does not make sense to use FDMA for GFSK and PWM systems.

Assuming CDMA is used as multiple access schemes for PWM and GFSK systems, what is the accommodated user number? Since there are two approaches to realize CDMA, we will discuss them respectively. The first scheme we discuss is DS-CDMA which is based on using spreading sequence. In DS-CDMA systems, the chip rate of spreading code is higher than the data rate, so the data is transmitted by signal with larger bandwidth. We will analyze the application result of DS-CDMA to PWM and GSFK under high and low speed conditions. Under high speed requirement, the signal bandwidth will occupy almost the whole range of 3.1-10.6 GHz. It seems that DS-CDMA is not suitable as multiple access scheme. If the DS-CDMA is used, the signal bandwidth is enlarged. However, the usable spectral range is limited by the FCC emission mask, so it is impossible to spread signal spectrum beyond the range of 3.1-10.6 GHz. Under a low speed requirement, we can use signal with narrow bandwidth. However, the minimum bandwidth requirement is 500 MHz of a single pulse and the total bandwidth is 1 GHz in both PWM and GFSK systems. Even we can use spreading code to spread the signal, the length of spreading code is no more than seven. And we need to construct an orthogonal spreading code under this length, the number is also very limited. For example, the most popular spreading sequence, gold sequence, can provide only two orthogonal codes under the length of seven. In FH-CDMA systems, the center frequency of signal spectrum hops to a

different frequency location. We will analyze this multiple access scheme as follows. Also we analyze it under the assumption of high speed and low speed conditions. It is apparent that it is impossible to use FH-CDMA multiple access scheme to PWM and GFSK systems under a high speed requirement, because the signal bandwidth will almost occupy the entire range of 3.1-10.6 GHz. If the center frequency of signal spectrum is hopped to other location, it will be out of the frequency range limited by the FCC emission mask. When low data rate transmission is considered, there are only seven positions to hop if we assume that the signal spectrum of single pulse is 500 MHz. The accommodated number of users is also very limited. If the bandwidth of single pulse is greater than 500 MHz, the number of positions to choose is much less than seven. It does not make sense to use a multiple access scheme which only can provide such limited number of users.

We will analyze TH multiple access in the following. Due to the high speed narrow pulse transmission characteristics of UWB signal, it is more efficient to separate the frame period into multiple chip intervals for different users. The suitable schemes can be TDMA or TH multiple access. However, all UWB systems use the TH multiple access scheme. We will compare these two schemes in the following. In both of these two schemes, the frame period is broken into multiple short chip intervals, the only difference is how to assign the chip intervals to users. In the TDMA scheme, the transmission between a pair of sender and receiver uses a fixed interval during the whole transmission period. In TH scheme, the user does not transmit data in a fixed chip interval, and system will assign a chip interval by pseudo-random sequence in every frame transmission. So the chip intervals assigned to a user can be different in different frame periods. At the receiver, a different user uses the same pseudo-random sequence as the transmitter side to recover data in specific chip interval. Why do UWB systems all use TH other than TDMA? The major benefit of using TH

are described as follows. Firstly, the TH scheme can remove the discrete spectrum line of the UWB signal [7]. In UWB systems, data is transmitted by pulses. If the pulse is transmitted periodically, discrete spectrum lines appear at the multiples of the average pulse repetition frequency. These discrete spectrum lines are harmful to systems, especially at the receiver side, it will affect the system performance and lead to decision error. The use of the TH multiple access scheme change the pulse repetition period of every user, so the discrete spectrum line is removed. Secondly, the use of the TH scheme also increase the security and protects user data from interception. When a vicious intrusion occurs, the intruder will have difficulty recovering the data of a specific user. Since the pulse repetition period is changed, the intruders can not know which pulse carries the user data they want. This increase the complexity of capturing the user data may force the intruder to give up their attempt. There, the TH scheme will greatly reduce the risk of interception and increase the security of data transmission. The TH scheme has much similarity to TDMA as the only difference is the assignment method of time slots. TDMA always assigns a fixed time slot for a user, so it will not have the ability to remove the discrete spectrum line and protect data from intrusion. This is the reason why TH is commonly used in UWB systems as the multiple access scheme. We also will use TH as multiple access scheme for our PWM and GFSK systems.

7.5 Summary

In this chapter, we analyze and compare the characteristics of different multiple access schemes and pick optimum multiple schemes for our PWM and GFSK systems. For these systems, the choice of multiple access schemes is similar to other UWB systems such as PPM and PAM systems. FDMA can not provide enough number of users, so it is obsolete in communication systems. Also, it is not suitable to our PWM

and GFSK UWB systems due to the very limited number of users that FDMA can provide. After an analysis of DS-CDMA and FH-CDMA multiple access schemes, we found that both of these schemes are not suitable for PWM and GFSK systems due to the frequency range limited by the FCC emission mask and the limited number of users of these two schemes under the limit of the FCC emission mask. Finally, we decide to pick TH as multiple access of PWM and GFSK systems. The reason to pick TH other than TDMA is that TH not only can accommodate a large number of users, but also can remove the discrete spectrum line and increase the ability to protect user data from intrusion.

The choice of TH as multiple access of PWM and GFSK system is similar to that of other UWB systems. This is absolutely not a coincidence and is determined by the characteristics of UWB systems: High speed transmission rate, wide bandwidth of pulse, the frequency range limited by FCC emission mask, and the appearance of discrete spectral line when using a fixed pulse repetition period to transmit signals. Since our PWM and GFSK systems all have these characteristics above, it will lead to the same choice of multiple access scheme as that of PAM and PPM systems. TH has become the most common multiple access scheme in UWB systems.

CHAPTER VIII

CONCLUSIONS AND FUTURE RESEARCH

8.1 Conclusions

In this dissertation, two new ED UWB systems, PWM and GFSK, are proposed. GFSK systems achieve the same BER performance as PPM systems in AWGN channels and the BER performance of PWM system are slightly worse than PPM systems in AWGN channels. When in the presence of CMI or synchronization errors, the BER performance of these two new systems both surpass that of PPM systems. When GFSK is compared to PWM, it exhibits better BER performance in AWGN channels, multipath channels, and in the presence of synchronization errors. However, PWM systems uses lower order Gaussian pulse generator than GFSK systems, so the pulse generator in PWM is easier to implement than that of GSFK. An adaptive threshold is applied to PPM system to mitigate the effect of CMI and synchronization error. The adaptive threshold always can find the optimum threshold which can

improve the BER performance in the presence of CMI and synchronization error. Especially, when severe CMI or synchronization errors occur, the improvement is very significant. Although the optimal threshold ED PPM system can achieve BER performance improvement, the BER performance of GFSK is always better than optimal threshold PPM. After the application of optimal threshold, PWM system still can achieve better BER performance than PPM systems, the only difference is that the BER of PWM will surpass that of optimal threshold PPM at greater CMI and synchronization errors values. Because of the spectral characteristic of PWM and GFSK signals, we also research and find appropriate parameters for these two systems to satisfy the emission mask set by FCC. The multiple access schemes is also discussed in this dissertation. After a detailed analysis of different multiple access schemes, we decide to use time hopping, which is the commonly used multiple access scheme in UWB field, as multiple access scheme for these two systems. The time hopping scheme can maximum the efficiency of these two systems.

8.2 Future Research

In this section, several important research topics are presented for future work.

8.2.1 Multiple Access Interference and Multiuser Capacity

The performance analysis of the two new energy detection UWB systems are both based on single user communication case and the effect of multiple access interference (MAI) has not been analyzed until now. To analyze the effect of MAI on system performance, the first step is to construct mathematical model of MAI in these two systems. The model of MAI for PPM and PAM have been modelled as Gaussian noise [193–196]. In PAM and PPM systems, the waveforms are all generated from the same pulses, and the modulation is achieved by changing the position or polarity of

the pulses. However, PWM systems use pulses with different widths and GFSK systems use different-order derivatives of the Gaussian pulse, so we can not simply take the MAI in these two systems as Gaussian noise. The work to establish the model of MAI in these two systems is interesting. After the MAI model is constructed, we must analyze the multi-user capacity of these two systems. In UWB signal transmission, every pulse will generate repeated multipath components in multipath channels. These multipath components will delay a very long time. If the period of chip interval is designed to too short, the MAI will occur among different users. However, if the chip interval is designed too long, the accommodated user number is small in a frame period. So there is a trade-off between the MAI and user numbers. We must research the user capacity under the consideration of the MAI and maintain acceptable BER simultaneously. In the analysis, we need to consider some parameters which are very important to our research. Firstly, the mean value of MAI with respect to the the chip interval must be considered. When the transmitting power of the signal is constant, the length of chip interval will have effect on the mean value of the MAI. Secondly, when the length of chip interval is fixed, we need to find the relationship of the mean value of MAI and the signal power. When we increase or reduce the transmitting power, it does not mean that the mean value of MAI also will change proportionally. Thirdly, the variance of MAI is also a very important parameter we need to know. We also will analyze the variance under two conditions: when the length of the chip interval is changed or when the length of chip interval is fixed but signal power is changed. The variance of MAI is also a very important parameter which can have great effect on system performance. If we just know the mean value , it still is not enough. For example, some MAI have very small average value, but its variance is very large and it can lead to a very large MAI noise power. Finally, some possible parameters are required by MAI noise model. If the MAI model is

like Gaussian noise, the average value and variance are enough to characterize MAI. However, if the model is not like Gaussian noise, some specific parameters maybe needed in that model. Besides these parameters we need to consider in our research, we also will compare the multi-user capacity under the requirements of different BER performances. The user number is usually fewer when the high requirement of BER is set. However, before we really carry out entire analysis, we can not draw a decision based on some common experience or knowledge.

8.2.2 Develop The Hardware Pulse Generator for High-order Derivative of The Gaussian Pulse

In GFSK systems, the modulation is achieved by transmitting different-order derivatives of the Gaussian pulse. So this system needs Gaussian pulse generators for different-order derivatives. Some pioneering works have been done to develop hardware implementation for pulse generators for some high-order derivatives. For example, in [38], a 7th-order pulse generator is proposed, and the generator in [39] is capable of producing a 13th-order pulse. In [40], the center frequency of the generated pulse is 34 GHz. However, the complete implementation for different-order derivatives is still under development. We need to develop a series of pulse generators to provide these pulses for systems. The pulse generator can be designed using different methods. In [39], the authors use two step recovery diode (SRD) components and microchip line and parallel stub to design their pulse generator. In [40], the authors design the pulse generator for optical fibre communications. The generator is designed using microwave-photonic tapped delay line filter. In [38], the analog 7th-order pulse is achieved from the 2nd-order derivatives of the fifth-order derivatives. Although we can keep using analog derivative circuit to generate higher pulse generator, it will make circuit very complicated and the consumption of power is not suitable for some UWB

devices which need low power. In modern digital circuit, many companies use ASIC or FPGA to implement their system. Usually a pulse shaping filter is built on FPGA or ASIC chips. The output from the chip is digital pulses and a D/A converter is used to convert the digital pulse to analog pulse which is suitable to transmitted in the air. This technology can easily achieve different pulse generator by using some hardware description language like VHDL or Verilog. This technology almost can generate digital pulse generators with any frequency responses. The mature design technology on chip design have lowered the expense to very cheap price. The only challenge is the D/A converter must work at very high frequency and this will increase the price of D/A converter. With the development of electronics industry, the performance of D/A converter is better than before, and the price is cheaper. We expect that the price of the high frequency D/A converter can be reduced to an acceptable price. Until now, there is still not a simple and general method to design different-order derivative pulses with a cheap cost. So it is valuable to carry out research on this topic. In the future, we will work to find a cheap and simple method to achieve pulse generation for different-order derivatives of the Gaussian pulse.

8.2.3 The Captured Energy with Respect to Integration Time for IEEE 802.15.4a Channel

In this dissertation, the theoretical BER in multipath channels and in the presence of synchronization errors is obtained by numerically calculating some parameters. Until now, there is still not a mathematical equation to calculate the captured signal energy with respect to integration time. In IEEE 802.15.4a model, the amplitude of multipath components obeys Nakagami distribution. The arrival of multipath components is grouped into clusters. The arriving time of clusters obeys Poison distribution. And in each cluster, the relative arriving time of each multipath component to the

first component all obeys Poison distribution with different parameters. What is the capture energy when the integration time is different? There is still no solution to this question. Some researchers use statistical and curves fitting method to derive the equation. Although these researchers acclaim that their result is accurate, it has not been accepted as an effective equation in calculation. Since these results are not based on strict mathematical derivations, it deserves to carry out research on this topic. Although this topic is very challenging, but it is very valuable. In the future, we will keep an eye on this topic.

8.2.4 MB-UWB

In the MB-UWB system, the modulation is achieved by using OFDM. In OFDM system, the sub-carriers are overlapped each other, and the separation of center frequency of these sub-carrier is $\frac{1}{T}$, where T is the symbol period. In MB-UWB systems, the bandwidth of each sub-carrier is at least 500 MHz to comply with FCC rule.

The overlapped spectrum of sub-carrier increase the spectral efficiency, so OFDM is very promising for high speed transmission systems. Also OFDM can avoid nonintentional interference in certain bands without using notch filter. And OFDM is already mature technology now and it has been widely applied to IEEE 802.11.a, IEEE 802.11.g, IEEE 802.11.n, ADSL, CDSL, and DVB-C2. The successful application of OFDM has brought great commercial profit and the market is booming in recent several years. Since the current OFDM systems already can provide a very wide bandwidth, it has been proposed as an alternative technology for UWB. Some researchers also combine OFDM with MIMO to generate a new technology called MIMO-OFDM. MIMO-OFDM has the advantage of OFDM and simultaneously it has the advantage of MIMO to achieve space diversity gain and improve system per-

formance. Due to the advantage of MIMO-OFDM, it was proposed for UWB system and it is called MIMO-OFDM UWB.

MB-OFDM is entirely different to the IR-UWB which use short pulse to transmit signal. Currently, the technology of IR-UWB is still not mature. However, OFDM is already mature technology. Although the concept of UWB originated from impulse radio, it is possible MB-UWB enter market earlier due to the successful application of OFDM technology to other fields. So it deserves us to keep an eye on MB-UWB systems.

BIBLIOGRAPHY

[1] F. Nekoogar, "Ultra-Wideband Communications: Fundamentals and Applications", *Prentice Hall*, Upper Saddle River, NJ, USA, 2005,

[2] G. Heidari, "WiMedia UWB technology of choice for wireless USB and bluetooth", *Wiley*, 2008

[3] M. Win and R. Scholtz, "Impulse radio: how it works," *IEEE Communications Letters*, vol. 2, No. 2, pp. 36-38, 1988.

[4] L. Yang and G.B. Giannakis, "Ultra-wideband communications: an idea whose time has come," *IEEE Signal Processing Mag.* , vol. 21, No. 6, pp. 26-54, 2004.

[5] D. Porcino and W. Hirt, "Ultra-wideband radio technology: potential and challenges ahead," *IEEE Communication Magazine*, vol. 41, No. 7, pp. 66-74, 2003.

[6] F. Wang, C. Xu, X. Ji and Y. Zhang, "Performance analysis of time-hopping pulse width modulation impulse radio," *IEEE the 4th International Conference on Wireless Communication, Networking and Mobile Computing*, pp. 1-5, 2008.

[7] M. Benedetto and G. Giancola, "Understanding ultra wide band radio fundamentals," *Prentice hall*, Upper Saddle River, NJ, USA, 2004.

[8] S. Dubouloz, B. Denis,S. de Rivaz and L. Ouvry" Performance analysis of LDR UWB non-coherent receivers in multipath environments," *Proc. IEEE Intern. Conf. Ultra-Wideband,*, Sep. 2005, pp. 491-496

[9] N. He and C. Tepedelenlioglu, "Performance analysis of non-coherent UWB receivers at different synchronization levels," *IEEE Transactions on Wireless Communications*,vol. 5, N0. 6, pp. 1266-1273, 2006.

[10] R. Hoctor, and H. Tomlinson, "Delay-hopped transmitted-reference RF communications," *2002 IEEE Conf. Ultra-Wideband Sys. and Tech.*, Baltimore, US. May 2002, pp. 265-269.

[11] X. Dong, L. Jin and P. Orlik, "A new transmitted reference pulse cluster system for UWB communications," *IEEE Transactions on Vehicular Technology*,vol. 57, N0. 5, pp. 3217-3224, 2008.

[12] X. Lu and G.B. Giannakis, "Achievable rates of transmitted-reference ultra-wideband radio with PPM," *IEEE Transactions on Communications*,vol. 54, No. 9, pp. 1536-1541, 2006.

[13] H. Khani and P. Azmi, "Weighted high data rate ultra wideband transmitted-reference system in dense multipath fading channels," *IET Communications*,vol. 3, No. 4, pp. 571-584, 2009.

[14] J. Tang, Z. Xu and B.M. Sadler, "Performance analysis of b-bit digital receivers for TR-UWB systems with inter-pulse interference," *IEEE Transactions on Wireless Communications*,vol. 6, No. 2, pp. 494-505, 2007.

[15] T. Jia and K. Dong, "Analysis of channel-averaged SINR for indoor UWB Rake and transmitted reference systems," *IEEE Transactions on Communications*,vol. 55, No. 10, pp. 2022-2032, 2007.

[16] S. Wang, Y. Chen, M. Leeson and N.C. Beaulieu, "Analysis of channel-averaged SINR for indoor UWB Rake and transmitted reference systems," *IEEE Transactions on Wireless Communications*,vol. 9, No. 6, pp. 1837-1842, 2010.

[17] J. Romme and K. Witrisal, "Transmitted-reference UWB systems using weighted autocorrelation receivers," *IEEE Transactions on Microwave theory and techniques*,vol. 54, No. 2, pp. 18751-1761, 2006.

[18] L. Fang and W. Namgoong, "An oversample channelized UWB receiver with transmitted reference modulation," *IEEE Transactions on Wireless Communications*,vol. 5, No. 6, pp. 1497-1505, 2006.

[19] Z. Franz and U. Mitra, "Generalized UWB transmitted reference systems," *IEEE Journal on Selected Areas in Communications*, vol. 24, No. 4, pp. 780-786, 2006.

[20] M. Ho, V.S. Somayazulu, J. Foerster and S. Roy, "A differential detector for an ultra-wideband communications system," *Proc. Vehicular Technology Conference, IEEE 55th,*, vol. 4, pp. 1896-1900, 2002.

[21] J.D. Choi, and W.E. Stark, "Performance of ultra-wideband communications with suboptimal receivers in multipath channels," *IEEE Journal of selected areas in communications* , vol. 20, No. 9, pp. 1754-1766, 2002.

[22] C. Carbonelli, and U. Mengali, "M-PPM noncoherent receivers for UWB applications," *IEEE Transactions on Wireless Communications*, vol. 5, 2006, pp.2285-2294, Aug. 2006.

[23] S. Paquelet and L-M. Aubert," An energy adaptive demodulation for high data rates with impulse radio," *IEEE Radio and Wireless Conference,*, Sep 19-22, 2004, vol. 4, pp. 323-326

[24] K. Witrisal, G. Leus, G. janssen, M. Pausini, F. Troesch, T. Zasowski and J.Romme, "Noncoherent ultra-wideband systems," *IEEE Signal Processing Magazine,*, 2009, vol. 26pp. 48-66

[25] D. Mu, and Z. Qiu, "Weighted non-coherent energy detection receiver for UWB OOK system," *The 9th International Conference on Signal Processing*, Oct. 2008, vol. 26, pp. 1846-1849

[26] A. Amico, U. Mengali and E.Arias-de-reyna, "Energy-detection UWB receivers with multiple energy measurements," *IEEE Trans. On Wireless Communications*, July. 2007, vol. 6, pp. 2652-2659

[27] X. Cheng and Y. Guan, "Mitigation of cross-modulation interference in UWB energy detector receiver," *IEEE Commun. Lett.* , 2009, pp. 375-377

[28] H. Urkowitz, "Energy detection of unknown deterministic signals," *Proceedings of IEEE* , 1967, pp. 523-531

[29] P. Humblet and M. Azizoğlu, "On the bit error rate of lightwave systems with optical amplifiers," *Journal of Lightwave Technology* , 1991, pp.1576-1582

[30] H. Celebi and H. Arslan, "Cross-modulation interference and mitigation technique for ultrawideband PPM signaling," *IEEE Trans. Veh. Tech.*, 2008, 57, (2), pp. 847-858

[31] R.F. Mills and G.E. Prescotte, "A comparison of various radiometer detection models," *IEEE Trans. on Aerospace and Electronics Systems*, vol. 32 1996, pp. 467-474

[32] Molisch A.F., Balakrishnan K., Cassioli D., Chong C., Emami S., Fort A., Karedal J., Kunisch J., Schantz H., Schuster U. and Siwiak K.: 'IEEE 802.15.4a channel model-final report', http://www.ieee802.org/15/pub/04/15-04-0662-02-004a-channel-model-final-report-r1.pdf, accessed December 2010

[33] H. Arslan, "Cross-modulation interference reduction for pulse-position modulation UWB signals," *IEEE VTC*, Montreal, Canada, September 2006, pp. 1-5

[34] Y. Karasawa, T. Kuroda, and H.Iwai, "The Equivalent Transmission-Path Model A Tool for Analyzing Error Floor Characteristics Due to Intersymbol Interfer-

ence in NakagamiRice Fading Environment," *IEEE Transactions on Vehicular Technology*, vol. 46, pp. 194-202, Feb. 1997.

[35] Y. Huang, and J.A.Ritcey, "16-QAM BICM-ID in Fading Channels With Imperfect Channel State Information," *IEEE Transactions on Communications*, vol. 2, pp. 1000-1007, Sep. 2003.

[36] B.D. Hart, "Maximum likelihood sequence detection using a pilot tone," *IEEE Transactions on Vehicular Technology*, vol. 49, pp. 550-560, Mar. 2000.

[37] R. Petrovic, and S.R. Filipovic,"Error floors of digital FM in simulcast and Rayleigh fading," *IEEE Transactions on Vehicular Technology*, vol. 47, pp. 954-960, Aug. 1998.

[38] Phan T., Krizhanovskii V., Han S., Lee S., Oh H. and Kim N.: '4.7pJ/pulse 7th derivative Gaussian pulse generator for impulse radio UWB', *IEEE International Symposium on Circuits and Systems*, New Orleans, USA, May 2007, pp. 3043-3046

[39] Kim D., Bang G. and Park C.: 'Design and characteristics of high order derivative Gaussian pulse generator for DS-UWB', *2006 Asian-Pacific Microwave Conference Proceedings*, Yokohama, Japan, December 2006, pp. 1110-1113

[40] Zadok A., Wu X., Sendowski J., Yariv A. and Willner A.E.: 'Reconfigurable generation of high-order ultra-wideband waveforms using edge detection', *Journal of Lightwave Technology*, 2010, 28, (16), pp. 2207-2212

[41] Y.R. Dixit, and S. Muhammed,"Performance Trade-offs of a Software Defined Radio for 2G and 3G Cellular Mobile Communication Standards," *IEEE First International Conference on Communication System Software and Middelware*, 2006, pp. 1-5

[42] M. Schreiner, M. Tangemann, D. Nikolai,"A new network-based positioning method for location services in 2G and 3G mobile communications," *IET The 5th European Personnel Mobile Communications Conference on Communication*, 2003, pp. 162-168

[43] H. Eul,"ICs for mobile multimedia communications," *IEEE International Solid-State Circuits Conference*, 2006, pp. 21-39

[44] A. Aragon-Zavala, J.L. Cuevas-Ruiz, G. Castanon, S.R. Saunders,"Mobility Model and Traffic Mapping for In-Building Radio Design," *IEEE International Conference on Electrical, Communications, and Computers*, Feb. 2009 , pp. 46-51

[45] J.S. Park; H.J. Lee; M. Kim,"Technical Standardization Status and the Advanced Strategies of the Next Generation Mobile Communications," *IEEE The 8th International Conference on Advanced Communications*, Feb. 2006 , pp. 884-887

[46] Z. Hunaiti, V. Garaj, W. Balachandran,"An Assessment of a Mobile Communication Link for a System to Navigate Visually Impaired People," *IEEE Transactions on Instrumentation and Measurement*, vol. 58, No. 9, Sep. 2009, pp. 3263-3268

[47] H. Setiawan, H. Ochi,"Study feasibility of common wireless communication services recognition for GSM, UMTS and LTE," *IEEE International Conference on Advanced Technologies for Communications*, 2009 , pp. 253-256

[48] M. Hildebrand, G. Piao; K. David, R. Sigle, D. Zeller, H. Karla,"Performance investigation of multi standard radio resource management for packet switched services," *IEEE 60th Vehicular Technology Conference*, 2004 , vol.5, pp. 3466-3470

[49] J. Wang, W. Zhou, Y. Luo, J. Song,"Performance Analysis of Random Access Algorithm Based on Power Capture," *IEEE 2nd International Conference on Mobile Technology, Applications and Systems*, 2005 , pp. 1-4

[50] I. Hatai, I. Chakrabarti,"Parameter controlled reconfigurable baseband modulator for SDR architecture," *IEEE 2nd International Conference on Mechanical and Electronics Engineering*, Aug. 2010 , pp. 29-33

[51] A.A. Kountouris, C. Moy, I. Rambaud, P. Le Corre,"A software radio approach for the transceiver transition from 2G to 2.5G to 3G," *IEEE Sixth Symposium on Signal Processing and Its Applications*, 2001, vol. 2, pp. 485-488

[52] Y. Zhang, Z. Gao,"An Adaptive Resource Allocation Scheme for GPRS/EDGE Towards 3G," *IEEE 5th International Conference on Wireless Communications, Networking and Mobile Computing*, 2009, pp. 1-4

[53] A.I. Zreikat, K. Al-Begain,"Soft handover-based CAC in UMTS systems," *IEEE 5th International Conference on Wireless Communications, Networking and Mobile Computing*, 2003, vol. 2, pp. 1307-1312

[54] F. Demmerle,"Integrated RF-CMOS Transceivers challenge RF Test," *IEEE International Test Conference* , 2006, pp. 1-8

[55] D.A. Humphreys, J. Miall,"Traceable RF Peak Power Measurements for Mobile Communications," *IEEE International Test Conference* , June 2004, pp. 467-468

[56] J.W. Matthews, W.R. Michalson,"Distributed Digital Radios and WLAN Interoperability," *IEEE Conference on Homeland Security*, May 2007, pp. 107-110

[57] J. Lin, K. Feher,"Noncoherent limiter-discriminator detection of standardized FQPSK and OQPSK," *IEEE Wireless Communication and Network*, March 2003 , vol. 2, pp. 795-800

[58] R.L. Li, B. Pan, T. Wu, K. Lim, J. Laskar, M.M. Tentzeris,"A broadband printed dipole and a printed array for base station applications," *IEEE Wireless Communication and Network*, July 2008, pp. 1-4

[59] A. Carr,"Development and trials for W-CDMA infrastructure," *IEEE Wireless Communication and Network*, Nov. 1998, pp. 1-7

[60] G. Hueber, R. Stuhlberger, A. Springer,"Concept for an adaptive digital front-end for multi-mode wireless receivers," *IEEE International Symposium on Circuits and System*, May 2008, pp. 89-92

[61] S.K. Bahl, "Cell searching in WCDMA," *IEEE Potentials*, vol. 22, No. 2, May 2003, pp. 16-19

[62] Y.S. Rao, W. Yeung, A. Kripalani,"Third-generation (3G) radio access standards," *IEEE International Conference on Communication Technology Proceedings*, Aug 2000, vol. 2, pp. 1017-1023

[63] H. Harada, S. Miyamoto,"Life cycle assessment of mobile communications networks," *IEEE 3rd International Symposium on Environmentally Conscious Design and Inverse Manufacturing*, Dec 2003, pp. 694-697

[64] A.C. Chen,"The evolution of wireless mobile data communication technologies and their market opportunities," *IEEE 28th Anual Conference of The Industry Electronics Society Symposium on Environmentally Conscious Design and Inverse Manufacturing*, Nov. 2002, vol. 2, pp. 3428-3433

[65] G. Hueber, R. Stuhlberger, A. Holm, A. Springer,"Multi-Mode Receiver Design for Wireless Terminals," *Eurapean Conference on Wireless Technologies*, Oct. 2007, pp. 126-129

[66] G. Hueber, R. Stuhlberger, A. Springer,"An Adaptive Digital Front-End for Multimode Wireless Receivers," *IEEE Transactions on Circuits and Systems II: Express Briefs*, vol. 55, No.4, 2008, pp. 349-353

[67] K. Yamauchi, W. Chen, D. Wei,"An Intensive Survey of 3G Mobile Phone Technologies and Applications in Japan," *IEEE Sixth International Conference on Computer and Information Technology*, Sep. 2006, pp. 265

[68] S.S. Prasad, R. Baruah,"Femtocell mass deployment: Indian perspective," *IEEE 3rd International Conference on Anti-counterfeiting, Security, and Identification in Communication* , Aug. 2009, pp. 34-37

[69] G.P. Perrucci, F.H.P Fitzek, Q. Sasso, W. Kellerer, J. Widmer ,"On the impact of 2G and 3G network usage for mobile phones' battery life," *European Wireless Conference*, May. 2009, pp. 255-259

[70] J. Yoo, H. Lee, S. Back, Y. Park,"Service quality management for value chain of wireless communication network," *30th Annual Conference of IEEE Industrial Electronics Society*, Nov. 2004, vol. 3, pp. 2758-2761

[71] Q. Wei, S. Su, J. Chen,"Study on application of softswitch in wireless networks," *IEEE International Conference on Communication Technology Proceedings*, April. 2003, vol. 1, pp. 127-130

[72] W. Chang, A. Gu,"Integration of RF front-end modules in cellular handsets," *IEEE 7th International Conference on Solid-State and Integrated Circuits Technology*, Oct. 2004, vol. 2, pp. 1285-1290

[73] S. Ratanamahatana, H.M. Kwon,"Channel estimation for power controlled 3G CDMA," *IEEE 51st Vehicular Technology Conference Proceedings*, May 2000, vol. 3, pp. 2429-2433

[74] W. Tang; C. Hu; C. Hsu,"A mobile phone based homecare management system on the cloud," *IEEE 2010 3rd International Conference on Biomedical Engineering and Informatics*, Oct. 2010, vol. 6, pp. 2442-2445

[75] Z.A. Colak, S. Helhel, I.B. Basyigit, S. Ozen,"Safety distance for medical equipments based on 2G and 3G mobile systems," *IEEE 15th National Biomedical Engineering Meeting*, April. 2010, pp. 1-3

[76] A.R. Karamchand Babu, Z.A. Abdul Rashid,"Performance evaluation of wideband CDMA air interface," *IEEE Student Conference on Research and Development*, 2002, pp. 145-148

[77] J.T Aguiar, L.M. Correia,"A framework for the evaluation of converged mobile and wireless communication systems," *IEEE 15th International Symposium on Personal, Indoor and Mobile Radio Communications*, Sep. 2004, vol. 2, pp. 752-756

[78] N.A. Al-Dabbous, B.S. Sharif,"Advance Detection Techniques for Beyond 3G Wireless," *IEEE The Third Advanced International Conference on Telecommunications*, May 2007, pp. 17

[79] K. Yamauchi, W. Chen, D. Wei,"3G mobile phone applications in telemedicine - a survey," *IEEE The Fifth International Conference on Computer and Information Technology*, Sep. 2005, pp. 956-960

[80] G. Rittenhouse,"Future of wireless networks," *IEEE 14th International Conference on Computer Communications and Networks*, Oct. 2005, pp. 480

[81] X. Qin, L. Mai, X. Dai,"Modeling of Hybrid-service in Broadband Wireless Communication System," *The Eighth IEEE/ACIS International Conference on Computer and Information Science* , June 2009, pp. 205-209

[82] J. Hausner, R. Denk,"Implementation of signal processing algorithms for 3G and beyond," *IEEE Microwave and Wireless Components Letters*, vol. 13, No. 8, Aug. 2003, pp. 302-304

[83] J. Perez-Romero, O. Sallent, R. Agusti,"Impact of indoor traffic on W-CDMA capacity," *IEEE 15th International Symposium on Personal, Indoor and Mobile Radio Communications*, Sep. 2004, vol. 4, pp. 2861-2865

[84] K. Hoque, R.R. Haque, M.A. Hossain, M.S.F. Farazi, G. Hossain,"Modeling and performance of TCP in a MC-CDMA system for 4G communications," *IEEE 10th International Conference on Computer and Information Technology*, Dec. 2007, pp. 1-5

[85] S. Sil, R. Bera, S. Bhattacharya, A. Chakraborty,"Realization of Vertical Handover - Applicable for 4G Communications," *IEEE 10th International Conference on Computer and Information Technology*, Feb. 2011, pp. 1-4

[86] I. Barbancho, A.M. Barbancho, L.J. Tardon, A. Peinado, "Multirate MC-DS-CDMA transmitter for 4G communications," *IEEE 60th Vehicular Technology Conference*, Sep. 2004, vol.2, pp. 904-908

[87] S. Yeh, "Green 4G communications: Renewable-energy-based architectures and protocols," *IEEE 2010 Global Mobile Congress*, Oct. 2010, vol.2, pp. 1-5

[88] A.F. Kamal, C.P. Wong, J.A. Copeland,"An original modeling process and technology with intra-package crosstalk consideration for compact array antennas on the 4G communications packages," *IEEE 2010 Global Mobile Congress*, Dec. 2002, pp. 37-39

[89] S. Shetty, A.S. Daryoush,"Circularly polarized broadband annular ring array

antenna for 4G communications" *IEEE Military Communications Conference*, Oct. 2005, vol. 5, pp. 3306-3309

[90] F. Dovis, R. Fantini, M. Mondin, P. Savi,"4G communications based on high altitude stratospheric platforms: channel modeling and performance evaluation," *IEEE Global Telecommunications Conference*, Nov. 2001, vol. 1, pp. 557-561

[91] J. Hu, W.W. Lu,"Open wireless architecture - the core to 4G mobile communications," *IEEE International Conference on Communication Technology Proceedings*, April 2003, vol. 2, pp. 1337-1342

[92] B. Chang, Y. Liang, C. Wu, Y. Huang, R. Hwang,"MDP-Based CAC for Two-Dimension Spreading VSF-OFCDM in 4G Cellular Communications," *IEEE Global Telecommunications Conference*, Nov. 2009, pp. 1-5

[93] A. Markhasin,"QoS-oriented medium access control fundamentals for future all-MPLS/ATM satellite multimedia personal communications 4G," *IEEE International Conference on Communications*, June 2004, vol. 7, pp. 3963-3967

[94] A. Hirata, S. Mitsuzono, T. Shiozawa,"Feasibility study of adaptive array antenna on handset for 4G mobile communications," *IEEE Antennas and Propagation Society International Symposium*, June 2004, vol. 3, pp. 3191-3194

[95] V.I. Slyusar, I.V. Titov,"Correction of smart antennas receiving channels characteristics for 4G mobile communications," *IEEE International Conference on Antenna Theory and Techniques*, Sep. 2003, vol. 1, pp. 374-375

[96] V. Gazis, N. Housos, A. Alonistioti, L. Merakos,"Generic system architecture for 4G mobile communications," *IEEE 57th Semiannual Vehicular Technology Conference*, April 2003, vol. 3, pp. 1512-1516

[97] J. Govil,"4G Mobile Communication Systems: Turns, Trends and Transition," *IEEE International Conference on Convergence Information Technology*, Nov. 2007, vol. 3, pp. 13-18

[98] L. Zhou, S. Shetty, R. Spring, H. Ariak, W. Zheng, J. Hyun, M.R. Tofighi, A.S. Daryoush,"IC based broadband digital receiver for 4G wireless communications," *IEEE Radio and Wireless Conference*, Sep. 2004, pp. 339-342

[99] S. Frattasi, M. Monti, R. Prasad,"A cooperative localization scheme for 4G wireless communications," *IEEE Radio and Wireless Symposium*, Sep. 2006, pp. 287-290

[100] A. Chun, E. Tsui, I. Chen, H. Honary, J. Lin,"Application of the Intel reconfigurable communications architecture to 802.11a, 3G and 4G standards," *IEEE 6th Circuits and Systems Symposium on Emerging Technologies: Frontiers of Mobile and Wireless Communication*, May. 2004, vol. 2, pp. 659-662

[101] V. Huang, W. Zhuang,"QoS-oriented access control for 4G mobile multimedia CDMA communications," *IEEE Communications Magazine*, March 2003, vol. 40, No. 3, pp. 659-662

[102] A.A. Youssef,"RF Wireless Integrated Architectures for 4G Communication Systems," *IEEE 49th International Midwest Symposium on Circuits and Systems*, Aug. 2006, vol. 1, pp. 1-5

[103] X. Jiang, X. Gu Xuemai, H. Li,"Based on 2.4G Wireless Communications System Design," *IEEE Second International Conference on Networks Security Wireless Communications and Trusted Computing*, April. 2010, vol. 2, pp. 553-556

[104] M.R. Chowdhury, C. Bose,"M-PSK TCM based MB-OFDM UWB communi-

cation system performance for 4G High-Rate Wireless Personal Area Networks," *IEEE 2010 Annual India Conference*, Dec. 2010, pp. 1-4

[105] P.W. Baier, M. Meurer,"Advanced CDMA transmission concepts for 3G and 4G mobile radio communications," *IEEE Eighth International Symposium on Spread Spectrum Techniques and Applications*, Aug. 2004, pp. 601-608

[106] J.W. Lee, O.C. Ugweje, C. Madubata,"Multi-code multi-carrier CDMA systems for 4G wireless communications," *IEEE Proceedings of the Thirty-Seventh Southeastern Symposium on System Theory*, March 2005, pp. 20-24

[107] W.C.Y. Lee,"Comparison of spectrum efficiency between FDMA and TDMA in digital cellular," *IEEE 39th Vehicular Technology Conference*, May 1989, vol. 1, pp. 165-168

[108] M. Wachira, D. Bossler, B. Skerry,"Comparison of spectrum efficiency between FDMA and TDMA in digital cellular," *IEEE Global Telecommunications Conference, 1989, and Exhibition. Communications Technology for the 1990s and Beyond*, Nov. 1989, vol. 2, pp. 754-759

[109] I.P. Kaminow, P.P. Iannone, J. Stone, L.W. Stulz, "Comparison of spectrum efficiency between FDMA and TDMA in digital cellular," *Journal of Lightwave Technology*, vol. 6, No. 9, 1988, pp. 1406-1414

[110] A.E. Willner, I.P. Kaminow, M. Kuznetsov, J. Stone, L.W. Stulz,"1.2 Gb/s closely-spaced FDMA-FSK direct-detection star network," *IEEE Photonics Technology Letters*, vol. 2, No. 3, 1988, pp. 223-226

[111] J. Capmany, M.A. Muriel,"1.2 Gb/s closely-spaced FDMA-FSK direct-detection star network," *Journal of Lightwave Technology*, vol. 8, No. 12, 1990, pp. 1904-1919

[112] A.A.M. Saleh, J. Stone,"Two-stage Fabry-Perot filters as demultiplexers in optical FDMA LANs ," *Journal of Lightwave Technology*, vol. 7, No. 2, 1989, pp. 323-330

[113] S.D. Elby, N.K. Shankaranarayanan, K.Y. Lau,"WDM-subcarrier FDMA lightwave networks: optical beat note interference ," *Conference Digest. LEOS Summer Topical on Optical Multiple Access Networks*, July 1990, pp. 64-65

[114] R.M. Gagliardi,"Optimal Channelization in FDMA Communications," *IEEE Transactions on Aerospace and Electronic Systems*, voL. AES-10, NO. 6, Nov. 1974, pp. 867-870

[115] G.J. Foschini,"Reliability of the repelling carrier method of implementing optical FDMA," *IEEE Transactions on Communications*, vol. 37, NO. 12, Dec. 1989, pp. 1275-1281

[116] S.H. Gardner, W.A. Shumate, B. Trumpis, A. Wardani,"A New FDMA Modem for Defense Satellite Communications," *IEEE Military Communications Conference - Communications-Computers: Teamed for the 90's*, vol. 2, NO. 9, Dec. 1986, pp. 669-672

[117] R. Lyons,"A Statistical Analysis of Transmit Power Control to Compensate Up- and Down-Link Fading in an FDMA Satellite Communications System," *IEEE Transactions on Communications*, vol. 24, NO. 6, June 1976, pp. 622-636

[118] K. Kinoshita, M. Hata, K. Hirade,"Digital mobile telephone system using TD/FDMA scheme," *IEEE Transactions on Vehicular Technology*, vol. 31, NO. 4, Nov. 1982, pp. 153-157

[119] N.J. Tolson,"A novel receiver for GSM TDMA radio," *IEEE 49th Vehicular Technology Conference*, vol. 2, July 1999, pp. 1207-1211

[120] B. Rohani, K.S. Chung, "Adaptive Equaliser With Time-reversal Strategy For Gsm Tdma Mobile Telephony," *IEEE Fourth International Symposium on Signal Processing and Its Applications*, vol. 2, Aug. 1996, pp. 523-526

[121] P. Decker, "A packet radio protocol for group communication suitable for the GSM mobile radio network," *IEEE 5th International Symposium on Personal, Indoor and Mobile Radio Communications*, vol. 3, Sep. 1994, pp. 934-938

[122] C. Brown, K. Feher, "A reconfigurable modem for increased network capacity and video, voice, and data transmission over GSM PCS," *IEEE Transactions on Circuits and Systems for Video Technology*, vol. 6, No. 2, April 1996, pp. 215-224

[123] B. Natarajan, C.R. Nassar, S. Shattil, "Throughput enhancement in TDMA through carrier interferometry pulse shaping," *IEEE 52th Vehicular Technology Conference*, vol. 4, Sep. 2000, pp. 1799-1803

[124] M. Yeon, J.J. Shynk, R.P. Gooch, "A Comparative Performance Investigation of Adaptive Beamformers with Iterative Weight Refinement for GSM Signal Detection," *IEEE Fourth Workshop on Sensor Array and Multichannel Processing*, vol. 4, July 2006, pp. 571-575

[125] A. Murase, A. Maebara, I. Okajima, S. Hirata, "Mobile radio packet data communications in a TDMA digital cellular system," *IEEE 47th Vehicular Technology Conference*, vol. 2, May 1997, pp. 1034-1038

[126] A. Murase, T. Utano, K. Yamamoto, "TDMA digital cellular systems in the second stage based on PDC standard in Japan," *IEEE 44th Vehicular Technology Conference*, vol. 1, June 1994, pp. 311-315

[127] T. Satoh, Y. Ohto, A. Murase,"TDMA half-rate digital cellular system based

on PDC standard in Japan," *IEEE 45th Vehicular Technology Conference*, vol. 1, July 1995, pp. 301-305

[128] S. Miyamoto, N. Morinaga,"Performance of radio communication systems under microwave oven interference environment," *IEEE International Symposium on Electromagnetic Compatibility Proceedings*, vol. 1, May 1997, pp. 308-311

[129] N. Spencer,"An overview of digital telephony standards," *IEE Colloquium on The Design of Digital Cellular Handsets*, vol. 1, Mar 1998, pp. 1-7

[130] P.D. Kenington,"Linearized transmitters: an enabling technology for software defined radio," *IEEE Communications Magazine*, vol. 40, No. 2, Feb. 2002, pp. 156-162

[131] C. Liu, H. Xiao, Q. Wu, F. Li,"Spectrum analysis of nonlinear distortion of RF power amplifiers for wireless signals," *IEEE International Conference on Communication Technology Proceedings* , vol. 2, April 2003, pp. 1468-1471

[132] K. Okada, A. Ohta, K. Shimokawa, M. Kawai,"A study on satellite-switched TDMA systems for applying to the asynchronous transfer mode," *IEEE International Conference on Communications*, vol. 1, June 1992, pp. 355-359

[133] S. Kato, M. Morikura, S. Kubota, H. Kazama, K. Enomoto, M. Umehira,"A TDMA satellite communication system for ISDN services ," *IEEE Journal on Selected Areas in Communications*, vol. 10, No. 2, Feb. 1992, pp. 456-464

[134] T. Kawabata, Y. Nagashima, Y. Moritani, T. Fujino,"Precise detection of the on-board IF-switch timing for SS-TDMA systems ," *IEEE Global Telecommunications Conference*, vol. 3, Nov. 1995, pp. 1899-1903

[135] H. Kazama, T. Atsugi, M. Umehira, S. Kato,"A feedback-loop type transmission

power control for low speed TDMA satellite communication systems," *IEEE International Conference on Communications*, vol. 1, June 1989, pp. 509-514

[136] J. Li, Q. Liang, M.T. Manry,"Adaptive channel equalization for satellite communications with multipath based on unsupervised learning algorithm," *IEEE Proceedings on 14th Personal, Indoor and Mobile Radio Communications*, vol. 1, Sep. 2003, pp. 730-734

[137] W. Mohr, M. Koukamp,"Downlink performance of IS-95 DS-CDMA under multipath propagation conditions," *IEEE 4th International Symposium on Spread Spectrum Techniques and Applications Proceedings*, vol. 3, Sep. 1996, pp. 1063-1067

[138] D.N. Kalofonos, E. Kurtas, J.G. Proakis,"Performance comparisons of concatenated codes with iterative decoding for DS-CDMA systems with application to IS-95-based cellular systems," *IEEE Wireless Communications and Networking Conference* , vol. 1, Sep. 1999, pp. 461-465

[139] Y.C. Yoon,"A simple and accurate method of probability of bit error analysis for asynchronous band-limited DS-CDMA systems," *IEEE Transactions on Communications*, vol. 50, No. 4, April 2002, pp. 656-663

[140] A. Ghosh, K. Rohani,"Effect of mobile power control saturation in DS-CDMA," *IEEE International Conference on Universal Personal Communications*, vol. 1, Sep. 1996, pp. 360-364

[141] Y. Chen, M.D. Zoltowski,"Blind RLS based space-time adaptive 2-D RAKE receivers for DS-CDMA communication systems," *IEEE Transactions on Signal Processing*, vol. 48, No. 7, July 2000, pp. 2145-2150

[142] G. Wetzker, F. Jondral,"Maximum likelihood acquisition of time and frequency shift in land mobile DS-CDMA systems," *IEEE International Symposium on Personal, Indoor and Mobile Radio Communications*, vol. 3, Sep. 1998, pp. 1208-1212

[143] P. Kauffmann,"Fast power control for third generation DS-CDMA mobile radio systems," *IEEE International Zurich Seminar on Broadband Communications*, Feb. 2000, pp. 9-13

[144] W.G. Phoel, M.L. Honig,"Fast power control for third generation DS-CDMA mobile radio systems," *IEEE 49th Vehicular Technology Conference*, July 1999, pp. 826-830

[145] F. Ling, E. Bruckert, T.A. Sexton,"Analysis of performance and capacity of coherent DS-CDMA reverse link communications," *IEEE 45th Vehicular Technology Conference*, July 1995, pp. 912-916

[146] P. Xiao, E. Strom,"Performance of iterative DS-CDMA m-ary demodulation in the presence of synchronization errors," *IEEE 53rd Vehicular Technology Conference*, vol. 3, May 2001, pp. 1703-1707

[147] Y. Lin, D.W. Lin,"Chip-interleaved WCDMA with parallel-interference-cancellation receiver in multipath Rayleigh fading channels," *IEEE International Conference on Acoustics, Speech, and Signal Processing*, vol. 4, May 2004, pp. iv - 961-4

[148] L. Qian, S. Berber,"3G WCDMA design, simulation and analysis using Ptolemy software tools," *IEEE Proceedings of the 2003 Joint Conference of the Fourth International Conference on Information, Communications and Signal Processing,*

2003 and the Fourth Pacific Rim Conference on Multimedia, vol. 2, December 2003, pp. 897-901

[149] A. Toskala, H. Holma, P. Muszynski,"ETSI WCDMA for UMTS," *IEEE 5th International Symposium on Spread Spectrum Techniques and Applications*, vol. 2, Sep 1998, pp. 616-620

[150] K. Waheed, F.M. Salem,"Blind information-theoretic multiuser detection algorithms for DS-CDMA and WCDMA downlink systems," *IEEE Transactions on Neural Networks*, vol. 16, No. 4, July 2005, pp. 937-948

[151] C. Li, K. Pu, Y. Chu,"An integrated pseudo-noise code acquisition processor for WCDMA, CDMA2000 and 802.11b systems," *IEEE International Symposium on Circuits and Systems*, May 2005, pp. 5043-5046

[152] C. Brunner, M. Haardt, J.A. Nossek,"On space-time RAKE receiver structures for WCDMA," *IEEE Conference Record of the Thirty-Third Asilomar Conference on Signals, Systems, and Computers*, vol. 2, Oct. 1999, pp. 1546-1551

[153] E. Kunnari, D. Tujkovic,"Convolutionally coded multi-antenna transmission in WCDMA over frequencyselective Rayleigh fading channel," *IEEE 53rd Vehicular Technology Conference*, vol. 1, May 2001, pp. 127-131

[154] M.A. Ouameur, D. Massicotte,"Wiener LMS Based Multipath Channel Estimation in WCDMA and cdma2000," *IEEE 64th Vehicular Technology Conference*, Sep. 2006, pp. 1-5

[155] M. Juntti, K. Pajukoski,"Blind spreading factor detection for DS-CDMA," *The 11th IEEE International Symposium on Personal, Indoor and Mobile Radio Communications*, Sep. 2000, pp. 1395-1399

[156] P. Lal Kafle, K. Makelainen, R.M.A.P. Rajatheva,"Performance of parallel concatenated interleaved codes in correlated multipath fading channels in a DS-CDMA system," *IEEE 49th Vehicular Technology Conference*, vol. 3, July 1999, pp. 1395-1399

[157] S. Mohan, R. Kapoor, B. Mohanty,"Enhanced HSDPA Mobility Performance: Quality and Robustness for Voice over HSPA Service," *IEEE 71st Vehicular Technology Conference*, May 2010, pp. 1-5

[158] M. Alvarez-Campana, E. Vazquez, J. Vinyes,"Performance modeling of web access over HSPA networks," *IEEE International Congress on Ultra Modern Telecommunications and Control Systems and Workshops*, Oct 2010, pp. 710-716

[159] K. Johansson, J. Bergman, D. Gerstenberger, M. Blomgren, A. Wallen,"Multi-Carrier HSPA Evolution," *IEEE 69th Vehicular Technology Conference*, April 2009, pp. 1-5

[160] S. Wanstedt, M. Ericson, K. Sandlund, M. Nordberg, T. Frankkila,"Realization and Performance Evaluation of IMS Multimedia Telephony for HSPA," *IEEE 17th International Symposium on Personal, Indoor and Mobile Radio Communications*, Sep. 2006, pp. 1-5

[161] B. Heder, C. Vulkan,"Improved Uplink Macro Diversity Combining in Evolved HSPA Systems," *IEEE 69th Vehicular Technology Conference*, April 2009, pp. 1-5

[162] A. Masmoudi, S. Tabbane,"Optimized dimensioning methods for HSPA based Beyond 3G mobile networks," *IEEE Global Information Infrastructure Symposium*, June 2009, pp. 1-8

[163] P. Gronsund, A. Jacobsen, T.O. Breivik, V. Hassel, G. Millstein, T. Haslestad,"Heterogeneous all-IP wireless broadband with WiMAX, WiFi and HSPA," *IEEE 20th International Symposium on Personal, Indoor and Mobile Radio Communications*, Sep. 2009, pp. 1128-1132

[164] T. Isotalo, J. Palttala, J. Lempiainen,"Impact of indoor network on the macro-cell HSPA performance," *IEEE International Conference on Broadband Network and Multimedia Technology*, Oct. 2010, pp. 294-298

[165] H. Holma, M. Kuusela, E. Malkamaki, K. Ranta-aho, T. Chen ,"VOIP over HSPA with 3GPP Release 7," *IEEE 17th International Symposium on Personal, Indoor and Mobile Radio Communications*, Sep. 2006, pp. 1-5

[166] K. Banitsas, S. Tachakra, E. Stefanidis, K. Boletis,"Using HSPA to improve the telemedical links on a moving ambulance," *IEEE 30th Annual International Conference Engineering in Medicine and Biology Society*, Aug. 2008, pp. 739-742

[167] A. Furuskar, J. Rao, M. Blomgren, P. Skillermark,"LTE and HSPA for fixed wireless broadband: Datarates, coverage, and capacity in an Indian rural scenario," *IEEE 2nd International Conference on Wireless Communication, Vehicular Technology, Information Theory and Aerospace and Electronic Systems Technology (Wireless VITAE)*, March 2011, pp. 1-5

[168] O. Ozturk, R. Kapoor, V. Chande, J. Hou, B. Mohanty,"Circuit-Switched Voice Services Over HSPA," *IEEE 71st Vehicular Technology Conference*, May 2010, pp. 1-5

[169] Y. Kim, W. Jang, N. Lim,"Self-encoded TH-PPM UWB system with iterative detection ," *IEEE 8th International Conference on Advanced Communication Technology*, vol. 1, Feb. 2006, pp. 5pp-714

[170] C. Han, G. Wang,"A novel multi-address chaotic sequence for TH-PPM-UWB system," *IEEE International Conference on Communications, Circuits and Systems* , July 2010, pp. 764-768

[171] S. Kim, B. Jung, J. Chong, C. Jung, D. Sung,"Capacity Analysis of a TH-PPM UWB System using a Near-Interference Erasure Scheme in Multi-User Environments ," *IEEE 18th International Symposium on Personal, Indoor and Mobile Radio Communications*, Sep. 2007, pp. 1-5

[172] Y. Jiang, J. Wu,"Enhanced Exact Modeling of Multiple Access Interference for TH-PPM UWB System," *IEEE 4th International Conference on Wireless Communications, Networking and Mobile Computing*, Oct. 2008, pp. 1-5

[173] T.K. Nguyen, T.H. Nguyen, T. Kaiser,"CMI and IFI mitigation for TH-PPM Ultra Wideband systems with a low complexity receiver ," *IEEE International Conference on Advanced Technologies for Communications*, Oct. 2009, pp. 223-228

[174] T. Tian, Q. Song, H. Zhang,"Analysis of Time-Hopping UWB Interference Effect on GPS Receivers," *IEEE International Symposium on Microwave, Antenna, Propagation and EMC Technologies for Wireless Communications*, Aug. 2007, pp. 1258-1262

[175] J. Xu, Y. Wang, C. Song,"EMD-Based BER Improvement of TH-PPM UWB Signal in AWGN Channel ," *IEEE 6th International Conference on Wireless Communications Networking and Mobile Computing*, Sep. 2010, pp. 1-3

[176] B. Liang, E. Gunawan, L. Choi, T. Kah,"Accurate bit error rate calculation for asynchronous TH-PPM UWB systems in Nakagami fading channel," *IEEE International Conference on Ultra-Wideband*, Sep. 2005

[177] M. Kim, B. Jung, J. Chong, D. Sung,"Performance Enhancement of a TH-PPM UWB System Using a Near-Interference Erasure Scheme ," *IEEE International Conference on Ultra-Wideband*, Sep. 2006, pp.399-404

[178] R. Pasand, S. Khalesehosseini, J. Nielsen, A. Sesay, "Exact evaluation of M-ary TH-PPM UWB systems on AWGN channels for indoor multiple-access communications," *IEE Proceedings on Communications* , vol. 153, No. 1, Feb. 2006, pp.83-92

[179] L. Fang, Z. Huang, "Low complexity multi-user detectors of TH-PPM UWB system ," *IEEE International Conference on Wireless Communications, Networking and Mobile Computing*, vol. 1, Sep. 2005, pp. 320-323

[180] Z. Liang, Z. Zhou, "Optimal Pulse Waveform Design for TH-PPM Ultra Wideband Systems ," *IEEE IFIP International Conference on Wireless and Optical Communications Networks*, vol. 1, July 2007, pp. 1-5

[181] S. Xu, Z. Bai, Q. Yang, K. Kwak, "Singular Value Decomposition-Based Algorithm for Suppression of IEEE 802.11 a Interference in TH-PAM UWB Systems," *IEEE International Symposium on Communications and Information Technologies*, Sep. 2006, pp. 599-604

[182] T. Shing, C. Ku, W. Feng, C. Lee, "Hopping Pilot Performance Analysis of PPM-TH and PAM-DS UWB Radio Link Based on Coherent Correlation Detection," *IEEE Fifth International Conference on Information, Communications and Signal Processing*, Sep. 2006, pp. 286-290

[183] H.B. Soni, U.B. Desai, S.N. Merchant,"Packet collision based Multiuser Interference (MUI) analysis for TH-PAM and TH-PPM ultra wideband (UWB) sys-

tem," *IEEE 3rd International Conference on Communication Systems Software and Middleware and Workshops*, Jan 2008, pp. 637-641

[184] G. Yue, S. Li, L. Ge ,"The PSD analysis of UWB time hopping impulse radio multi-user aggregate signals ," *IEEE International Conference on Communications, Circuits and Systems*, vol. 1, May 2005, pp. 441-445

[185] P. Yaddanapudi, N. Vallepali, D.C. Popescu, M. Shadaram,"Performance Analysis of Multiband TH-PAM and Multiband-OFDM UWB Communications Systems," *IEEE Radio and Wireless Symposium*, vol. 1, May 2005, pp. 503-506

[186] A.Y. Abdalkarim, Sh. Shaaban, Kh. Shennawy,"Hybrid Modulation Schemes for UWB Wireless Systems," *IEEE Proceedings of the Twenty Third National Radio Science Conference*, vol. 0, March 2006, pp. 503-506

[187] D.C. Popescu, P. Yaddanapudi, N. Vallepalli, G.V.S. Raju,"A simulation comparison of time-hopping PAM and interference suppressing OFDM in multiuser ultra wideband communications systems ," *IEEE Radio and Wireless Symposium* , Jan. 2008, pp. 875-878

[188] A. Maali, A. Ouldali, H. Mimoun, G. Baudoin,"An evaluation of UWB localization under non line-of-sight (NLOS) propagation ," *IEEE 3rd International Symposium on Wireless Pervasive Computing*, May 2008, pp. 379-382

[189] M. Herceg, T. Matic, T. Svedek,"Performance of hybrid pulse shape amplitude modulation for UWB communications systems over multipath channels," *IEEE 9th International Conference on Telecommunication in Modern Satellite, Cable, and Broadcasting Services*, Oct. 2009, pp. 427-431

[190] W. Wu,"Design of Blind Mobile Receiver in UWB Communication System Em-

polying Time-Hopping PAM Modulation ," *IEEE Singapore International Conference on Communication systems* , Nov. 2006, pp. 1-5

[191] F. Kharrat-Kammoun, P. Ciblat, C. Martret,"Error probability approximation and codes selection in presence of multi-user interference for IR-UWB ," *IEEE 19th International Symposium on Personal, Indoor and Mobile Radio Communications*, Sep. 2008, pp. 1-5

[192] G. Khuandaga, A. Iqbal, K. Kwak,"Error probability approximation and codes selection in presence of multi-user interference for IR-UWB ," *IEEE Performance analysis of modulation schemes in Intra Vehicle Communications (IVC) channel* , Feb. 2011, pp. 725-729

[193] S. Niranjayan, A. Nallanathan, B. Kannan,"Modeling of multiple access interference and BER derivative for TH and DS UWB multiple access system," *IEEE Transactions on Wireless Communications*, vol. 5, No. 10, Oct. 2006, pp. 2794-2804

[194] A. A.D'Amico, U. Mengali and L. Taponecco,"Impactor of MAI and channel estimation errors on the performance of Rake receivers in UWB Communications," *IEEE Transactions on Wireless Communications*, vol. 4, No. 5, September 2005, pp. 2435-2440

[195] Y. Shen, F. Ueng , J. Chen and S. Huang,"A high-capacity TH multiple-access UWB system with performance analysis," *IEEE Transactions on Vehicular Technology*, vol. 59, No. 2, February 2010, pp. 742-753

[196] L. Li, and J.K. Townsend,"M-ary PPM for transmitted reference Ultra-Wideband communications," *IEEE Transactions on Communications*, vol. 58, No. 7, July 2010, pp. 1912-1917